

UNIVERSIDADE FEDERAL DO RIO GRANDE DO SUL
INSTITUTO DE INFORMÁTICA
PROGRAMA DE PÓS-GRADUAÇÃO EM COMPUTAÇÃO

BÁRBARA BELLAVER GONÇALVES

**A Quantum Physics Approach for
Simulating Agate Colors**

Thesis presented in partial fulfillment of the
requirements for the degree of Master of
Computer Science

Prof. Dr. Manuel Menezes de Oliveira Neto
Advisor

Porto Alegre, July 2012.

CIP – CATALOGING-IN-PUBLICATION

Gonçalves, Bárbara Bellaver

A Quantum Physics Approach for Simulating Agate Colors /
Bárbara Bellaver Gonçalves. – Porto Alegre: PPGC da UFRGS,
2012.

15 f.:il.

Advisor: Manuel Menezes de Oliveira Neto.

Thesis (Master) – Universidade Federal do Rio Grande do Sul.
Programa de Pós-Graduação em Computação. Porto Alegre, BR –
RS, 2012.

1. Agates. 2. Determination of color. 3. Quantum physics. 4.
Minerals. I. Oliveira Neto, Manuel Menezes de. II. Title

UNIVERSIDADE FEDERAL DO RIO GRANDE DO SUL

Reitor: Prof. Carlos Alexandre Netto

Vice-Reitor: Prof. Rui Vicente Oppermann

Pró-Reitor de Pós-Graduação: Prof. Aldo Bolten Lucion

Diretor do Instituto de Informática: Prof. Luís da Cunha Lamb

Coordenador do PPGC: Prof. Álvaro Freitas Moreira

Bibliotecária-Chefe do Instituto de Informática: Beatriz Regina Bastos Haro

*With love,
to Eduardo Camaratta and
my parents Rosa and Selvino*

ACKNOWLEDGEMENTS

I would like to thank God, my family, my friends and my advisor.

Eduardo, Mom and Dad, mere words are not enough to thank you for everything: All the support, the patience and mainly lots and lots of love that you gave me during the development of this work. You're amazing!

CONTENTS

LIST OF ABBREVIATIONS AND ACRONYMS	8
LIST OF FIGURES.....	9
LIST OF TABLES	12
ABSTRACT.....	13
RESUMO.....	14
1 INTRODUCTION.....	15
2 MINERALS	17
2.1 Properties of Minerals.....	18
2.1.1 Luster	18
2.1.2 Cleavage.....	19
2.1.3 Refractive Index, Birefringence and Dispersion.....	20
2.1.4 Color	20
2.1.5 Hardness.....	22
2.1.6 Emission of Light.....	23
2.1.7 Streak	27
3 AGATES	28
3.1 Silicates	28
3.2 Quartz.....	29
3.3 Chalcedony	29
3.4 Agates.....	30
3.4.1 The Formation of Agates	30
3.4.2 Agate Properties	30
3.4.3 Types of Agates	31
3.5 Additional Information about Agates.....	33

4	RELATED WORK.....	34
4.1	Rendering Minerals and Optical Effects	34
5	QUANTUM PHYSICS APPROACH FOR SIMULATION OF COLOR	39
5.1	Acquiring geometric information.....	39
5.2	Generating absorption curves	41
5.2.1	Molecular Orbital Theory	42
5.3	Calculating the Transition Energy.....	43
5.3.1	Input file for Orca	44
5.3.2	Methods and parameters we used with Orca	45
5.3.3	The Absorption spectra	48
5.4	Obtaining Color from a Spectrum.....	49
5.5	Generating textures to represent the surface of an agate	50
5.6	Rendering of the Colored Volume Representing an Agate	52
6	AGATE SURFACE FROM A 2D IMAGE	53
6.1	Solid Texture Synthesis from 2D images.....	53
6.2	The Proposed Method for Generating Solid Textures for Agates	57
6.3	Description of the Technique – Spreading the Colors.....	58
6.4	Examples of Generated Solid Textures	62
6.5	Limitations	64
7	RESULTS AND DISCUSSION	66
7.1	Single Molecule	66
7.2	The Unit Cell	68
7.3	Expansions.....	69
7.4	Unit Cell with Impurities	71
7.5	Discussion	76
8	CONCLUSIONS AND FUTURE WORK	78
9	REFERENCES.....	79
	APPENDIX A: PHYSICAL AND CHEMICAL BACKGROUND	86
A.1	Orbitals.....	86
A.1.1	Quantum Numbers	86
A.1.2	Electron configuration	88
A.1.3	The Shape of Orbitals	90
A.2	Definition of Mass and Matter	91

A.3	Light.....	92
A.3.1	Definition of Light	93
A.3.2	Photons.....	95
A.3.3	Wave-Particle Duality	95
A.3.4	Polarized Light.....	95
A.3.5	Refraction and Reflection	96
 APPENDIX B: THE CAUSES OF COLOR		98
B.1	Incandescence	98
B.2	Gas Excitation	99
B.3	Vibrations and Rotations	100
B.4	Presence of transition metal in the original compound or as an impurity	101
B.5	Molecular Orbitals	103
B.6	Charge transfer.....	103
B.7	Band theory	104
B.8	Color centers	106
B.9	Dispersion.....	107
B.10	Scattering.....	107
B.11	Interference and Diffraction.....	108
 APPENDIX C: DEVELOPING THE IDEA		110
 ANNEX A		112
 ANNEX B		113

LIST OF ABBREVIATIONS AND ACRONYMS

API	Application Programming Interface
CIF	Crystallographic Information File
DFT	Density Functional Theory
HF	Hartree-Fock
KS	Kohn-Sham
MOT	Molecular Orbital Theory
RI	Resolution of the Identity
RKS	Restricted Kohn-Sham
SCF	Self-Consistence Field
TDDFT	Time-Dependent Density Functional Theory

LIST OF FIGURES

Figure 2.1: Seven crystal systems	17
Figure 2.2: Graphite (left) and Diamond (right).....	18
Figure 2.3: Internal structure of graphite (left) and diamond (right).....	18
Figure 2.4: Metallic (left) and non metallic (right) luster.....	19
Figure 2.5: Crystalline structure and cleavage surface for NaCl.....	19
Figure 2.6: Examples of cleavage	19
Figure 2.7: Sulfur.....	21
Figure 2.8: Influence of the chemical composition in the color.....	21
Figure 2.9: Different colors of Fluorite	22
Figure 2.10: Fluorite exposed to visible (left) and ultraviolet light (right)	23
Figure 2.11: Fluorescence effect in several minerals	23
Figure 2.12: Alexandrite exposed to sunlight (left) and artificial light (right).....	24
Figure 2.13 Sapphire (left) and ruby star (right)	24
Figure 2.14: Cat's eye effect.....	24
Figure 2.15: Zinc sulfide (left) and aluminate (right) lit (up) and dark (bottom).....	25
Figure 2.16: Thermoluminescence in fluorite before (left) and after heating (right)	25
Figure 2.17: Triboluminescence effect.....	26
Figure 2.18: Aventurescence effect	26
Figure 2.19: Adularescence effect	27
Figure 2.20: Labradorescence effect	27
Figure 2.21: Examples of streaks	27
Figure 3.1: Silica tetrahedron.	28
Figure 3.2: Transition temperatures for silica	29
Figure 4.1: Real yellow diamond (left) and synthesized image (right)	34
Figure 4.2: Real aventurine (left) and synthesized image (right)	35
Figure 4.3: Real labradorite (left) and synthesized image (right).....	35
Figure 4.4: A lightened marble texture.....	36
Figure 4.5: Real tourmaline (left) and synthesized image (right).....	36
Figure 4.6: Effects of volume absorption in glass material shaped as cube (left) and as a diamond cut (right)	37
Figure 4.7: Light dispersion in a scene formed by crystal polyhedrons on a mirrored surface surrounded by several light sources	37
Figure 4.8: A crystal rendered without (left) and with dispersion effect (right)	38
Figure 5.1: Silica unit cell (left), supercell (middle), and the same supercell from a different angle (right).	40
Figure 5.2: Atom A surrounded by six atoms B within a fixed distance.	42
Figure 5.3: Orca input file for molecular silica	44
Figure 5.4: Absorption spectra obtained as output from Orca.	49

Figure 5.5: Example of an absorption/transmission spectrum (top) and the obtained color (violet) using the Eq. (5.1) (bottom).	50
Figure 5.6: Equation of an ellipse centered at the origin.	51
Figure 5.7: Example of image generated using the Algorithm 5-1.	52
Figure 5.8: Image obtained using the Algorithm 5-1 (left) and real agate (right).	52
Figure 6.1: A 2D image and the generated solid texture applied to a complex object... ..	54
Figure 6.2: Example of input image and several objects on which the solid texture was applied on	54
Figure 6.3: Kiwi model and different cuts.....	55
Figure 6.4: 2D images with their respective solid textures and intermediate layers	55
Figure 6.5: 2D image (a) and the synthesized vector solid texture applied to an object	56
Figure 6.6: Several fruits synthesized using the technique	56
Figure 6.7: A vector volume (a) and the zoomed view of the selected area in the previous image (b and c)	57
Figure 6.8: Arrows indicating how the colors spread in the volume.....	58
Figure 6.9: A transversal section, with a red dot indicating the approximate center of symmetry of the nested bands (a). Vertical (b) and horizontal profile mask (c)... ..	58
Figure 6.10: An 8x8-pixel set of image and masks: transversal (left), vertical mask (center) and horizontal mask (right).	59
Figure 6.11: List of possible movements for the color of a pixel (x_i, y_i) in the volume.	59
Figure 6.12: Movements in one slice of the volume.	60
Figure 6.13: The colors in positions A and B have two options of movement. The one in A spread to left and in B, down.	60
Figure 6.14: Example of discontinuity in the colored pixels.....	61
Figure 6.15: The borders of a vertical slice and a horizontal slice.....	62
Figure 6.16: Original image (a), vertical (b) and horizontal (c) masks and final volume with Marching Cubes and post processing (d).	62
Figure 6.17: Volume before (left) and after (right) post processing	63
Figure 6.18: Comparison between a volume generated by (TAKAYAMA and IGARASHI, 2009) (left) and our method (right).	63
Figure 6.19: Carrot and Kiwi volumes generated with our method.	64
Figure 6.20: Example of mismatched colors and squared surface.	64
Figure 6.21: Differences in the volume resulting from external parameters.....	65
Figure 6.22: Agate with crystals in its interior	65
Figure 6.23: The external surface of the resulting volume generated with the proposed technique may not look like a stone.	65
Figure 7.1: Silica unit cell. It is formed by six silicon (Si) and six oxygen (O) atoms. ..	66
Figure 7.2: Molecules based on the unit cell, treated separately.....	67
Figure 7.3: Absorption spectra obtained from individual molecules (top) and the colors represented by the resulting curves (bottom).	67
Figure 7.4: Molecular angles presented by the different molecules.....	68
Figure 7.5: Absorption spectra for the silica unit cell inside the visible region of the spectrum, obtained using the methods B3LYP and RI-B2PLYP.....	68
Figure 7.6: Absorption spectra for the silica unit cell for a larger portion of the electromagnetic spectrum obtained using the methods B3LYP and RI-B2PLYP.	69
Figure 7.7: Absorption spectra for the silica unit cell for a larger portion of the electromagnetic spectrum obtained using the methods B3LYP and RI-B2PLYP, after the RI-B2PLYP curve has been translated to the left to better match the B3LYP curve.	69

Figure 7.8: Unit cell (a) expanded along the X, Y and Z directions, (b), (c) and (d) respectively.....	70
Figure 7.9: Absorption spectra of the unit cell expanded into X, Y and Z directions....	70
Figure 7.10: Scaled version of the absorption spectra of the expanded unit cell	71
Figure 7.11: Absorption spectra of a molecule, the unit cell and its expanded versions	71
Figure 7.12: Unit cell after the insertion of impurities. The blue spheres represent iron (<i>Fe</i>) atoms, while the red spheres represent titanium (<i>Ti</i>) atoms.	72
Figure 7.13: Set of obtained impure spectra.....	73
Figure 7.14: Spectra of <i>Fe</i> (top) and <i>Ti</i> (bottom) atoms individually replaced.....	74
Figure 7.15: Influence of the concentration of an element.....	75
Figure 7.16: <i>Ti</i> atom at position #3 with <i>Fe</i> atom at #2 and the inverse situation	75
Figure 7.17: Spectra obtained from a mixture of <i>Ti</i> atoms at position #3 with <i>Fe</i> atoms at position #1 (top) and #2 (bottom).....	76
Figure A.1: Simplified representation of the Periodic Table.....	88
Figure A.2: Phase Diagram	91
Figure A.3: Structure of a crystalline (left) and an amorphous material (right).....	92
Figure A.4: Only items (a), (b) and (c) are crystals.....	92
Figure A.5: Electromagnetic spectra	93
Figure A.6: Wave propagation in the c direction and its electric and magnetic fields...	93
Figure A.7: Distance of a wavelength λ , with amplitude A.	94
Figure A.8: Non polarized light.....	96
Figure A.9: Polarized light	96
Figure A.10: Propagation of a light wave.....	96
Figure A.11: Propagation of a white light beam through a prism	97
Figure B.1: Spectrum of colors.....	99
Figure B.2: Piece of hot iron	99
Figure B.3: Light emitted by a sodium lamp.....	100
Figure B.4: Directions of vibration for molecules of iodine (left), and water (right) .	100
Figure B.5: Possibilities of rotation for a diatomic molecule.....	101
Figure B.6: Iodine in solid state (left), and vaporized (right).....	101
Figure B.7: Aluminum atom surrounded by six atoms of oxygen	102
Figure B.8: From left to right, the crystals of aluminum oxide, ruby and emerald.....	102
Figure B.9: Alexandrite effect	103
Figure B.10: A crystal of aluminum oxide (left). Iron impurities result in a pale yellow color (center). Iron plus titanium impurities result in the blue (right).....	103
Figure B.11: Slightly distorted octahedral aluminum sites occupied by Fe^{+2} and Ti^{+4}	104
Figure B.12: Energy band.....	104
Figure B.13: Silver ore	105
Figure B.14: Color sequence of a continuous series	106
Figure B.15: Example of the formation of color centers	106
Figure B.16: Different colors of topaz.....	106
Figure B.17: Sparkles in a diamond	107
Figure B.18: Red sunset	107
Figure B.19: Constructive (left) and destructive (right) interference.....	108
Figure B.20: Bubble soap	108
Figure B.21: Corona (left)and iridescent clouds (right)	109
Figure AnnexA.1: Example of a silica CIF file.....	112

LIST OF TABLES

Table 2.1: Values for Mohs and absolute hardness.	22
Table 3.1: Agate properties	31
Table 3.2: Types of Agate.	32
Table A.1: Possible values for n , l and m	87
Table A.2: Exceptions of the electron configuration.....	89
Table A.3: Graphical representation of the orbitals.	90
Table Annex B.1: CIE 1931 standard colorimetric observer	113
Table Annex B.2: CIE Standard Illuminant D65	114

ABSTRACT

Color simulation is the essence of realistic image synthesis. In the case of minerals, the presence of a given impurity, or a variation of its concentration, can cause some materials to experience dramatic changes in color. For instance, while pure quartz is transparent, amethyst is a violet type of quartz, whose color is determined by the presence of traces of iron. The amount of iron defines the perceived hue. The color presented by a mineral can be determined based on its absorption spectrum. However, defining all possible variations is impractical and, therefore, such information is available only for a subset of the existing minerals. This thesis presents an approach for simulating the colors of existent agates, as well as for predicting the colors for (non-existent) synthetic ones. The approach is based on the fundamentals of quantum theory, and starts with the description of the silica molecule one wants to simulate. One can add different amounts of impurities, and alter the number of atoms included in the simulation. The obtained result is the absorption spectra of the mineral, which can then be used for determining the color of the agate with the desired composition. Although a detailed simulation of the entire process is extremely computationally-expensive, the thesis presents some results that corroborate the correctness of the proposed solution. It also introduces a standalone technique for defining agate volumes based on 2D images of agates.

Keywords: Agates, Color Computation, Quantum Physics, Minerals.

Uma Abordagem Quântica para Simulação das Cores de Ágatas

RESUMO

A simulação de cores corresponde à essência do processo de síntese de imagens realistas. Em se tratando de minerais, a presença de uma dada impureza, ou uma variação de sua concentração, pode fazer com que alguns materiais sofram alterações dramáticas em suas cores. Por exemplo, enquanto o quartzo puro é transparente, a ametista é um tipo violeta de quartzo, cuja cor é determinada pela presença de traços de ferro. A quantidade de ferro define o matiz percebido. A cor apresentada por um mineral pode ser determinada com base no seu espectro de absorção. No entanto, a definição de todas as variações possíveis é impraticável e, portanto, tal informação está disponível apenas para um subconjunto dos minerais existentes. Esta dissertação apresenta uma proposta para estimar a cor de ágatas, bem como para simular as cores de ágatas sintéticas (inexistentes). A abordagem utilizada baseia-se nos fundamentos da teoria quântica, e parte de uma descrição da molécula de sílica que se deseja simular. À esta, pode-se adicionar quantidades diferentes de impurezas e alterar o número de átomos incluídos na simulação. O resultado obtido é o espectro de absorção do mineral, que pode então ser utilizado para determinar a cor da ágata com a composição desejada. Embora uma simulação detalhada de todo o processo seja uma tarefa computacionalmente extremamente cara, esta dissertação apresenta alguns resultados que corroboram com a correção da solução proposta. Também é apresentada uma técnica independente que pode ser utilizada para definir um volume de ágata com base em uma imagem 2D.

Palavras-chave: Ágatas, Determinação de Cor, Física Quântica, Minerais.

1 INTRODUCTION

Several classes of minerals present an extraordinary beauty. Realistic color and appearance simulation of minerals is a difficult problem. It requires a significant amount of effort to determine, through practical experiments, functions that approximate the result of light interaction with such materials. Thus, the development of a general technique for simulating such interaction, taking the material properties into account is, therefore, very desirable, finding innumerable practical applications. These range from the synthesis of images in computer graphics, to the development of new materials with pre-determined optical and visual characteristics. Our main goal is to simulate realistic color of materials based on first principles, *i.e.*, using a quantum-theory approach. It is therefore a very bold goal that will require several years of effort. The work described in this thesis is, therefore, a first step in this direction. As the range of existent materials is extremely wide, we decided to focus our attention on minerals. The presence of certain elements or even a trace of others determines what colors a mineral will exhibit, or can cause it to change colors (NASSAU, 1978). For example, consider the pure quartz, which is colorless, while amethyst, a variation of quartz with traces of iron as impurity, is violet. The color of a mineral can also vary with illumination, heating, radiation, and imperfections in the crystal structure or the molecular bonding. Color in minerals is, ultimately, determined by the composition and organization of their molecules.

Therefore, if we want a general technique to simulate the colors of minerals, we have to work at the molecular level. A model for simulating the interaction of light with some material in such a fundamental level would lead us to the desired general color model. Besides, it would also allow us to predict the color of nonexistent minerals. A detailed investigation is required for determining a specific cause of color in most minerals (NASSAU, 1978). Thus, one could use such a general technique to test the same original molecule with different kinds and degrees of impurities and try to determine what impurities are most likely to cause a given color.

Given the huge number of different minerals, we had to restrict the scope of this thesis. Lapidated gemstones, such as tourmalines (GUY and SOLER, 2004) or diamonds (SUN, FRACCHIA and DREW, 1999), (SUN, FRACCHIA and DREW, 2000a), are the types of minerals that received most attention in computer graphics. On the other hand, the most abundant minerals are silicates. They represent 95% of the Earth's crust (BRITANNICA, 2008). Therefore, it is needless to state the importance of being able to simulate them. Thus, we decided to focus our work on silicates. However, since silicates represent a very large class of minerals, we had to restrict the scope our work even more. Therefore, this thesis focuses on the colorful and interesting group formed by agates. Agates define a large class of minerals. They can be found worldwide, but most of the commercially available agate come from deposits in the state of Rio

Grande do Sul, in Brazil (O'DONOGHUE, 2006), (GRANDE, AUGUSTYN and WEINSTEIN, 2009).

In computer graphics, rendering techniques based on the simulation of light interaction at molecular or atomic level have not been explored. Moreover, to the best of our knowledge, there has been no work specifically targeted at the rendering of agates. Even in a broader spectrum, one will find only few works related to rendering of gemstones and minerals. The thesis describes a pipeline of methods I used for simulating agate colors. I do not provide a deep description of the quantum algorithms, as this is beyond the scope of this work. However, I show the fundamental ideas of the proposed technique, so that the concepts can be applied to other areas of visual simulation.

This thesis is organized as follows: Chapters 2 and 3 introduce some concepts and a brief overview of minerals and agates, respectively. Chapter 4 reviews some related works that represent some efforts towards rendering minerals and optical effects. Chapter 5 describes our technique and the fundamentals on which it is based on. Chapter 6 presents a method we proposed for rendering of agate surface from a 2D image. Chapter 7 presents the obtained results and a general discussion. Conclusions and future work are presented in Chapter 8. Appendices Appendix A: and Appendix B: introduce some theoretical background and definitions required for a better understanding of the proposed technique.

2 MINERALS

This chapter briefly reviews the main properties responsible for the appearance of minerals. While it includes many properties not required for simulating agate colors, such properties were kept as they provide a source of inspiration for future research in computer graphics.

A mineral is a homogeneous solid substance formed through geological processes and presenting characteristic chemical composition, an atomic structure often crystalline, and specific physical properties (NICKEL, 1995), (PRICE and WALSH, 2005). Minerals can be divided into *amorphous* (with undefined internal structure) and *crystalline* (with an organized internal structure). Crystalline minerals are then divided into seven Crystalline Systems, according to their fundamental atomic structure. This fundamental cell (called the unit cell) repeats itself in order to form the mineral. Figure 2.1 presents the seven Crystalline Systems with an example of mineral which belongs to each one of them.

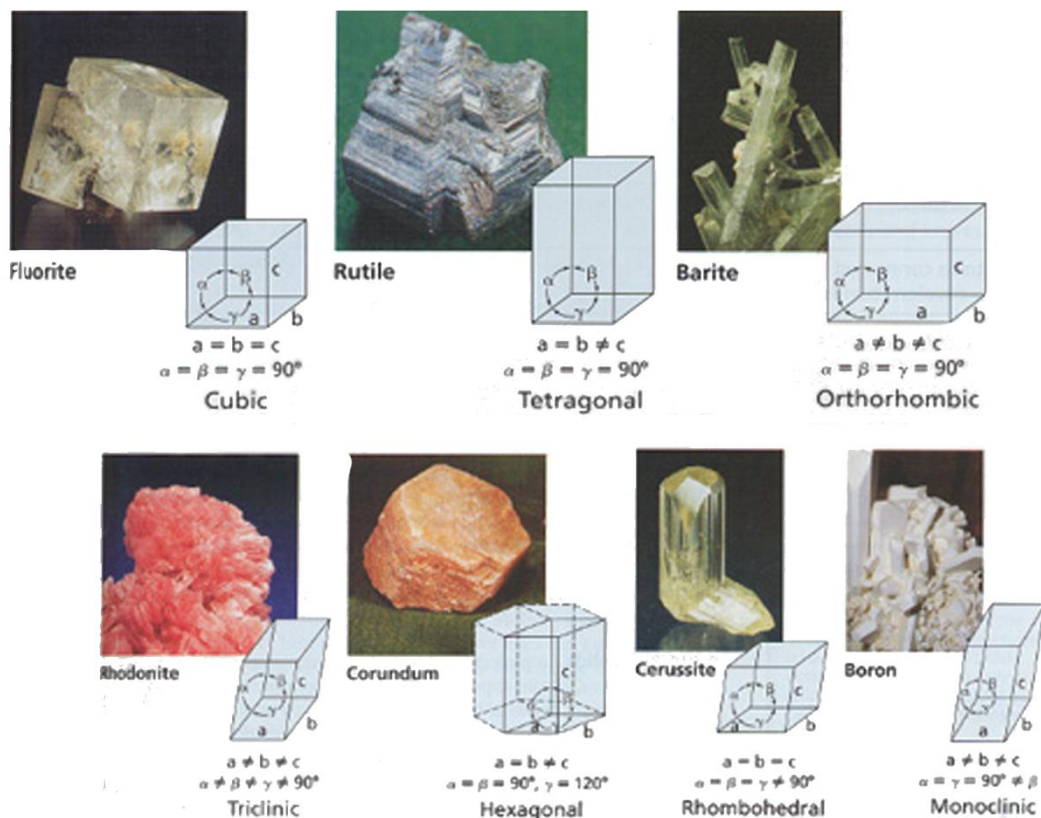


Figure 2.1: Seven crystal systems: cubic, tetragonal, orthorhombic, triclinic, hexagonal, rhombohedral, and monoclinic (SMOOT, PRICE and SMITH, 1983).

There are some minerals that present the same chemical composition, but their atoms are organized in different structures resulting in complete different materials. A classic example is *graphite* and *diamond*. They are both constituted of Carbon atoms but graphite crystallizes in the hexagonal and the diamond in the cubic crystalline system. Figure 2.2 presents graphite (left) and diamond (right), where it is easy to see the big difference between them. Figure 2.3 compares the internal structure of the graphite (left) and diamond (right).



Figure 2.2: Graphite (left) and Diamond (right) (Source: <http://preo.aps.org/story/v22/st5>. Access in June, 2012).

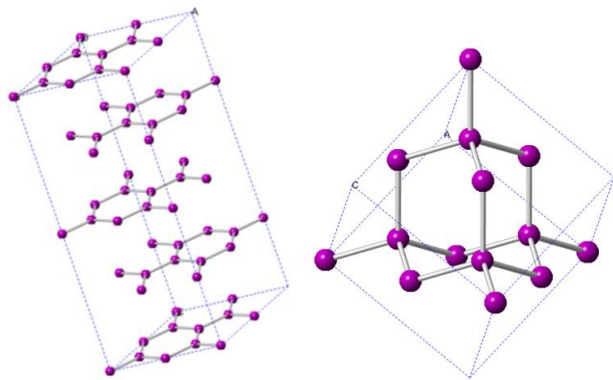


Figure 2.3: Internal structure of graphite (left) and diamond (right).

Minerals can be classified according to their physical and chemical properties, such as color and hardness. The following section presents a description of such properties.

2.1 Properties of Minerals

This section presents a description of some mineral's physical and optical properties, such as luster, color, hardness, etc. These properties can be sometimes used to identify a mineral.

2.1.1 Luster

The luster of a mineral is the way its surface reflects, absorbs, or refracts light. There are some self-explanatory terms to define the kind of luster, such as adamantine, metallic, and vitreous (ZIM, SHAFFER and PERLMAN, 1989) Figure 2.4 shows the

pyrite (left) and the kaolinite (right) as examples of metallic and non-metallic luster, respectively.



Figure 2.4: Metallic (left) and non metallic (right) luster(Source: <http://geology.csupomona.edu/alert/mineral/luster.htm>. Access in March, 2009).

2.1.2 Cleavage

Cleavage is the gentle break of a mineral, producing what looks like a flat crystal face. In some minerals, the connections between layers of atoms aligned in certain directions are weaker than others. In this case, the break occurs along smooth, flat surface parallel to the zone of weakness. It is a very important property for lapidary as it allows the creation of beautifully faceted gems (ZIM, SHAFFER and PERLMAN, 1989), (READ, 2005). Figure 2.5 presents the crystal structure (left) and the surfaces of cleavage (right) for NaCl (Sodium Chloride) and Figure 2.6 shows different examples of cleavage in some minerals.

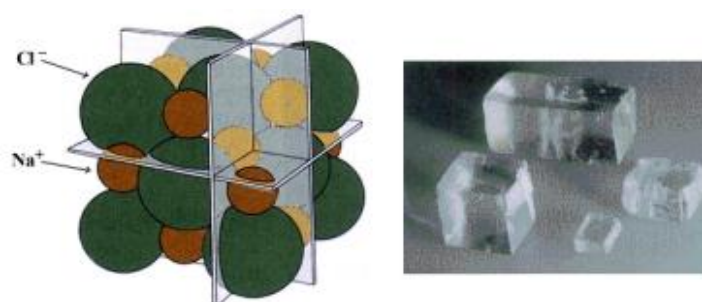


Figure 2.5: Crystalline structure and cleavage surface for NaCl (Source: <http://geology.csupomona.edu/alert/mineral/cleavage.htm>. Access in March, 2009).



Figure 2.6: Examples of cleavage (Source: <http://geology.csupomona.edu/alert/mineral/cleavage.htm>. Access in March, 2009).

2.1.3 Refractive Index, Birefringence and Dispersion

These are consistent properties in the sense that the mineral is never far away from their known values, which makes them important in the process of mineral identification (READ, 2005).

As discussed in Appendix A:, refractive index is the ratio of the geometric angle at which light falls on the crystal (called the angle of incidence) by the angle with which light is bent upon entering the crystal (called the angle of refraction). Metallic minerals do not have a refractive index because they do not allow light to enter deep in the crystal. The laws of refraction (Snell's Law) were presented in 1621 by Snellius Willebrod and have the simplified formula:

$$\eta = \frac{(\sin i)}{(\sin r)}$$

where i is the incident angle; r is the refraction angle, and η is the refractive index. η also expresses the ratio of the speed of light in air and in the crystal. This relationship shows the impact of density on the refractive index; the higher the density, the lower the speed of light inside the crystal. Chemical composition, symmetry, and the speed of light also influence this index.

Isometric minerals have essentially the same crystal structure in all directions, while amorphous minerals have no structure at all. So, isometric minerals have only one refractive index and are called isotropic minerals. Uniaxial minerals have two refractive indices: one when light falls along its primary axis (or optical axis) and one for the other directions. Biaxial minerals have two optic axes and three refractive indices (HERBERT, 1958).

The difference between the highest and lowest refractive index in a mineral is called birefringence. The birefringence is low for most minerals. But it is high for some carbonates and other minerals. The calcite (a uniaxial mineral) has one of the highest degrees of birefringence and this causes the phenomenon of double refraction. Double refraction occurs when a ray of light enters the calcite crystal and it is split into two beams, a very fast and a very slow (relative to one another). When these beams leave the crystal they are reflected in two different angles (the angles of refraction) because the angle is directly affected by the speed of the beams. A person looking into the crystal will see two images. Both beams only have the same velocity when the direction of incidence is parallel to the primary axis of the crystal (HERBERT, 1958).

Dispersion is an important property used to identify and classify gems. It is also affected by the refractive index. As already mentioned, the speed of light also influences this index. For example, blue light reflects more than the green light. That is, if the dispersion in a mineral is low then an incident white light can pass through this mineral almost unaffected and emerge as white light. But if the dispersion is high, the white light will have the wavelengths (colors) that compose it scattered through an increasing refraction. Dispersion is the reason why we have rainbows and why the prisms can separate light into many colors (READ, 2005).

2.1.4 Color

The color is the feature that draws most attention in minerals. The beautiful colors of some gems and agates, for example, have great appeal and are used in the production of

jewelry and decorative objects. Appendix B: presents a detailed description of how colors are formed. In this section, we present only a brief summary of the cause of color in minerals.

The color of a mineral is directly related to its chemical composition. Each element forming the mineral when exposed to light (visible or not) will absorb and re-emit a certain amount of energy. The energy emitted in the form of wavelengths is interpreted as color. Figure 2.7 shows an example of sulfur (S), whose characteristic color is yellow.



Figure 2.7: Sulfur (Source: <http://geology.csupomona.edu/alert/mineral/color.htm>. Access in March, 2009).

Figure 2.8 shows an example of the influence of chemical composition in color. As you can see, in spite of very similar constitution, minerals *malachite* (left) and *azurite* (right) have different colors.



Figure 2.8: Influence of the chemical composition in the color (Source: <http://geology.csupomona.edu/alert/mineral/color.htm>. Access in March, 2009).

The way the elements are arranged within the crystal also affects the color, because it implies how the light will pass through it. This causes minerals with different internal (crystalline) structures to have different colors. The presence of impurities changes the crystalline structure of the mineral, resulting in elements of the same family with different colors, as seen, for example, in Figure 2.9 which shows different colors of Fluorite (CaF_2).



Figure 2.9: Different colors of Fluorite (Source: <http://geology.csupomona.edu/alert/mineral/color.htm>. Access in March, 2009).

2.1.5 Hardness

It is a measure of abrasion resistance offered by a surface. The hardness is determined by comparing how easy or difficult it is for a mineral be scratched by another. It can be tested by scratching a mineral with the other. A scratch is actually a groove produced by micro fractures on the surface of the mineral. It requires either the breaking of the bonds or the displacement of atoms. A mineral can only be scratched by another harder than it. Thus, a relative scale can be established. This scale was proposed in 1812 by the mineralogist Friedrich Mohs (READ, 2005). Table 2.1 presents the values for Mohs and absolute hardness. Note that the Mohs scale is only relative. That is, it only indicates that a mineral is harder than other, but not how much harder.

Table 2.1: Values for Mohs and absolute hardness.

Mohs Hardness	Mineral	Absolute Hardness
1	Talc	1
2	Gypsum	3
3	Calcite	9
4	Fluorite	21
5	Apatite	48
6	Feldspar	72
7	Quartz	100
8	Topaz	200
9	Corundum	400
10	Diamond	1600

(Source: http://en.wikipedia.org/wiki/Mohs_scale_of_mineral_hardness. Access in June, 2012).

2.1.6 Emission of Light

There are different processes by which a mineral can emit light, shine. In the following sections these processes will be reviewed.

2.1.6.1 Fluorescence

Fluorescent minerals are those that emit visible light when exposed to ultraviolet light, X-rays and / or electrons beams. Some electrons in the mineral absorb the energy from these sources and move to a higher-energy level. The fluorescent light is emitted when these electrons return to lower energy level. The visible light emitted by the mineral is colored and can be different from its original color. Figure 2.10 presents an example of fluorite exposed to visible (left) and ultraviolet (right) lights. Figure 2.11 presents the effect of fluorescence in several minerals.

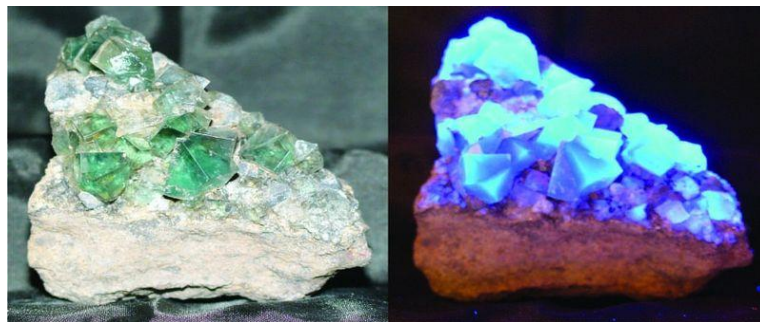


Figure 2.10: Fluorite exposed to visible (left) and ultraviolet light (right)(Source: <http://smc.cnes.fr/lexique/f.htm>. Access in June, 2012).

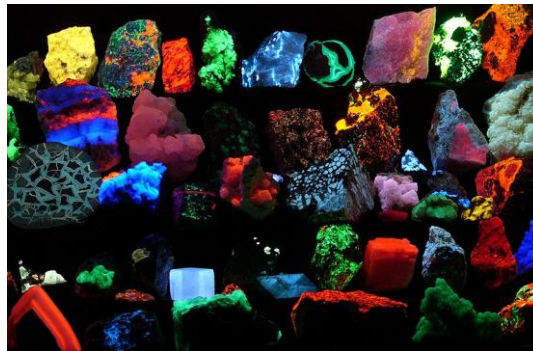


Figure 2.11: Fluorescence effect in several minerals (Source: <http://en.wikipedia.org/wiki/Fluorescence>. Access in June, 2012).

2.1.6.2 Pleochroism

Pleochroic minerals are those that present different colors depending on which direction the observer is looking at the crystal. Some minerals have a wide variation in color. Often the color change is limited to the change of tone, such as a light pink to a dark one. The pleochroism is caused by the absorption of different wavelengths passing through different directions in a crystal. Isometric minerals cannot be isometric pleochroic as they have the same structure, and hence the same absorption capacity in all directions. Figure 2.12 presents the alexandrite exposed to daylight (left) and artificial light (right).



Figure 2.12: Alexandrite exposed to sunlight (left) and artificial light (right) (Source: http://www.realgems.org/edelsteine_lexikon.html. Access in June, 2012).

2.1.6.3 Asterism

It is a star-shaped effect known in some gems such as sapphires, rubies and pink quartz. It is caused by the presence of small needle-shaped crystals. These crystals are microscopic, but there are thousands of them, and the result is the interference in the reflection of light resulting in bands that appear to be light rays (CIBJO, 2010),(READ, 2005). Figure 2.13 shows a *sapphire* (left) and a *ruby star* (right).



Figure 2.13 Sapphire (left) and ruby star (right) (Source: <http://aboutgemstones.blogspot.com.br/2008/10/star-gemstones-star-sapphire-star-ruby.html>. Access in June, 2012).

2.1.6.4 Cat's Eye

It is similar to asterism and is also caused by the inclusion of small crystals. But in this case, the bands of light are limited to a single band from top to bottom of the stone which resembles to a bright cat's eye. Figure 2.14 presents the effect of cat's eye.



Figure 2.14: Cat's eye effect (Source: <http://www.lahariaastroscience.com>. Access in March, 2009).

2.1.6.5 Phosphorescence

Many minerals which have the property of fluorescence can also phosphoresce. Phosphorescence is the ability that a mineral has of shining after the removal of a light source which was initially focused on it. The electrons in the mineral essentially keep the energy absorbed and then re-emit it gradually. Figure 2.15 presents the pulverized minerals zinc sulfide (left) and aluminate (right) lit (up) and dark (bottom).

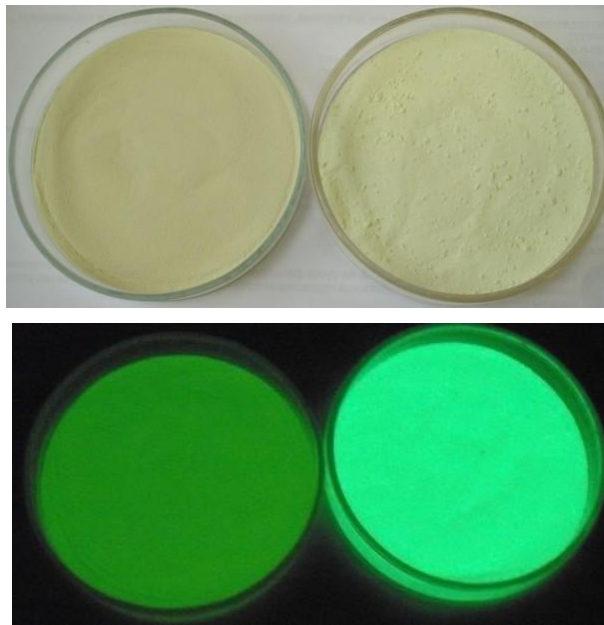


Figure 2.15: Zinc sulfide (left) and aluminate (right) lit (up) and dark (bottom)(Source: <http://www.enotes.com/topic/Phosphorescence>. Access in June, 2012).

2.1.6.6 Thermoluminescence

It is the property that some minerals (insulator or semiconductor), which had previously absorbed energy from radiation, have of shining when heated. This process happens just once: the excited electrons crystallize at higher energy levels and only by heating they can return to their lower energy levels emitting photons of light. In order to repeat the process, the mineral must be re-exposed to radiation. Figure 2.16 shows the thermoluminescence effect of fluorite before (left) and after heating (right).



Figure 2.16: Thermoluminescence in fluorite before (left) and after heating (right) (Source: <http://en.wikipedia.org/wiki/Thermoluminescence>. Access in June, 2012).

2.1.6.7 Triboluminescence

It is the property some minerals present of shining when crushed, polished, scratched or rubbed. They have chemical bonds that emit light even when mechanical energy is imposed upon them. It is a not reliable property because it is not consistent from species to species. Figure 2.17 shows an example of triboluminescence by rubbing two crystals in each other.



Figure 2.17: Triboluminescence effect(Source: <http://1hour2sunrise.livejournal.com/43997.html>. Access in June, 2012).

2.1.6.8 Aventurescence

It is the effect caused by small inclusions of a mineral with a highly reflective surface into another. These inclusions originate an effect of small bright points within the mineral when rotated or viewed from different angles. It is as if it had been mixed with glitter. Figure 2.18 shows two examples of this effect.



Figure 2.18: Aventurescence effect (Source: <http://www.bwsmigel.info/GEOL.115.ESSAYS/Gemology.Aventurescence.html>. Access in June, 2012).

2.1.6.9 Adularescence

It is a white or bluish glow effect exhibited by some gemstones when they are rotated in different directions (CIBJO, 2010). Figure 2.19 presents an example of this effect in a moonstone.



Figure 2.19: Adularescence effect (Source: <http://www.gemstones-guide.com/Feldspar.html>. Access in June, 2012).

2.1.6.10 Labradorescence

It is an effect that causes a dark metallic sheen, usually blue or green. The most representative mineral to present this property is labradorite. The orientation of the stone influence the effect obtained. Figure 2.20 presents a bluish labradorite.



Figure 2.20: Labradorescence effect (Source: <http://www.jewelinfo4u.com/Labradorescence.aspx>. Access in June, 2012).

2.1.7 Streak

The color of a mineral when it is pulverized is called the streak of this mineral. It can be determined by rubbing the mineral on a hard porcelain surface. The streak and color are the same for some minerals. For others, it may be quite different (ZIM, SHAFFER and PERLMAN, 1989), as for example, the dark red streak of hematite, a usually silvery mineral. Figure 2.21 shows examples of streaks in cinnabar and pyrite.



Figure 2.21: Examples of streaks (Source: <http://geology.csupomona.edu/alert/mineral/luster.htm>. Access in March, 2009).

3 AGATES

Agates are known for their amazing colors and different formation patterns, being widely used for jewelry and craft making. Despite their beauty and popularity, they are mainly composed by silica (a small molecule formed by only few atoms of silicon (Si) and oxygen (O)) with some sort of impurities. Thus, the combination of working with a small-sized molecule and the possibility of obtaining simulations of a beautiful and popular mineral became a good reason for us to focus this work on agates.

This chapter starts with an introduction to silicates, quartz, and chalcedony. These concepts are important for a better understanding of the final sections about agates, which are a sub-variety of chalcedony. There are many books related exclusively to silicates. Therefore, we just present a brief summary of the topics. For further reading, we recommend, for example (DAKE, FLEENER and WILSON, 1938), which is an interesting book and most of the concepts it presents still remain up-to-date. The book by Deer et al. (DEER, HOWIE, *et al.*, 2004) is a recent and good source of information about silicates.

3.1 Silicates

The internal structure *silica* (SiO_2) is formed only by SiO_4 tetrahedron, where each atom of oxygen is shared by two of them. Figure 3.1 presents this tetrahedron.

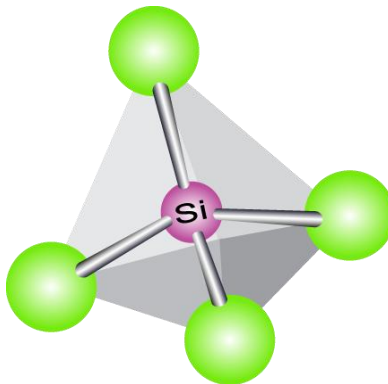


Figure 3.1: Silica tetrahedron.

This structure is affected by temperature rising, thus presenting three principal crystalline forms with low (α) and high (beta) temperature forms (DOUGLAS and HO, 2006). Figure 3.2 presents the temperature for transitions between α and beta (top), and at which structural changes happen (bottom) (DOUGLAS and HO, 2006):

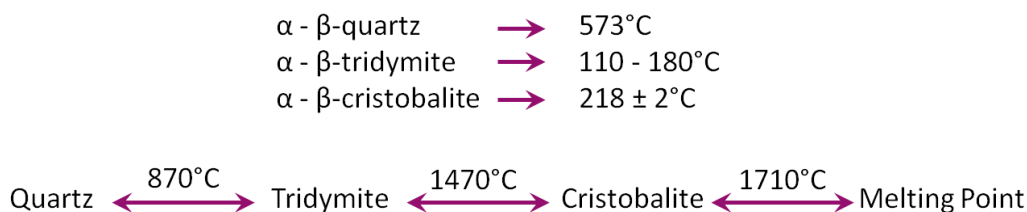


Figure 3.2: Transition temperatures for silica (DOUGLAS and HO, 2006).

Quartz is the most relevant structure to this work, as it is the most common. It will be presented in the following section. A detailed explanation about *tridymite* and *cristobalite* can be found in (O'DONOGHUE, 2006) and (DOUGLAS and HO, 2006). One interesting thing to note is that after melting, silica solidifies as glass, an amorphous material (DOUGLAS and HO, 2006).

3.2 Quartz

Quartz is a member of the silicates and it is the most common mineral on Earth (MACKENZIE and GUILFORD, 1994). It can be found in its fully crystalline form (amethyst, pink quartz, etc.) or *crypto-crystalline* (*chalcedony*). Generally the name quartz is associated only with its crystalline varieties (SYMES and HARDING, 2007). Its internal structure is affected by temperature rising. Thus, it is only present as stable crystalline silica (SiO_2) in temperatures up to 570°C. Quartz's hardness is around 7 (it scratches glass and steel). Its indexes of reflection are 1.544 and 1.553 and, therefore, its birefringence is 0.009. Quartz does not fluoresce and its streak is white (O'DONOGHUE, 2006), (CULL, 2009).

Crystalline quartz is abundant all over the world. Its main characteristics are its nice appearance (sometimes even before lapidating) and distinct color. They can be colorless or present some different colors due to impurities. There are for example the *white quartz*, whose color is the result of the presence of minute cavities filled with water or liquid carbon dioxide; *smoky quartz*, whose color is due to aluminum impurity; *citrine*, a yellowish quartz due to the presence of traces of ferric iron (Fe^{+3}); *amethyst*, the violet variety of quartz due to the presence of iron ions, either (Fe^{+2}) or (Fe^{+3}), in a color center. There are also other varieties of quartz presenting other colors due to mechanisms such as charge transfer, inclusions, color centers and impurities. For instance, *rose quartz*, *blue quartz*, and *green quartz* (O'DONOGHUE, 2006).

The group of crypto-crystalline quartz is formed by *chalcedony* and its varieties. Due to its importance to our work, we are going to present it separately in the following sections.

3.3 Chalcedony

Chalcedony is the name generally given to any quartz that presents a microcrystalline structure (O'DONOGHUE, 2006), (DAKE, FLEENER and WILSON, 1938). It frequently presents a grayish waxy surface (O'DONOGHUE, 2006). Sometimes a small birefringence and other optical properties are seen. It can be found in different colors, mainly white, grayish or pale brown with different intermediate shades (DAKE, FLEENER and WILSON, 1938). Its brown and reddish colors are often due to

presence of Fe_2O_3 ; A variety called *chrysoprase* presents a translucent bright apple-green color which is believed to be due to Ni^{+2} ; The *mtrolite* variety presents a green color due to chromium; And the bluish shade in some varieties is due to the Tyndall scattering (O'DONOGHUE, 2006).

Chalcedony presents different varieties such as *jasper*, *chrysoprase* and *plasma* (PRICE and WALSH, 2005). According to (BECKWITH, 1972), (PRICE and WALSH, 2005) and (MOXON and REED, 2006), agates are not a variety of chalcedony, but indeed a form of it which often presents a colored concentric banding pattern. As agates are an important concept to this work, a deeper description is presented in the following section.

3.4 Agates

Agates are beautifully colored semi-precious gemstones. One of the forms of chalcedony, they are composed by a microcrystalline structure organized as concentric bands or other formats in which successive layers present different colors and translucency (O'DONOGHUE, 2006), (GRANDE, AUGUSTYN and WEINSTEIN, 2009). The organization of the microcrystals depends on factors from the environment during the process of formation of the agate, such as the presence of different minerals, pressure, and temperature. The wide range of possible combinations of environmental factors results in somewhat random patterns and therefore in no agate being equal to another.

3.4.1 The Formation of Agates

There are several theories about how do agates form. But, basically all of them state that agates form by the systemic deposition of silica in cavity walls generally resulting in banded patterns (O'DONOGHUE, 2006). A very simple (and somewhat naïve) description of this process is that high temperature, pressure or ionized surface and magmatic waters are capable of dissolving the silica from the rocks where they pass through (DAKE, FLEENER and WILSON, 1938). When these water flow or evaporate, there is the formation of silica deposition.

3.4.2 Agate Properties

Table 3.1 presents a summary of some agate properties, adapted from (IBGM, 2005).

In order to enhance its commercial value, many agates are dyed before selling. There are different dyeing processes. O'Donoghue (O'DONOGHUE, 2006) presents some examples:

Immersion in a hot sugar solution followed by immersion in concentrated sulphuric acid and heating gives black; a blue color, once called Swiss lapis, is produced by immersion in potassium ferrocyanide and subsequent warming in a solution of ferrous sulphate to give a precipitate of Berlin blue. Chromium alum or potassium dichromate may be used to give green or bluish green, and nickel compounds give a brighter, apple green. Impregnation with iron compounds and heating may give reddish Brown and red colors. Yellow to greenish yellow is obtained by heating dry agate that has been treated with concentrated hydrochloric acid.

The difference in porosity in agate layers is related to the organization of the microcrystalline structure. This variation will then interfere in the dyeing process,

resulting in a non uniform and sometimes messy colorization (DAKE, FLEENER and WILSON, 1938).

Table 3.1: Agate properties(IBGM, 2005).

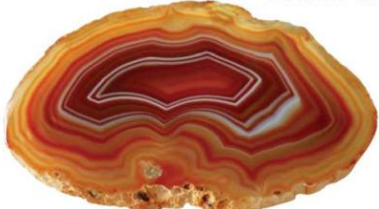



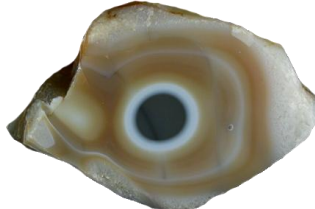
Mineral Class	Silicates
Mineral Specie	Crypto-crystalline quartz
Crystal System	Hexagonal (Trigonal)
Chemical Compound	SiO ₂
Variety	Chalcedony
Names	Many, i.e. moss, iridescent and fire agate
Color	Several, usually bluish gray, white, brown and red; Presents a banded structure with layers of different colors, thickness and porosity; Most agates in the market are artificially colored
Transparency	From semi-transparent to opaque
Luster	From waxy to glassy
Optical Phenomena	It can present iridescence
Refraction Indexes	1,535 – 1,539
Birefringence	It can present a small birefringence of 0,004. But it is normally not detectable
Dispersion	It does not present
Pleochroism	It does not present
Fluorescence	Generally inert; Some species can fluoresce from weak to strong yellowish green
Cleavage	It does not present
Hardness	6,5 – 7
Stability to Heat	It can change color
Stability to Sun Light	Stable
Stability to Chemical Reactions	It can be attacked by hydrofluoric and nitric acids



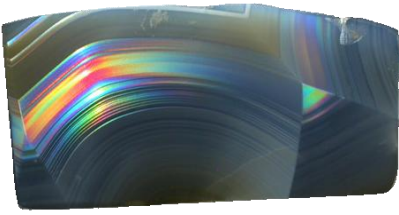
3.4.3 Types of Agates

There are many types of agates (GRANDE, AUGUSTYN and WEINSTEIN, 2009) , (SCHUMANN, 2009). And it seems that there is no consensus or a closed list of the types/names of agates in literature. But what can be perceived is that, in general, they are named according to their formation type, band/color pattern, and location where

they formed. For example, *banded agate*, *onyx*, or *Brazilian agate*. Table 3.2 presents some examples of different types found in the literature. It also includes a brief description and illustrations of each one of them.

Table 3.2: Types of Agate.

Type	Description	Image
Banded agate	It is a general term applied to chalcedony which presents parallel concentric curved bands (BECKWITH, 1972, p. 31), (POLK, 2010, p. 52).	 <p>(POLK, 2010, p. 53)</p>
Fortification Agate	The bands form concentric parallel layers that resemble the shape of an aerial view of the old-time fortifications (DAKE, FLEENER and WILSON, 1938). This shape is determined by the cavity where the agate was formed. The difference between fortification and banded agate is that the former presents more complex and irregular band patterns (POLK, 2010, p. 62).	 <p>(POLK, 2010, p. 62)</p>
Shadow Agate	It presents a shadow effect which resembles a movement across the layers depending on the position of the observer in relation to the agate. This effect happens when there is an alternation between translucent and opaque bands which causes the eye to perceive depth in the agate (WOLTER, 1996, p. 82).	 <p>(GUMEE, 2011)</p>
Tubular Agate	Presents numerous tubes with usually concentric opening (SCHUMANN, 2009).	 <p>(SCHUMANN, 2009)</p>
Eye Agate	It presents concentric rings of contrasting colors, giving it the appearance of an eye. They are cut, polished and colored in order to increase the similarity with an eye (DAKE, FLEENER and WILSON, 1938).	 <p>(FRIEDMAN, 2011)</p>

Plume Agate	It is a vein or nodular type of agate which presents clear colors and three-dimensional plume-like inclusions (POLK, 2010, p. 71).	 (POLK, 2010, p. 71)
Moss Agate	It is a vein or nodular type of agate which presents pale or clear colors and small inclusion of different oxides with moss like appearance. These inclusions can present different colors such as black, red or green (POLK, 2010, p. 67), (O'DONOGHUE, 2006).	 (POLK, 2010, p. 68)
Iris Agate	A highly translucent agate which presents very small bands. When a thin slab of this agate is exposed to light, a rainbow effect can be seen due to dispersion of light by the tiny bands (THOMAS, 2008, p. 36).	 (FRIEDMAN, 2011)

3.5 Additional Information about Agates

Agates present a chemical composition of around 97% of silica and less than 1% of non-volatile impurities (FLÖRKE apud (MOXON and REED, 2006)). The concentration of impurity from H₂O and Si-OH is up to 2% (GRAETSCH apud (MOXON and REED, 2006)). The silica in agates is composed by two of its polymorphs: α -quartz and up to 20% of *moganite*¹.

Götze et al. (1999) present the results of a series of studies, including the confirmation that “the agate structure can probably be interpreted as alternating formation of fine-grained, highly defective chalcedony intergrown with moganite, and coarse-grained low-defect quartz”.

Several works, such as (WANG and MERINO, 1990) and (ORTOLEVA, CHEN and CHEN., 1994) tried to model the agate growth. Heaney and Davis (1995) suggested that fractal geometry could be used to describe the banding pattern in agates. Inspired by such works, Holten et al. (1998) demonstrated that indeed the color bands present a fractal zoning pattern.

¹ A silica polymorph first described by (FLÖRKE, KÖHLER-HERBETZ, *et al.*, 1982), (DEER, HOWIE, *et al.*, 2004).

4 RELATED WORK

To the best of our knowledge, there has been no work in computer graphics focused on rendering agates. There have been, however, several works on rendering optical effects, molecules and, mostly, materials in general, such as marble and wood. This chapter discusses the works more closely related to the rendering of minerals and to the work described here².

4.1 Rendering Minerals and Optical Effects

SUN, FRACCHIA and DREW (2000a) proposed a technique for the rendering of diamonds. The approach uses a combination of Fresnel effect, volumetric absorption, and light dispersion. The authors used an extended version of the traditional Ray Tracing algorithm (WHITTED, 1979) that includes these mechanisms. Their technique is limited to gemstones with specific optical characteristics and cuts. Figure 4.1 presents a comparison of an image of a real yellow diamond (left) and a synthesized one (right).



Figure 4.1: Real yellow diamond (left) and synthesized image (right)(SUN, FRACCHIA and DREW, 2000a).

Weidlich and Wilkie (2008a) presented a technique to model the property of aventurescence³ which can be found in some minerals. The authors simulated the appearance of the material by using multi-layered surfaces procedurally textured. In

² All images presented in this chapter were extracted from the original related work.

³ Effect that resembles small shining points in the interior of the mineral. It is visible when the mineral is rotated or seen from different angles. It is as if the mineral had been mixed with glitter.

order to generate these textures, they used Voronoi diagrams and colored some of their cells with metallic and the others with non-metallic colors. Later, the layers were rearranged generating the desired effect. Figure 4.2 shows a real aventurine (left) and a synthetic image rendered in a similar environment.

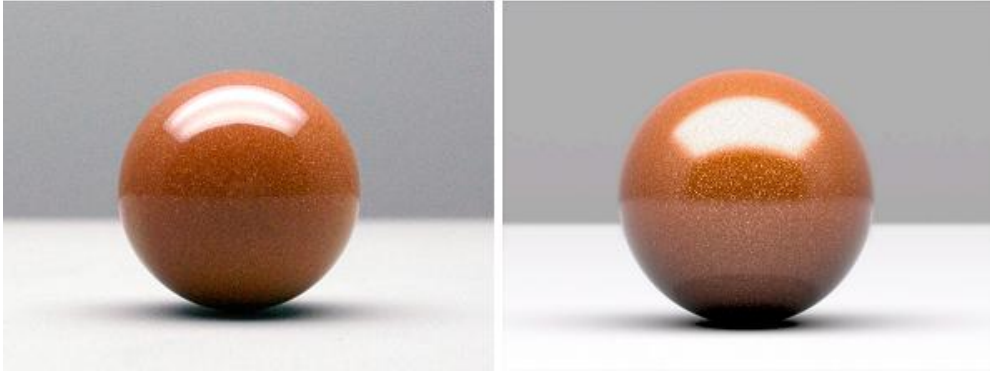


Figure 4.2: Real aventurine (left) and synthesized image (right)(WEIDLICH and WILKIE, 2008a).

Weidlich and Wilkie (2009) also introduced a technique to model the property of *labradorescence*⁴, which is highly dependent on the orientation in which the object is observed. It consists in a reflection model based on the physical characteristics of *labradorite*. The authors use texture maps that are applied on the objects' surfaces to perform reflection calculations. These maps are obtained by using the Perlin noise function (PERLIN, 1985) to simulate color zones. Figure 4.3 presents a comparison of a real labradorite (left) and a synthetic image rendered using Perlin's noise (right).

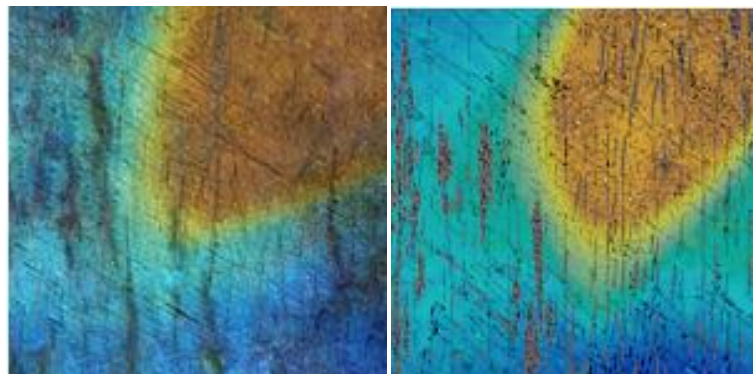


Figure 4.3: Real labradorite (left) and synthesized image (right)(WEIDLICH and WILKIE, 2009).

Carter (2007) proposed a method for modeling subsurface scattering in materials with highly scattering property, such as marble. The marble texture was generated using Perlin noise functions (PERLIN, 1985). To lighten the marble, the authors use a two-

⁴ Effect that causes a dark metallic luster, generally blue or green. It is mainly presented by the mineral labradorite. See Section 2.1.6.10.

step technique which first processes the diffusion of light on the surface and then uses a modified version of ray tracing algorithm to account for this diffusion. Figure 4.4 presents a lightened marble texture.



Figure 4.4: A lightened marble texture(CARTER, 2007).

Guy and Soler (2004) proposed a technique for the synthesis of images of lapidated gems which approximates some optical phenomena such as reflection and refraction. Such an approach considers only homogeneous materials and is not capable of simulating the appearance of a determined mineral based on its crystal structure. Besides, the algorithm assumes the existence of faceted forms resulting from the process of lapidating and it is not applicable to arbitrary shapes. Figure 4.5 presents a comparison of a real tourmaline and a synthetic image generated in a similar environment.

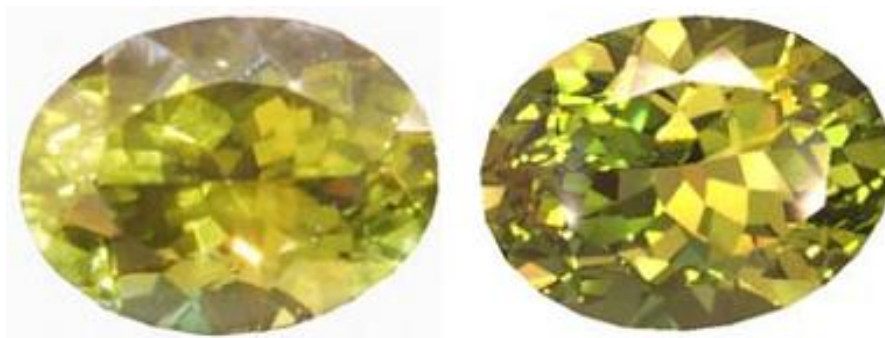


Figure 4.5: Real tourmaline (left) and synthesized image (right)(GUY and SOLER, 2004).

SUN, FRACCHIA and DREW (1999) proposed a technique for rendering light dispersion. The authors developed a dispersive ray tracer that is similar to a regular one. The difference is that the former works with several rays, each with their own path and wavelength. The contributions from all rays are then summed to determine the final shade. This technique is effective for emulating the light dispersion in materials that are translucent, such as crystal quartz. And, it can be combined with other methods to synthesize more realistic gemstones images. Figure 4.6 presents the effects of volume absorption, which causes a variation of color intensity and saturation in both images.

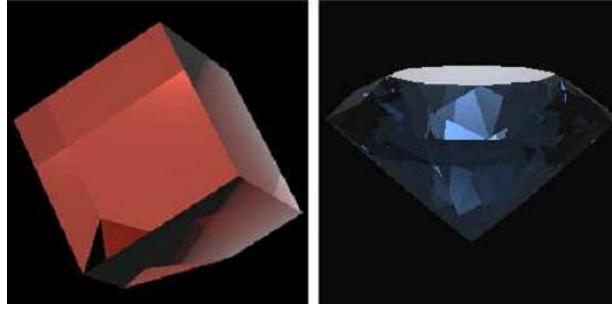


Figure 4.6: Effects of volume absorption in glass material shaped as cube (left) and as a diamond cut (right)(SUN, FRACCHIA and DREW, 1999).

SUN, FRACCHIA and DREW (2000b) presented a model of volume absorption for homogeneous transparent materials. The authors developed an extended version of a regular ray tracer. Their version requires the spectral absorptivities for all transparent objects and applies an attenuation factor for light shading based on Bouguer-Lambertian law, which relates the absorption of light with the properties of the material it is passing through. As in (SUN, FRACCHIA and DREW, 1999), this is an effective method for what it is proposed. Interesting images could be obtained if combined with other approaches. As for example the one presented in Figure 4.7, where the effect of light dispersion is applied to a scene formed by crystal polyhedrons on a mirrored surface surrounded by several light sources.



Figure 4.7: Light dispersion in a scene formed by crystal polyhedrons on a mirrored surface surrounded by several light sources(SUN, FRACCHIA and DREW, 2000b).

WILKIE, TOBLER and PURGATHOFER (2000) presented an extended version of the ray tracing algorithm that efficiently renders dispersion effects. The authors use a spectral rendering system in order to achieve colorimetric accuracy and to be able to treat optical and natural phenomena, such as dispersion. The proposed method first divides the spectra into n non-overlapping spectral bands. Next, it stochastically determines the contribution of each band. This process consists of getting the average value of the band's wavelength and randomly jitter it with a value inferior to half of the width of the band. The results were similar to those of (SUN, FRACCHIA and DREW, 2000b). Figure 4.8 presents a crystal paperweight rendered without (left) and with (right) light dispersion effect.

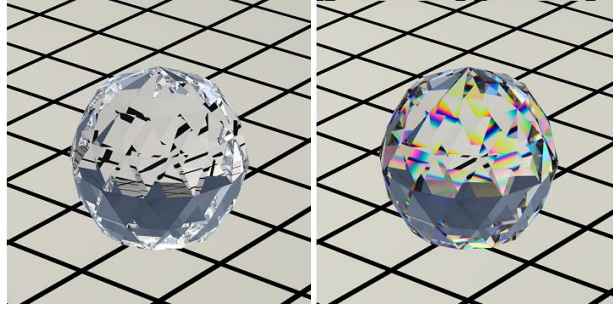


Figure 4.8: A crystal rendered without (left) and with dispersion effect (right)(WILKIE, TOBLER and PURGATHOFER, 2000).

5 QUANTUM PHYSICS APPROACH FOR SIMULATION OF COLOR

Currently, there is not yet a generic formalism that completely describes all the causes of colors observed in nature, or even among minerals. However, it is known that the colors we see are the result of how light interacts with matter and with the photoreceptors in our eyes. At its most basic level, the interaction of light with matter depends on the molecular structure of the material. This chapter describes a framework for simulating the colors of minerals based on such a fundamental principle, aiming to achieve a methodology as generic as possible. From a wide view, the technique developed in the context of this thesis consists of the following steps:

1. Acquiring information about the molecular geometry of the mineral we want to simulate;
2. Using the geometry information to generate spectral absorption curves;
3. Generating textures representing the agate's surface based on the absorption curves calculated in step (2);
4. Rendering of the colored volume representing an agate.

Each of these steps consists of several sub-steps, which are going to be described in the next sections. Note that in step (2), it is still not practical (due to computational limitations) to work with molecules with more than just a few hundred atoms. Removing such a restriction would be desirable for representing bigger structures or even entire objects with visible imperfections at naked eye, or with small variations in the way the atoms are organized. The number of atoms also directly influences the concentration of impurities, with just a few replacements leading to impurity concentrations of 25-50%. In nature, one only finds traces or maximum impurity concentrations of 1-5%. Thus, in this case, it is not only desirable, but it is necessary to be able to use a large number of atoms in the simulations. Thus, we begin the simulations using a small number of atoms, and increase this quantity until it is computationally feasible. Using such an approach, we would like to find a relationship between the number of proper and impurity atoms and the corresponding spectral curves. Such a relationship would allow us to extrapolate the obtained results for structures with larger numbers of atoms.

5.1 Acquiring geometric information

Our technique takes as input a Crystallographic Information File (CIF) file, which is the standard format for the exchange of crystallographic data (HALL, ALLEN and BROWN, 1991). This file contains the description of the *unit cell* of the mineral. The

unit cell is defined as the smallest structure of atoms for any crystalline material that describes the symmetry and properties of this material. Based on the unit cell, it is possible to build mineral structures of any sizes just by replicating the unit cell along the mineral's crystal axes (DYAR, GUNTER and TASA, 2007). In this thesis, we need information about the silica unit cell (SiO_2). It is known that molecules under different temperatures and pressure have different molecular structure (*i.e.*, the way the atoms are organized varies). Thus, we have to choose the CIF representation that describes the molecule in the desired condition. It is interesting to note that although there are several different CIF files for the same kind of mineral (*i.e.*, different quartzes stones from all over the world analyzed in different experiments), when we plot their unit cell, the geometry obtained is the same for all of them.

The information contained in a CIF file is obtained from practical measurements. Therefore, they are available only for existent minerals. Thus, to simulate non-existent ones, we start from an existent mineral whose chemical composition is similar to the one we want to simulate (*e.g.*, SiO_2 , at 1 atm and 25°C). We then replicate the unit cell to the size we want and replace the atoms of the original molecule with those of the impurities we want to test. As we want to compare results obtained simulating the original molecule and the modified structure, we keep the original geometry and do not consider the distortion to this geometry that the impurity atom we included may have caused. Note that not considering this distortion may result in a divergence from the value that would be obtained otherwise. An approach to solve this issue would be to perform some simulation with and without considering the distortion in order to determine an approximate divergence factor.

After we manipulate the original molecule to turn it into the one we want, the only information we are interested in are the spatial coordinates (geometry) and the new molecule's composition. An example of a CIF file describing a quartz molecule is presented in Annex A. Figure 5.1 shows the geometries obtained according to this file. From left to right, a silica unit cell (left), a supercell, *i.e.*, the unit cell replicated in the x, y and z axes, and the same supercell seen from a different point of view (right). The images in Figure 5.1 were obtained by loading the CIF file in the CrystalMaker® software (CRYSTALMAKER SOFTWARE LTD, 2011). It would also be possible to simulate a complete random molecule instead of using CIF files or to consider the distortion caused by the addition of impurities. But, in both cases, it would be necessary to consider molecular dynamics in order to know, for example, the bonds, the distance between atoms, if the configuration is plausible or not, etc.

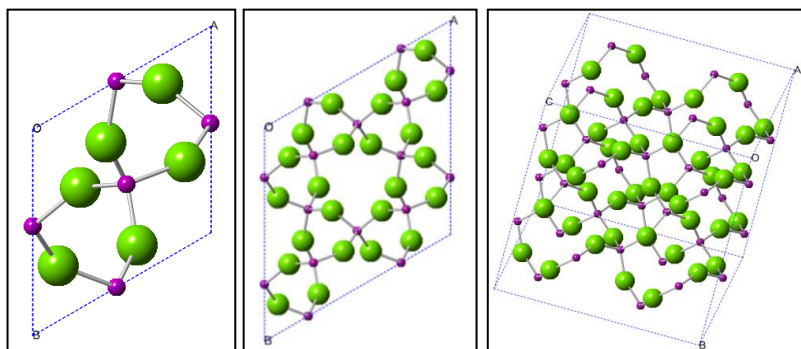


Figure 5.1: Silica unit cell (left), supercell (middle), and the same supercell from a different angle (right).

5.2 Generating absorption curves

The next two paragraphs present a very brief description of key concepts required to understand the work done in this thesis. A slightly more detailed presentation of these subjects is presented in Appendix A:. For a deeper and more technical discussion of these concepts, we refer the readers to (LEVIN, 2002), (GILLESPIE and POPELIER, 2001), (GREINER, 2001), and (OLMSTED and WILLIAMS, 1996).

The Heisenberg Uncertainty Principle states that it is not possible to determine both the position and momentum (*i.e.*, speed and direction) of a small particle like an electron. This implies that we cannot accurately describe the movement of electrons. Thus, it is only possible to determine in which region in space there is the greatest probability of finding a specific electron. This region is called *orbital*. The solution of the Schrödinger wave equation describes the position and energy of an electron in an atom, *i.e.*, describes an atomic orbital.

Each orbital corresponds to an *energy level*. For an electron to make a transition from one level to another, it needs to emit/absorb energy. The *Pauli Exclusion Principle* states that an orbital can have at most two electrons and they must be spinning in opposing directions. An electron that is spinning in one way and does not have another electron spinning in the opposite direction is said to be *unpaired*. An atom is in its *fundamental state* when it has the largest possible number of unpaired electrons. This corresponds to its state of least energy. The electrons in the outermost shell (the valence shell) are called the *valence electrons*, and the chemical bonds occur between these electrons (GILLESPIE and POPELIER, 2001).

Given the unit cell (or its multiple copies) of the original molecule, the problem now is how to simulate the interaction of light with the available geometry. As we are dealing with the elements in their molecular size and form, a molecular approach is required, and the use of quantum theory is needed.

What we are willing to obtain from the light-matter interaction simulation is the color a mineral would have when being exposed to a light with a given spectral distribution. In (NASSAU, 1978), Nassau describes four formalisms that are responsible for the color in minerals, which are discussed in Appendix B: as well as other causes of color:

- 1) **Crystal Field Theory:** Based on the fact that electrons in a determined energy level need to absorb/emit energy to change to another level. This explains the color in ionic crystals, which contain unpaired electrons. Only unpaired electrons can interact with visible light emitting/absorbing energy, thus resulting in color. Generally speaking, elements such as V, Cr, Mn and Fe (*i.e.* Vanadium, Chrome, Manganese and Iron) present unpaired electrons;
- 2) **Molecular Orbital Theory (MOT):** Based on the premise that the energetic levels used to describe a molecule are not related to only one atom, but to all atoms that form the molecule. This explains, for example, the color in blue sapphire and organic materials, such as amber, pearl, etc.;
- 3) **Band Theory:** Considers that the free electrons in the mineral do not belong to one atom or molecule, but to the mineral as a whole. The color in conductors and semi-conductors is explained by this theory;

- 4) **Physical Optics:** This formalism is not directly related to the electrons in the molecule and it is well known and explained by physical optics principles, such as dispersion, scattering, interference, and diffraction.

According to van Vleck (1978), the Molecular Orbital is a more generic approach than the Crystal Field Theory. And, according to Gil (2000), MOT can also be used to explain Band Theory. Therefore, considering these four formalisms, we can divide them in two groups: one explained by Molecular Orbital Theory, and another explained by Physical Optics. As the physical optics approach is well explored and has limited scope for the problem at hand, we decided to work with Molecular Orbitals.

5.2.1 Molecular Orbital Theory

Molecular Orbital Theory (MOT) is a method for the determination of the transitions in energy levels. It considers that the valence electrons do not belong to only one atom, but to the molecule as a whole (SOLE, BAUSÁ and JAQUE, 2005). For example, consider the ideal situation shown in Figure 5.2 of a molecule composed of an atom A surrounded by six atoms B, within a fixed distance.

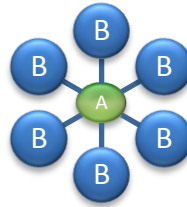


Figure 5.2: Atom A surrounded by six atoms B within a fixed distance.

The energy levels of A are modified by the influence of the electric field produced by ligand B ions. To determine the energy levels E_i of the molecule AB_6 , we must solve the Schrödinger molecular equation:

$$H\psi_i = E_i\psi_i,$$

where H is a Hamiltonian that defines the interactions between the valence electrons in the molecule, and ψ_i are the wave functions of the orbitals (SOLE, BAUSÁ and JAQUE, 2005).

When using MOT, we must consider that atoms A and B share their valence electrons. Thus, an approximate solution for the equation above is obtained by a linear combination of the atomic orbitals $\psi(A)$ and $\psi(B)$ generating the molecular orbitals $\psi(MO)$ (MIESSLER, 2003). The molecular orbitals $\psi(MO)$ can be written as:

$$\psi_{MO} = N(\psi_A + \lambda\psi_B)$$

where N is a normalized constant and λ is an adjustment coefficient (SOLE, BAUSÁ and JAQUE, 2005). These transitions in energy levels can also occur when we focus

light over the molecule. This set of transitions will originate the absorption/emission spectra.

Molecular Orbital Theory is a very complex subject and it is way beyond the scope of this thesis to provide a more advanced or detailed explanation of it. We just wanted to present some basic fundamentals in order to show the principles in which our technique is based on. We tried to use a more conceptual than mathematical/chemical approach in this description, as these topics are largely covered in the literature. We refer the interested reader to (SOLÉ, BAUSÁ and JAQUE, 2005), (SMART and MOORE, 2005) and (MIESSLER, 2003).

5.3 Calculating the Transition Energy

Our intention in using the theory described in the previous section was to determine transitions energy, as these energies are the responsible for the absorption/emission properties. And, therefore, they can be used to predict color. Implementing such calculations can be very cumbersome and susceptible to errors. Therefore, we decided to adopt existing software to perform these computations. For this purpose, we use free software called Orca (NEESE, 2008), a tool that implements a wide variety of standard methods for quantum chemistry calculi (NEESE and WENNMOHS, 2010).

The use of this software (or any other one that implements similar methods) requires a lot of previous knowledge about quantum chemistry and the problem you want to solve. This is necessary because Orca's main features are also its biggest problem for beginners: it offers you a lot of methods and you need to know them to decide what to use to solve your problem. Therefore, it was necessary to spend several weeks studying the methods and parameters before we could decide for a final set of methods that would solve our problem. At first, we studied all the methods implemented in Orca (around 60) to determine to what kind of molecule they could be applied to. The methods that did not apply for the type of molecules we intended to work with were discarded. After defining the algorithms, it was necessary to choose which parameters would be used with each method. These parameters will define, for example, if the calculus will consider polarization or not. After discovering which methods would be tested and which parameters must be provided, it is necessary to write an input file according to the specified syntax in order to call these methods. After that, it is possible to run the software and begin the calculation. A detailed explanation of how to use Orca and the methods and analyses it supports can be found in its manual (NEESE and WENNMOHS, 2010).

In total, only for the silica molecule, we performed around 50 tests just to determine the best set of method/parameter. In these tests, we considered the quality of the obtained results and the time required achieving them.

Our main problem was to determine the transition energies. So, comparing existing methods and analyzing what would best fit our problem, we decided to use as our main method the Time-Dependent Density Functional Theory (TDDFT), which can be used, for example, to determine the electronic excited states and to predict the absorption spectra (BURKE, WERSCHNIK and GROSS, 2005). In the next section, we present a brief overview of the methods and parameters that were used as well as a description of an example input file. Note that the approach we used here will not necessarily solve

any transition energies problem. The characteristics of the molecules that you are working with must be taken into account when deciding the methods and parameters.

5.3.1 Input file for Orca

This section presents the description of an input file we used for generating the spectra of molecular silica. Figure 5.3 represents such a file. The explanations on the remainder of this section are going to be based on this figure. Not necessarily all simulations will follow this same pattern. This is just a simple example in order to illustrate a possible structure of an input file. The Orca manual provides many other parameters that can be set, and input instructions that can be used.

```

1 ! RKS RI-B2PLYP RIJONX Def2-aug-TZVPP Aug-TZVPP/C DIIS ZORA/RI TightSCF NoMOPrint PRINTGAP
2
3 $pal nprocs 6
4   end
5
6 $tddft NRoots 80
7       MaxDim 240
8   end
9
10 $base "SiO2-Mol"
11
12 * xyz 0 1
13
14 O      -4.76115    -2.75315    -2.49342
15 O      -2.95987    -3.23898    -0.62325
16 Si     -3.60275    -3.75773    -1.99993
17
18 *
```

Figure 5.3: Orca input file for molecular silica

Here is a brief description to help the reader interpret the file:

Line 1: Set of methods and parameters. The word “TightSCF” indicates the convergence threshold; “NoMOPrint” indicates that the Molecular Orbitals are not going to be printed in the output file; And “PRINTGAP” prints the difference between the highest occupied and the lowest unoccupied Molecular Orbital, which is useful for detecting convergence problems. The remainder terms are going to be detailed in Section 5.3.2.

Lines 3-4: Indicates the number of processors being used for the calculation.

Line 6-8: The word “tddft” indicates the method used for calculating the excited states (detailed in Section 5.3.2). “NRoots” is the number of excited states we want to calculate. This number was chosen experimentally. We tested several numbers and opted for the smallest one that would result in energy being absorbed / emitted in the visible light region. We chose the smallest one because the more excited states calculated, the longer the software execution takes. “MaxDim” is a multiple of NRoots. It is used internally by Orca as a control parameter for the size of the expansion vectors in the iterative algorithm.

Line 10: The expression (SiO₂-Mol) after the word “base” indicates the name for the output files.

Lines 12-18: They contain the description of the geometry of the molecule. The word “xyz” indicates the type of coordinates. The second parameter is the total charge of the molecule and the third is the multiplicity⁵ of the molecule. Lines 14-16 present the atom and its xyz coordinates.

Bellow, we present the descriptions of the methods.

5.3.2 Methods and parameters we used with Orca

The literature has many books related to one or more of the topics we address here. As new discoveries are being made every day, new books and papers are released. However, it is still difficult to find one book that presents in a succinct form all the required concepts for the understanding of this work. Therefore, in this section we are going to briefly present the basic idea of the methods we used in most of our simulations. This is not an exhaustive list, and others could have been used. For those covered here, we opted to organize them in an easier to understand order rather than in the exact order they are used by the software. For further reading and mathematical derivations, we suggest (MENNUCCI, 2010), (LIPKOWITZ, CUNDARI and BOYD, 2008), (SZABÓ and OSTLUND, 1996) and (JENSEN, 2007).

Landau and Lifshitz (1977) said:

Schrödinger’s equation for atoms containing more than one electron cannot be solved in an analytical form. Approximate methods of calculating the energies and wave functions of the stationary states of the atoms are therefore important.

This statement remains true, and there are still only approximate (although some are highly accurate) methods for evaluating Schrödinger’s equation.

The Hartree-Fock (also called Self-Consistent Field - SCF) formalism is an approximation for the description of an orbital. That is, it is basically a method which solves a one-electron Schrödinger-like equation and operates over the results until convergence is reached. It is used for determining the wave function and the energy of the ground-state of an n -electron interacting system. Many *ab initio* methods⁶ use this formalism as a starting point for more accurate approximations (SZABÓ and OSTLUND, 1996).

Another approach is the *Density Functional Theory* (DFT). According to Schrödinger’s equation the wave function ψ for an n -electron molecule is a computational demanding function depending on $3n$ spatial coordinates and n spin coordinates. On the other hand, the electron density of a system can be described by only three spatial coordinates. Therefore, a theory based on the electron density would be simpler and faster. This resulted in the development of the DFT (DYALL, 1995).

⁵ Multiplicity is the sum of the spins of all electrons in a molecule (GLICK, 2009).

⁶ According to (IUPAC, 1997-2011), *ab initio* quantum mechanics methods are those in which the calculations are “independent of any experiment other than the determination of fundamental constants [..]. In practice, approximations are necessary to restrict the complexity of the electronic wavefunction and to make its calculation possible.”

DFT is a method that can be used to calculate the energy of a molecule. One of the main advantages it presents when compared to other related methods is that the DFT computation can be done for large molecules, with more than 100 heavy atoms (MUELLER, 2001). DFT computation usually starts with an initial guess for the density, which is a Hamiltonian for an ideal many-electron system with an exact known wave function. With this initial guess, it calculates another density and the process repeats until it converges to a specified threshold (LOWE and PETERSON, 2006).

The energy of the system is given by the sum of the following energies: (i) the energy of a single electron; (ii) the energy of the repulsion between the nuclei; (iii) the energy of the repulsion between electrons; and (iv) the exchange energy. Exchange energy is the difference in energy from the exact solution of Schrödinger's equation to the approximation method used to evaluate it. This approximation states that the nuclei are in fixed positions (MUELLER, 2001). In the DFT model, this energy is a function of the *electron density matrix*, $\rho(r)$. This matrix is determined from the Kohn-Sham (KS) orbitals (KOHN and SHAM, 1965), $\psi(i)$. The Kohn-Sham formalism assumes that there is an unrealistic system formed by n non-interacting electrons under a real external potential and with exactly the same density of the real system. This assumption allows one to see an n -electron system as a superposition of n one-electron systems (PACCHIONI, 2007). Therefore, for an n -electron system the density matrix is given by (VASILIEV, ÖGÜT and CHELIKOWSKY, 2002):

$$\rho(r) = \sum_i n_i |\psi_i(r)|^2$$

DFT has the limitation of considering only the ground-state charge density. To properly consider the electronic excitations it was necessary to generalize this theory, resulting in the development of Time-Dependent Density Functional Theory (TDDFT). The fundamentals of TDDFT are similar to those of DFT. The difference is that with TDDFT the wave function $\psi(r, t)$ and effective potential $\rho(r, t)$ explicitly depend on time (BURKE, WERSCHNIK and GROSS, 2005).

Although there are other similar methods that were successfully applied for absorption spectra calculation, as for example Time-Dependent Local Density Approximation (TDLDA) (VASILIEV, ÖGÜT and CHELIKOWSKY, 2002), we have chosen TDDFT because it is a standard tool in the area for calculating electronic excitations. It has been used, for example, in inorganic chemistry for the calculation of optical properties of transition metal complexes (BURKE, WERSCHNIK and GROSS, 2005).

A close analogy between KS and HF methods can be done, but density functional treatments are more stable (BAUERNSCHMITT and AHLRICHS, 1996). We use the Restricted Kohn-Sham (RKS) method in our simulation. A restricted calculation is the one where you assume there are two electrons per occupied orbital (SZABÓ and OSTLUND, 1996). And it can be performed considering a closed (the one we use) or open shell⁷ system (ROKS).

⁷ An open shell system is the one in which there are unpaired electrons in the orbitals (IUPAC, 1997-2011). Analogously, a closed shell system is the one which possess an

When working with KS or HF methods, we have to consider that each molecular orbital is expressed as a linear combination of a set of mathematical functions whose coefficients and weights are later determined; this set is called the *basis set*. The theoretical ideal would be to use a set of infinite size. But this cannot be done in practice (CRAMER, 2004). Therefore, it is necessary to select the best set for using within each situation. We decided to use Ahlrichs-TZV (SCHÄFER, HORN and AHLRICHS, 1992) basis sets as they are available for almost all elements.

One issue that must be taken into account is that the energy-optimized basis sets tend to consider the *1s* electrons as responsible for most of the energy. Therefore, this approach can be good for determining the energy of core electrons, but not for those properties not related to energy of the valence electrons. If we wanted a better description of the valence electrons, it would be necessary to use very larger basis sets, which is not efficient. Therefore, these basis sets are explicitly augmented with *diffuse functions*, which are basis functions with small exponents. The use of such functions is required when valence electrons are involved, for example for anions or excited states (CRAMER, 2004), (JENSEN, 2007). Another issue is that mathematical flexibility is required when describing a molecule as opposed to an atom using Schrödinger's equation. This flexibility can be achieved by also adding as auxiliary basis functions the *polarization functions*, which corresponds to “one quantum number of higher angular momentum than the valence orbitals” (CRAMER, 2004, p. 173).

Thus, we used a basis set with auxiliary polarized functions and augmented with diffuse functions (as we are going to calculate excited states). As we opted for the Ahlrichs-TZV basis set, we decided to use the polarization and diffuse functions from the same group, Def2-aug-TZVPP (WEIGEND and AHLRICHS, 2005) and Aug-TZVPP/C, respectively (WOON and DUNNING, 1993).

We also need to inform the functionals we are going to use in the calculations⁸. We decided to use Hybrid Functionals which are those that are mixtures of the exact HF exchange⁹ with approximations of the DFT correlation¹⁰ energy functional. Therefore, they present better results than non-hybrid ones, because the use of an exact exchange term helps partially correcting problems of approximation methods which otherwise would remain. One widely used example of these functionals is B3LYP (SHOLL and STECKEL, 2011). Gancheff and Denis (2011) performed a study of the UV-vis spectra of Rhenium (III) (Re^{+3}) complexes using TDDFT with, among others, B3LYP and the B2PLYP functionals. One of their conclusions is that using B2PLYP leads to more efficient computation. As will be seen in Section 7.2, we perform preliminary tests using both methods and indeed the use of B2PLYP leads to a faster computation. It is

even number of electrons and they are organized in pairs in the orbitals (IUPAC, 1997-2011).

⁸ Note that there is a difference between a function and a functional: although both output a number, the input for a function is a number, while the input for the functional is an entire function.

⁹ The exchange calculations in HF theory, gives the amount of exchange repulsion which is the correction to the value of the repulsion of two parallel electrons in different orbitals (IUPAC, 1997-2011).

¹⁰ Correlation energy is the “difference between the Fock energy calculated for a system and the exact non-relativistic energy of that system” (IUPAC, 1997-2011).

important to observe that, being more specific, we used a combination of the B2PLYP functional and the Resolution of the Identity approximation.

According to (NEESE, 2011, p. 236), the *Resolution of the Identity (RI) approximation* “consists of fitting the electron density to an auxiliary basis set”. Thus, reducing the required amount of calculation up to three orders of magnitude if the provided set has small size and sufficient quality (NEESE, 2011). This reduction, consequently, makes it an interesting approach for being used in calculations of large systems, which is our case. So, whenever possible, we opted for using this approximation.

B2PLYP is a double-hybrid functional, that is, a hybrid functional with a perturbative second-order correlation part. It was first proposed by (GRIMME, 2006) for ground state problem, and later by (GRIMME and NEESE, 2007) for the excited states problem. Perturbation theory, in general, is a set of approximations that allows the description of a complex system in terms of a simpler one. The original Møller-Plesset perturbation theory is an extension to the Hartree-Fock method, where they added electron-correlation effects (MOSS, PLATZ and JONES, 2004). In the case of B2PLYP, it is obtained from Khon-Sham orbitals (GRIMME, 2006), (GRIMME and NEESE, 2007). A good description of the dispersion energy can be obtained by using second-order Møller-Plesset (MP2), which is the lowest level that can be used for such calculations (MOSS, PLATZ and JONES, 2004).

The complete functional description we provided to Orca was RI-B2PLYP RIJONX, where RI-B2PLYP indicates we are using B2PLYP with RI approximation to the MP2 part and RIJONX is an Orca’s keyword indicating that RI is also being applied to the SCF part (NEESE and WENNMOHS, 2010, p. 41).

There is also ZORA, the Zeroth Order Regular Approximation, first presented by van Lenthe et al. (1993). It introduces relativistic effects to the calculation. That is, it includes “Corrections to exact non-relativistic energy from the fact that inner shell electrons in heavy atoms move with velocities comparable in order of magnitude to the velocity of light.” (IUPAC, 1997-2011). ZORA/RI is ZORA with RI approximation.

For convergence acceleration, we used the default method, the Direct Inversion in the Iterative Subspace (DIIS), which is a robust approach which combines direct and iterative methods (HIRATA, 2003).

5.3.3 The Absorption spectra

The software output provides lots of information about the computation it performed. In our work, we use the information about the set of calculated transition energies. These energies can be interpreted as the intensity of the energy absorbed/emitted when one electron moves from one state to another.

Then we can generate a chart of wavelength versus absorption intensity as the one presented in Figure 5.4. This chart represents an absorption spectrum. Similar charts obtained from simulating our samples will later be used to determine absorbed / re-emitted colors. As we are interested in obtaining color, we limit ourselves to the visible region of the electromagnetic spectrum. But it is possible to get information about the whole spectrum. Note that although we are using Orca, any program that performs TDDFT and produces the absorption spectra could have been used instead.

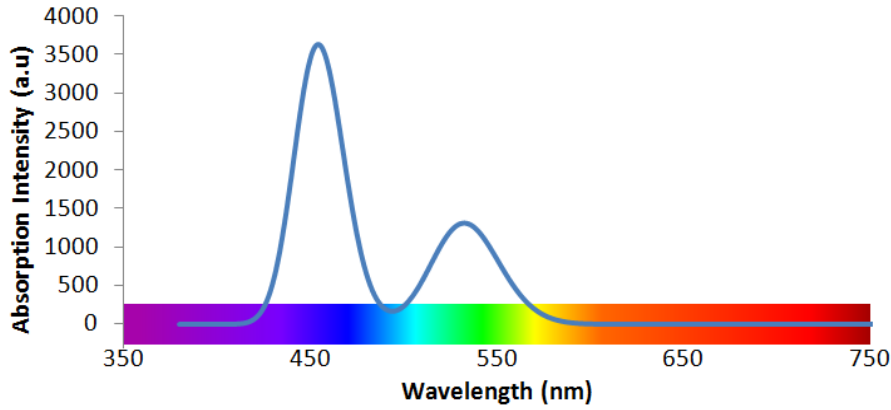


Figure 5.4: Absorption spectra obtained as output from Orca.

5.4 Obtaining Color from a Spectrum

Once we have determined the absorption spectra (Figure 5.4), we need to obtain the color it represents. This color must be in a color space that can be used to generate the texture of an agate. We decided to use the RGB color space. Therefore, as described in (LEE, 2005), it is necessary first to convert the spectrum to CIE XYZ color space and then to RGB. For a given spectral distribution of the sample, $S(\lambda)$, and a reference illuminant $I(\lambda)$, the XYZ tristimulus are computed according to:

$$X = \frac{1}{N} \int_{\lambda} \bar{x}(\lambda) S(\lambda) I(\lambda) d\lambda$$

$$Y = \frac{1}{N} \int_{\lambda} \bar{y}(\lambda) S(\lambda) I(\lambda) d\lambda$$

$$Z = \frac{1}{N} \int_{\lambda} \bar{z}(\lambda) S(\lambda) I(\lambda) d\lambda$$

$$N = \int_{\lambda} \bar{y}(\lambda) I(\lambda) d\lambda$$

where \bar{x} , \bar{y} and \bar{z} are the CIE standard observer functions. The reference illuminant is needed because we are working with materials that are not light emitters. Thus, the only way it will be possible to see it is if it is under some incident illumination. The integrals are computed over the visible spectrum (from about 380 to 830 nm). But, as in practice these values are represented by discrete values obtained from experiments, the above integrals are replaced by summations.

Considering that X, Y and Z are in the range [0, 1], the values for R, G and B coordinates (in the same range) are obtained as (LEE, 2005):

$$r = 3.2410 * X - 1.5374 * Y - 0.4986 * Z,$$

$$g = -0.9692 * X + 1.8760 * Y + 0.0416 * Z,$$

$$b = 0.0556 * X - 0.2040 * Y + 1.0570 * Z.$$

A second step is used to perform gamma correction to each channel individually:

$$K = \begin{cases} 12.92 * k, & k \leq 0.003040 \\ (1.055 * k)^{1/2.4} - 0.055, & \text{Otherwise,} \end{cases} \quad (5.1)$$

where $K \in \{R, G, B\}$ and $k \in \{r, g, b\}$, respectively.

In our example calculations, we used the CIE 1931 standard colorimetric observer and the sunlight, CIE D65, as reference illuminant (CIE, 2012), with a 5 nm interval between values. Annex B presents both tables. It is important to note that these values and formulae consider a reflectance/transmission spectrum. Thus, as we have an absorption spectrum, it is necessary to use its inverse. Figure 5.5 presents an example of an absorption/transmission spectrum (top) and the color obtained from it (bottom). In this example, we have light transmission in the region corresponding to blue and red parts of the spectrum. Thus, the resulting color presents a violet tone. Note that the spectrum shown in Figure 5.5 was manually defined by plotting the values of a curve in a known region in order to verify if the expected color would be obtained after the calculation.

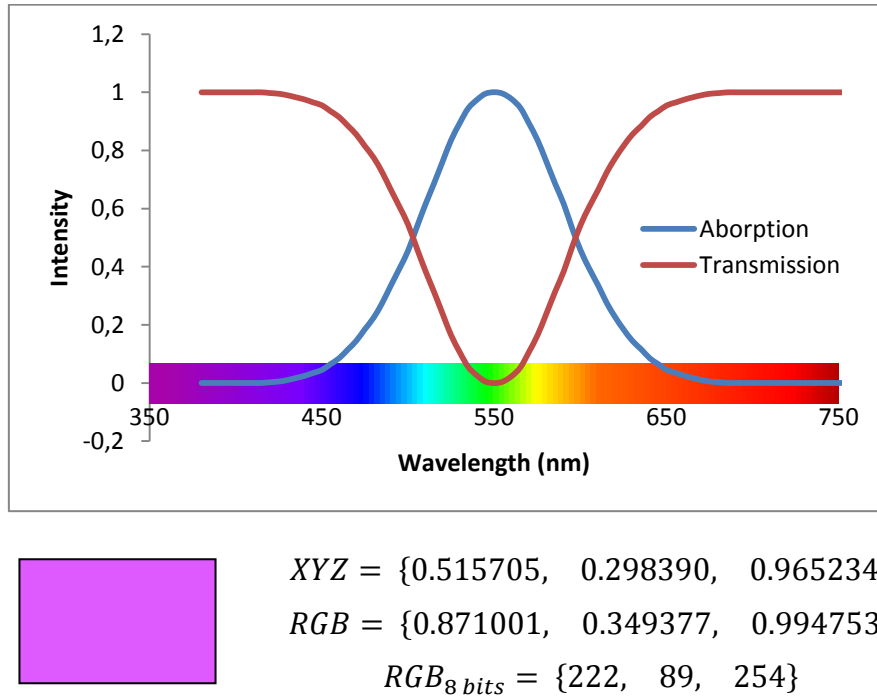


Figure 5.5: Example of an absorption/transmission spectrum (top) and the obtained color (violet) using the Eq. (5.1) (bottom).

5.5 Generating textures to represent the surface of an agate

Given the colors corresponding to the absorption/transmission spectrum obtained with the use of time-dependent density functional theory (TDDFT), we want to create the banded-stone appearance characteristic of agates. As described by Perlin (PERLIN, 1985), the use of noise functions is very suitable when it comes to simulating natural phenomena such as banding formation. Therefore, this was the selected approach.

Our base image is an ellipse with center in the origin of the coordinate system, as described in Figure 5.6. As the center is fixed, by altering parameters a and b , it is possible to obtain concentric ellipses with different sizes.

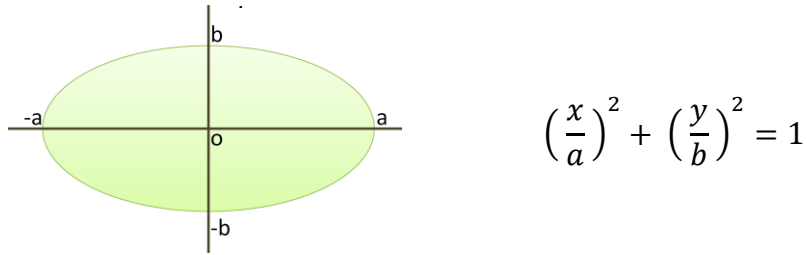


Figure 5.6: Equation of an ellipse centered at the origin.

We want to generate an image that is closer to the representation of an agate. Thus, for each ellipse, we apply a noise function over all its x coordinates which affects the range of y -coordinate values. For each region we inform a color to fill it. In order not to use a single color for the whole region, we jitter the value of each RGB channel of the informed color by a random value of at most 10% of it. Thus, the new color obtained is different but not perceptually far from its neighboring colors.

The pseudo code for the algorithm we use to generate each region is presented bellow. Our function is a modified version of the one presented in (VANDEVENNE, 2004), which can be used for creating marble-like textures:

1. For each x coordinate in the ellipse
 - Determine the value of y according to the function

$$y_square = (1 - (x^2/a^2)) * b^2$$
 - Determine the noise value as

$$noise = k * \sin(v * d)$$

where d is the distance from the point (x, y) to the center of the ellipse; and k and v are variable values chosen generally by trial and error which define the final shape of the image
 - Determine the range for y as

$$yMin = center - \sqrt{y_square} + noise$$

$$yMax = center + \sqrt{y_square} + noise$$
2. Define an initial color
3. For each pixel of the region
 - Define the color of the pixel by jittering the value of each RGB channel of the initial color by at most 10%

Algorithm 5-1: Pseudo code for generating each region of the image.

Note that all parameters are variable. Therefore, it is possible, for example, to render half of the ellipse with a set of values and the remainder with another. This characteristic is important because it allows us to obtain innumerable different shapes. Figure 5.7 presents an example of image generated using the Algorithm 5-1.

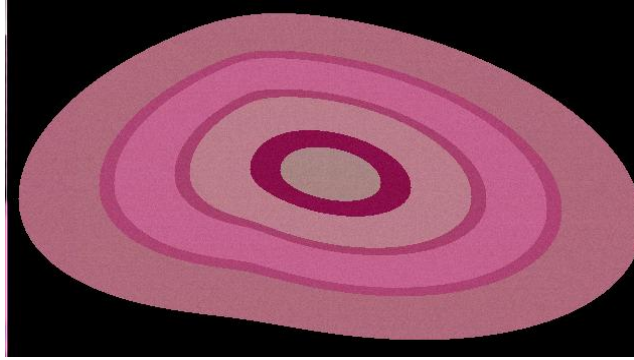


Figure 5.7: Example of image generated using the Algorithm 5-1.

The image presented in Figure 5.8 (left) was also generated using the Algorithm 5-1. The objective was to obtain an image with similar appearance to a real agate (Figure 5.8 (right)). For determining the shape we defined the parameters of the algorithm by trial and error. For each region of the generated image, we performed a visual random selection of a pixel in the respective region of the real image. The color of such a pixel was then used as the initial color of the generated region.

However, the use of this approach is not enough to obtain an image that looks realistic (Figure 5.8, (left)). As can be seen in Figure 5.8 (right), a real agate presents some kind of translucence and subsurface scattering. Barnard and Ural (BARNARD and URAL, 2005) presented a method that renders a translucent material with Perlin noise (PERLIN, 1985). Using this technique for our agate representation is an interesting future work and would allow us to obtain more realistic images.



Figure 5.8: Image obtained using the Algorithm 5-1 (left) and real agate (right).

5.6 Rendering of the Colored Volume Representing an Agate

The goal of the previous steps was to obtain an image of a simulated agate. The idea was to randomly generate some bands and then paint each one of them according to its composition. Based on this image, we would then construct a volume. Although first conceived to be only one step in the whole process, the method we proposed for the synthesis of a volume based on a 2D image became a standalone technique. Therefore, we are going to describe it in details in Chapter 6.

6 AGATE SURFACE FROM A 2D IMAGE

The generation of volumes based on a 2D image, although being a fairly explored field, still presents some problems that are not solved by existing methods. To the best of our knowledge, there is no technique that can be directly used for the purpose of creating volumes of banded agates from a single image. Thus, we decided to develop a method for this particular application. More specifically, we restrict ourselves to those agates which present the property of being formed by parallel concentric curved bands. This definition is very important, as it is the fundamental characteristic in which our method is based.

The problem of synthesizing banded agates can be defined as follows: given a 2D image of the center of an agate, we need to generate a volume that can be cut and seen from different angles. A framework with such characteristics could be very useful, for example, for someone who works crafting objects which the base material is agate. It would be possible for (s)he to verify how a cut in the agate they are working with would look like before actually cutting it. One way to solve this problem is to use a volume generation method.

Texture and volume generation are subjects widely studied in computer graphics. Therefore, it is beyond the scope of this work to perform a complete discussion of such topics. However, in the following sections we briefly review the techniques that were more relevant to the development of the work described in this thesis, as well as their limitations to the render agates.

6.1 Solid Texture Synthesis from 2D images¹¹

Kopf, Fu, et al. (2007) presented a method for synthesizing solid textures from 2D exemplars. The first step consists of texture optimization where they determine the color of each voxel based on the best neighborhood which results in smaller difference between the texture and the original image. Then, they perform global histogram matching. This re-weights the synthesized texture so that its histogram becomes similar to the one from the original image. Figure 6.1 presents a 2D image and the generated solid texture applied to a complex object, obtained using the technique by Kopf, Fu, et al. (2007).

¹¹ All images presented in this Section were extracted from the original related work.



Figure 6.1: A 2D image and the generated solid texture applied to a complex object(KOPF, FU, *et al.*, 2007).

Dong, Lefebvre, et al. (2008) presented a technique for rendering solid-texture volumes, whose main feature is to synthesize only a subset of the voxels. They use a group of three images (generally the same image rotate in different directions), which are positioned according to the X, Y and Z orthogonal planes. Then, they execute a pre-process where they select the neighbor candidates from these images having similar colors and being closely located to each other. The generated solid textures present good quality and can be used on complex surfaces. It also allows the interactive cutting of objects. Figure 6.2 illustrates this with an image that was used to generate a solid texture, and several objects on which the solid texture has been mapped to.



Figure 6.2: Example of input image and several objects on which the solid texture was applied on(DONG, LEFEBVRE, *et al.*, 2008).

Takayama, Okabe, et al. (2008) proposed a technique for synthesizing solid objects that present an oriented variation in the texture. The method requires as input a solid volume and a tetrahedral mesh representing the object. As several variations are possible, the algorithm performs distinct steps for each one and let the user determine which type (s)he wants. The result is a tetrahedral model which can be cut in different shapes. Figure 6.3 presents a kiwi model cut into different shapes.

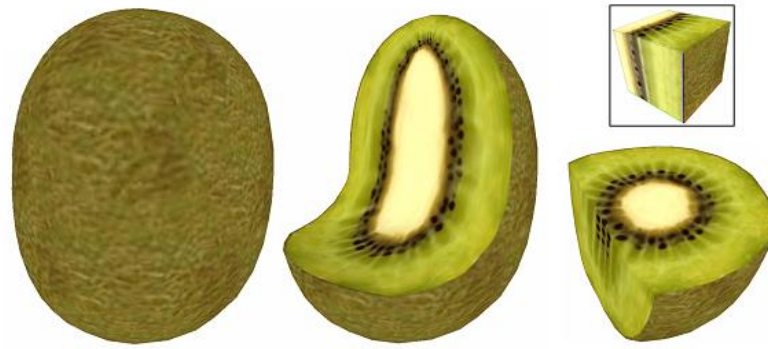


Figure 6.3: Kiwi model and different cuts(TAKAYAMA, OKABE, *et al.*, 2008).

Takayama and Igarashi (2009) proposed a method for synthesizing layered solid textures which is an extension of the work described in (KOPF, FU, *et al.*, 2007). The extension consists of: (i) adding a depth map; and (ii) performing a search and an optimization only in x and y directions. The changes in the searching processes allowed them to reduce the artifacts in the depth direction of the generated solid texture. Figure 6.4 presents some examples of 2D images with the generated solid textures and intermediate layers.

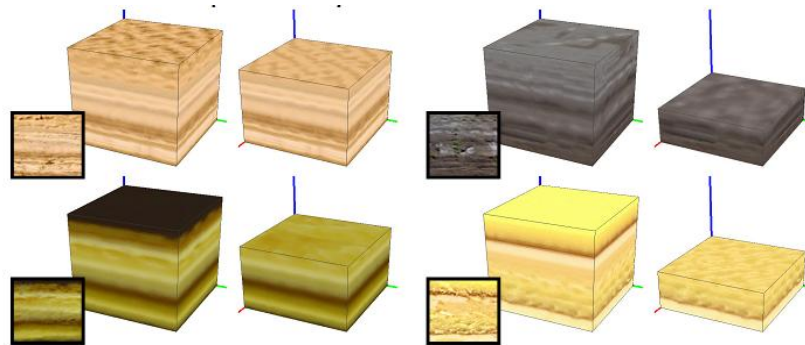


Figure 6.4: 2D images with their respective solid textures and intermediate layers (TAKAYAMA and IGARASHI, 2009).

Wang, Zhou, et al. (2010) presented a compact vector structure for representing solid textures which allows random-access. The input can be a 2D color image and a binary mask of this image (in which case they use the algorithm described in (KOPF, FU, *et al.*, 2007) to generate the solid texture) or an existent solid texture. Then, they compute a signed distance function, which implicitly represents the texture's features such as, for example, sharp edges in the image. Next, they evaluate this function and divide the texture into regions according to the results obtained by this evaluation. At last, the authors color the regions according to the members that are part of each region. Figure 6.5 presents an example of a 2D image (a) and the synthesized vector solid texture applied to an object.

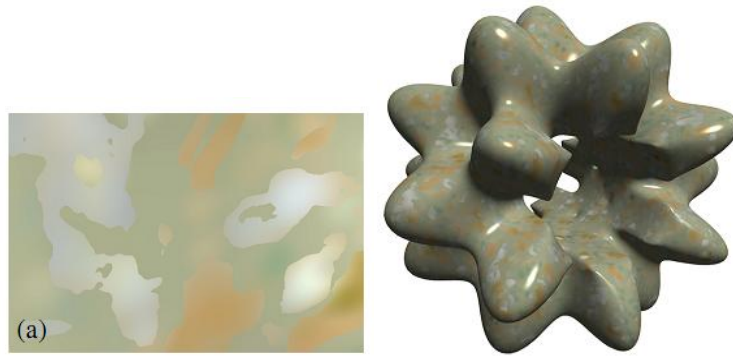


Figure 6.5: 2D image (a) and the synthesized vector solid texture applied to an object (WANG, ZHOU, *et al.*, 2010).

Takayama, Sorkine, et al. (2010) presented a technique called *diffusion surfaces* for modeling volumetric objects with smooth variation in color, such as those of fruits and vegetables. The method consists basically of computing the colors in both sides of a 3D surface and then diffusing the colors in the interior of the volume. The input consists of two images: one represents a vertical cut of the object, and the other represents a horizontal cut. Based on these images, they generate a mesh onto which they apply the algorithm. The authors use non-photorealistic rendering (NPR) as a post-process to generate the final results. Figure 6.6 presents several pieces of fruits synthesized using the proposed technique.

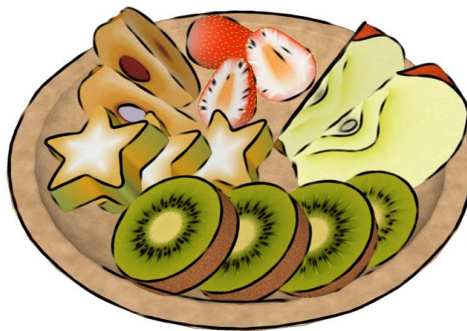


Figure 6.6: Several fruits synthesized using the technique (TAKAYAMA, SORKINE, *et al.*, 2010).

Wang, Yu, et al. (2011) proposed a novel data structure which allows the modeling of volumetric objects using a compact vector representation. This work can be seen as an extension of (VST) with some important differences such as, for example, the fact that VST has limited resolution while the new data structure can represent unlimited details. Figure 6.7 presents a vector volume (a) and the zoomed view of the selected area in the previous image (b and c).

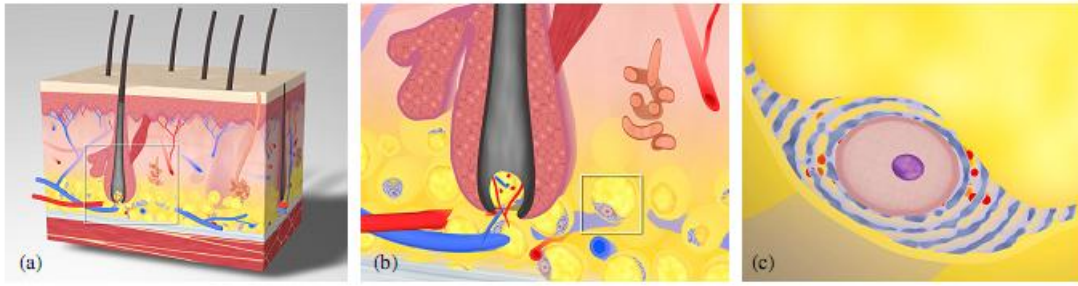


Figure 6.7: A vector volume (a) and the zoomed view of the selected area in the previous image (b and c)(WANG, YU, *et al.*, 2011).

6.2 The Proposed Method for Generating Solid Textures for Agates

Several changes would be required to allow the use of the techniques described in the previous section to render agates. For instance, the algorithm described by (KOPF, FU, *et al.*, 2007) would have to be altered in order to represent concentric bands as the solid texture is generated in only one direction. As (TAKAYAMA, OKABE, *et al.*, 2008), (WANG, ZHOU, *et al.*, 2010) and (WANG, YU, *et al.*, 2011) also use the volume described by (KOPF, FU, *et al.*, 2007) as input, they would require modifications too. An extension to the method was proposed by (TAKAYAMA and IGARASHI, 2009), however, the changes were not enough to solve the concentric bands problem.

Although Dong, Lefebvre, *et al.* (2008) use only a similar method to the one described by (KOPF, FU, *et al.*, 2007) for generating the solid texture, it also needs adjustments for concentric bands. Besides, it requires different images. For common abstract images, there is no problem in using the rotated version of the same image, but, for agates this approach would not work. Thus, in this case, this method would not be reliable due to the fact that, for example, someone who works with or collect agates would probably not want to cut the agate in more than one place just to see how other cuts would look like. A similar problem is presented by (TAKAYAMA, SORKINE, *et al.*, 2010), where more than one cut is required, resulting in the same infeasibility.

Considering the problem we want to solve and the limitations of the existent techniques, we propose a method that generates a solid texture volume. Our approach requires the image of only one cut of the agate, plus some external views of the stone (to define its shape). The generated volume can be used as input for other methods. The results we present were generated using the resulting volume as input for the Marching Cubes algorithm (LORENSEN and CLINE, 1987).

Thus, our approach can be stated as follows: given a 2D colored image of the center of the agate as input, we place this image in the center of the volume formed by the external views and spread the colors in order to fill the volume as indicated by the arrows in Figure 6.8. To avoid polluting the picture, only one set of arrows is represented in Figure 6.8, but this process repeats for each pixel of the image. The way the color of a pixel spreads depends on its location in the image: the closer to the center of the agate, the least it will spread. Then, after spreading all the pixels' colors, we obtain a volume containing the appearance of concentric bands. Details of how we spread the colors are given in the next section.

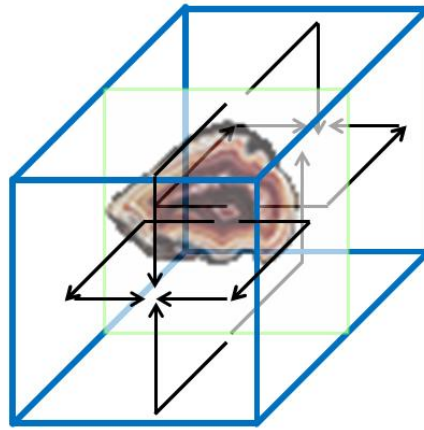


Figure 6.8: Arrows indicating how the colors spread in the volume.

6.3 Description of the Technique – Spreading the Colors

In this section we describe a fundamental part of our technique, which is the algorithm we use to spread the colors of each pixel of the original image across the volume.

The technique uses three input images (Figure 6.9): a transversal section of the agate and two binary masks representing the vertical and horizontal profiles of the agate stone (Figure 6.9 (b) and (c), respectively). Figure 6.9 (a) presents a half section of an agate. The red dot inside of it, does not belong to the original image, and indicates “the origin” of the agate’s bands. This position should be informed by the user; The vertical profile mask represents how the agate’s volume would be seen from its side; The horizontal profile mask indicates how the agate’s volume is seen from the top. It is important to note that the masks are not images from the cuts of the object; they are indeed only pictures of the external structure of the object.

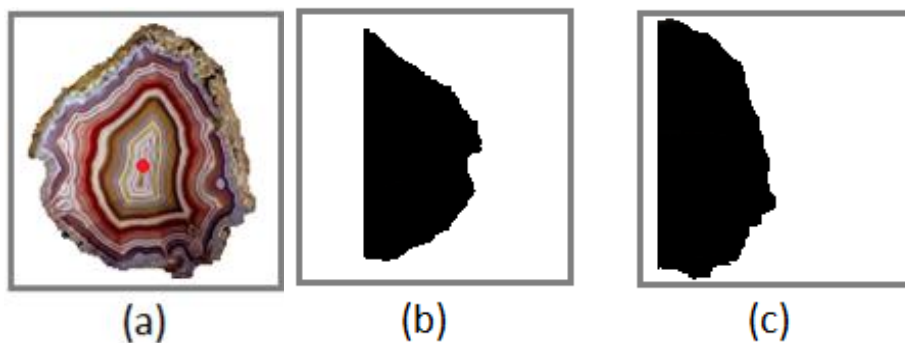


Figure 6.9: A transversal section, with a red dot indicating the approximate center of symmetry of the nested bands (a). Vertical (b) and horizontal profile mask (c).

Based on this set of images, we generate a volume that represents the external structure of the object. We do not create a mesh or anything to represent the volume, but use the depth information obtained from the masks. Figure 6.10 illustrates the process using a hypothetical example described as a set of 8x8-pixel image and masks. As can

be seen in the figure, each pair (x_i, y_i) of the transversal image is limited by two pairs (y_v, z_v) and (x_h, z_h) from the vertical and horizontal masks respectively. The z axis gives us the depth information.

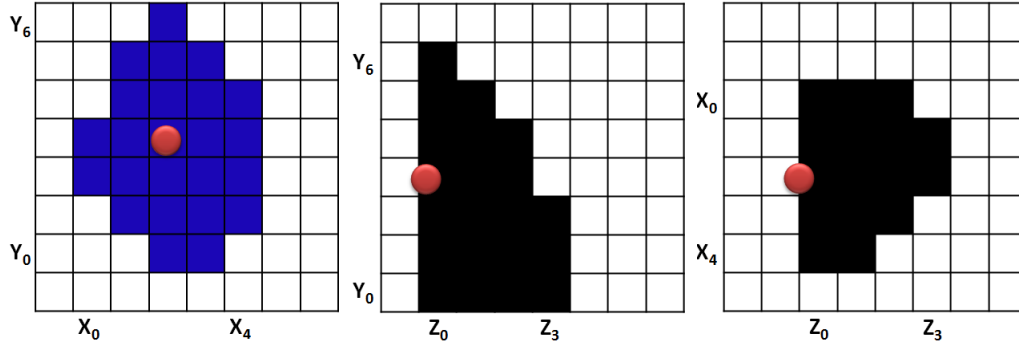


Figure 6.10: An 8x8-pixel set of image and masks: transversal (left), vertical mask (center) and horizontal mask (right).

So, the problem of creating a synthetic volumetric representation for the agate can then be stated as: given a pixel (x_i, y_i) in the transversal image, and a volume defined by the masks, which positions in the volume should have the same color as in the pixel (x_i, y_i) . How far a certain color will be spread is determined by the depth information in the generated volume.

The user indicates the approximate of the center of symmetry for the bands. In Figure 6.10 the red dot represents this point. For the masks, the whole line where this point is located is considered to be the middle line.

As we want to spread the color according to the masks in order to form the colored volume, we have four possible straight directions for the color of the pixel to spread to: left, right, up and down. We do not consider any diagonal direction. Considering these four movement possibilities, for each pixel (x_i, y_i) there will be 16 options of situations which describe where it can go considering the masks, Figure 6.11 presents the list of such possible movements.

Number of Directions	
0	
1	
2	
3	
4	

Figure 6.11: List of possible movements for the color of a pixel (x_i, y_i) in the volume

The number of possible directions where it can move to and the movements that will be executed depends on the number of existing neighbors a pixel has. To determine those neighbors, we divide the volume into vertical and horizontal slices and work with each one of them individually. For each line in the slice, we have a list of possible columns and rows, which represents four surrounding neighbors. As we perform movements on the slice, we remove that position and a new set of neighbors is determined. Figure 6.12 presents the movements in a sample slice of the volume. Figure 6.12 (a) is the initial slice. The arrows represent the movements executed by the colors. The "X" indicates where the color propagation process for one band stopped. Each color is spread only until the middle. Figure 6.12 (b) shows the slice with the remaining positions after the execution of the movements.

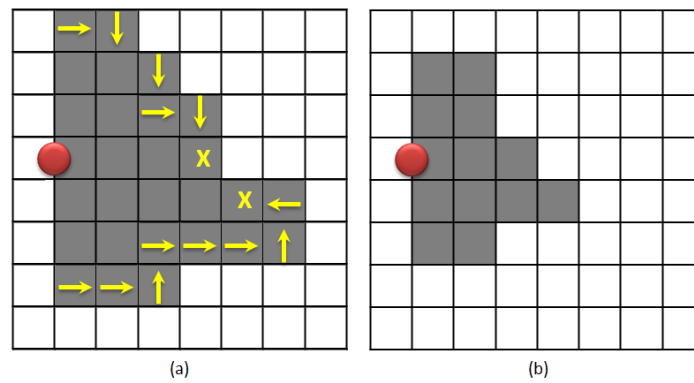


Figure 6.12: Movements in one slice of the volume. (a) The initial slice. (b) The slice after the execution of the movements.

We always try to spread the color to the most external and central position. Thus, when there is more than one option of direction, we choose the one that fulfills this requirement. For example, Figure 6.13 presents two pixel positions A and B which have more than one option of direction. In position A, we chose to go left and in B we moved down. Column 0 always keeps its original value as it represents the center of the volume and is filled with the original color of the image. Also, our first attempt is always to move right, because, as we start from left to right, there is no pixel in its left side and it cannot go up or down as these positions are already filled by the original colors.

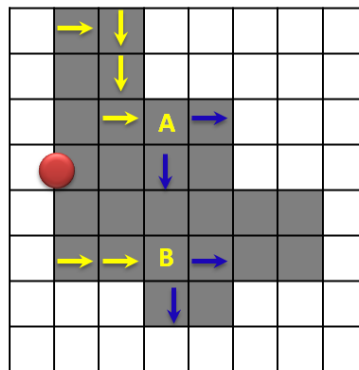


Figure 6.13: The colors in positions A and B have two options of movement. The one in A spread to left and in B, down.

We repeat this spreading process for all the vertical and horizontal slices. Thus we obtain two possible colors for each position in the volume and we need to decide which color will be used. To define a color, we first determine if both colors are valid. An invalid color is the one generated by the discontinuity in the colored pixels of a line/column of the original image. For example: Figure 6.14 (left) shows an image formed by different shades of blue, which presents line (position (X_2, Y_0)) and column (positions (X_6, Y_3) and (X_7, Y_3)) discontinuities; Figure 6.14 (center) is the corresponding horizontal mask; And Figure 6.14 (right) represents the horizontal spread corresponding to the slice Y_0 . We verify that the background color belonging to this hole is not spread resulting (as expected) in empty spaces inside the volume. Note that the colors from neighboring positions ((X_1, Y_0) and (X_3, Y_0)) do not spread over this empty space either.

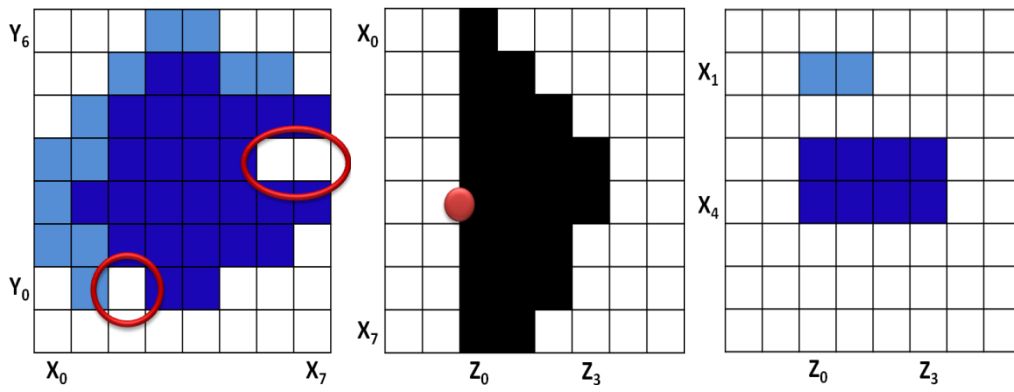


Figure 6.14: Example of discontinuity in the colored pixels. Image formed by different shades of blue presenting discontinuities in line (position (X_2, Y_0)) and column (positions (X_6, Y_3) and (X_7, Y_3)) (left); The corresponding horizontal mask (center); And the horizontal spread corresponding to the slice Y_0 (right).

The verification of the validity of the colors leads us to the following options:

1. None or only one of the options is valid;
2. Both indicated colors are valid.

Option 1 indicates that the position receives no color as an invalid index in one direction indicates a discontinuity in the exterior, and, therefore, that the line/column it belongs to is empty.

Option 2 requires that we verify if the colors are similar¹². Such a process is necessary because a lack of similarity indicates that they probably belong to distant regions of the original image. For example, one came from the outer edge of the agate and the other one, from the interior.

To determine the similarity we compare the luminance of the color indicated by one slice with the luminance presented by the surrounding neighbors (of the texel being considered) in the other slice. For example, Figure 6.15 presents a vertical slice (for clarity of the image only its borders are represented) and a horizontal slice. If we

¹² Note that such verification is not necessary if the colors are equal.

consider the texel represented in red (belonging to the vertical slice), its surrounding neighbors in the horizontal slice will be those represented in blue.

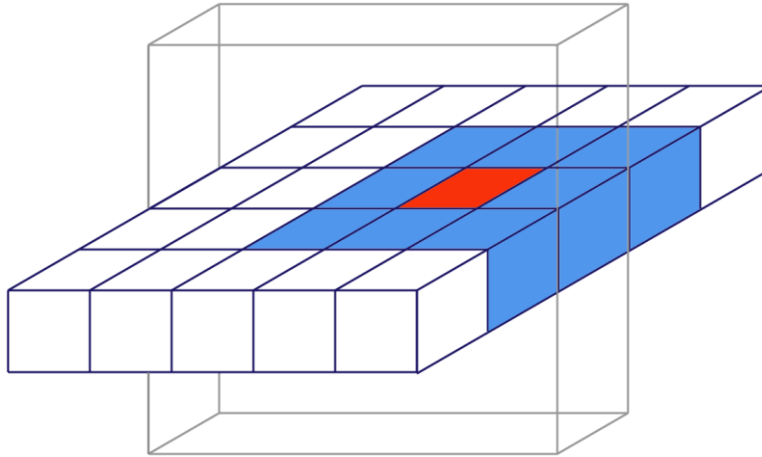


Figure 6.15: The borders of a vertical slice and a horizontal slice. The red texel belongs to the vertical slices and the texels represented in blue are its surrounding neighbors in the horizontal slice.

If they are similar, any one of them can be used and therefore they are randomly chosen. Otherwise, the color of the texel being considered will be set as undefined and, after all slices were processed, the texels in this situation will be reprocessed and will receive an interpolated value according to their neighbors' colors. At last, to achieve a smoother effect we apply, as post process, the optimization method described by (KOPF, FU, *et al.*, 2007) which was presented in Section 6.1.

6.4 Examples of Generated Solid Textures

This section presents several volumes generated using our technique. Figure 6.16 shows the input center image with 64x64 pixels (a), the vertical (b) and horizontal (c) masks and the final volume obtained using Marching Cubes (d).

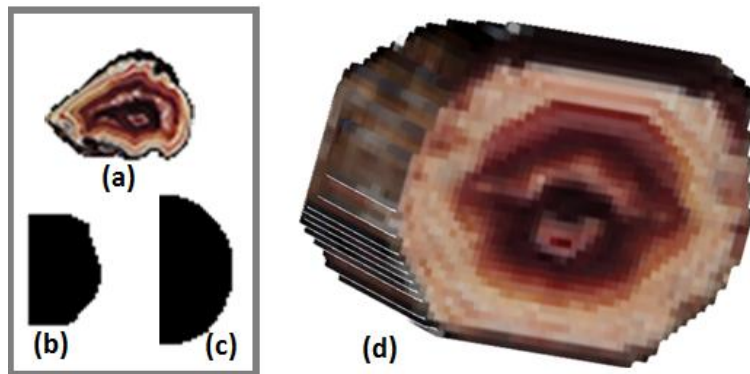


Figure 6.16: Original image (a), vertical (b) and horizontal (c) masks and final volume with Marching Cubes and post processing (d).

Figure 6.17 presents a volume before (left) and after (right) applying the post processing to the final volume. For comparison, Figure 6.17 also presents the respective enlargement of a portion of each volume. Note that in the detailed portion of the post processed image there was a blur in the colors resulting in a slight aliasing reduction.

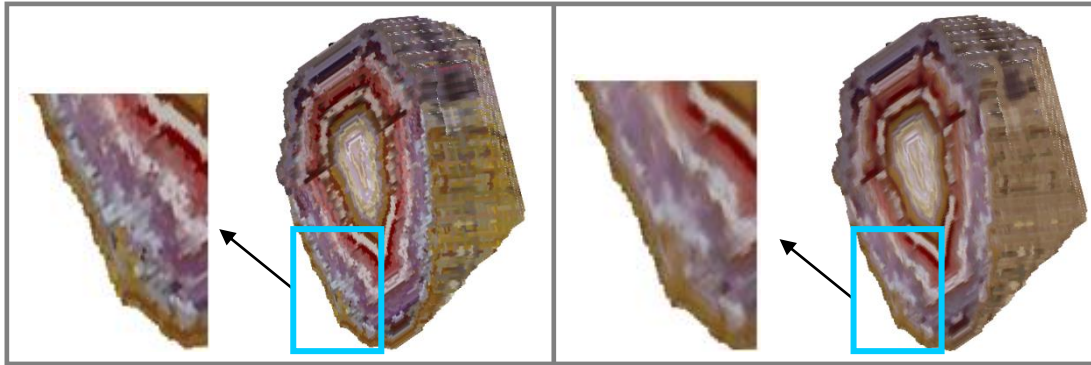


Figure 6.17: Volume before (left) and after (right) post processing, along with a detailed portion of each volume.

Figure 6.18 presents a comparison between a volume generated using the technique proposed by (TAKAYAMA and IGARASHI, 2009) and our method. This image summarizes the main difference between the methods. It illustrates the reason why the previous methods could not have been used for concentric bands. The image was colored with a blue background just to highlight the generated volume.

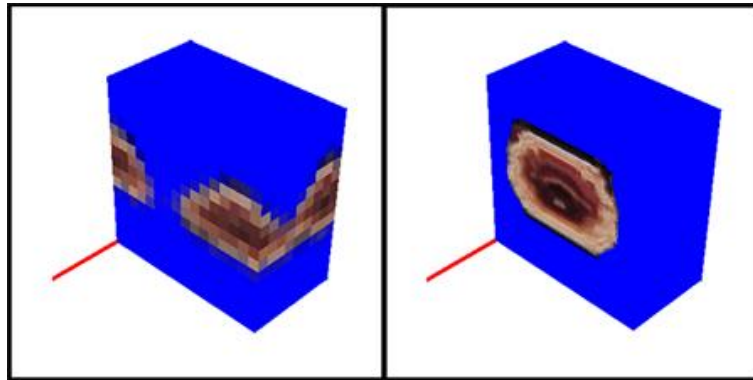


Figure 6.18: Comparison between a volume generated by (TAKAYAMA and IGARASHI, 2009) (left) and our method (right).

Although our approach was originally conceived for agates, with only few minor changes it can be used for generating volumes of different objects with cylindrical geometry. As mentioned in Section 6.3, we spread the color in vertical and horizontal directions, due to the characteristics of the agate's structure. However, other objects may present symmetry in only one direction; therefore, the adaption required for these objects is just to spread the color in the required direction, instead of spreading in both. Figure 6.19 presents the cuts from volumes of a carrot and a kiwi fruit, respectively.

They were generated with minor changes to the method, from 64x64 images. They show the original volume, before any post process.

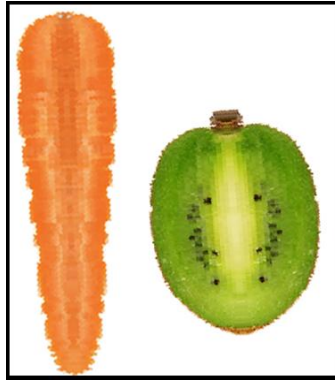


Figure 6.19: Carrot and Kiwi volumes generated with our method.

6.5 Limitations

The main limitation of our volumetric texture technique is that we cannot precisely determine how the agate actually is. This is due to the fact that we only have information about one dimension of cutting. Our results are then plausible representations (approximations) of actual agates. Furthermore, this fact also implies abrupt changes in color when the left side of the symmetry is different from the right side (or bottom/up), as the colors "collide" in the center resulting in mismatched colors. For example, in Figure 6.20 (left) we have the original onion image, which presents a slightly darker color in its right side. The consequence of this difference is that a horizontal cut of the volume generated presents a discontinuity (mismatch) in its color (Figure 6.20 (center)). Other limitation is the dependence the final volume has from external conditions: Our approach is imaged based. Thus, the quality of the results is directly related to the quality of the center image and accompanying masks. The resolution and artifacts that might be present affect the obtained volume. For example, the onion in Figure 6.20 (center) presents a squared surface due to the square shape of the borders of the horizontal mask (Figure 6.20 (right)) and not a half circle as it was expected to be.



Figure 6.20: Example of mismatched colors and squared surface. Original onion image (left). Horizontal cut (center) of the generated volume presenting mismatched colors (due to the color differences in the original image) and squared surface (due to the shape of the horizontal mask (right)).

In Figure 6.21 we present several differences in the volume resulting from external parameters. Images (a) and (b) present the volume before post processing. In image (a) the symmetry center was considered to be the middle of the agate and in (b) the middle of the bands. Image (c) is the same as image (b) but after post processing. Image (d) is the same as (c) but with different luminance threshold. Therefore, as can be seen, changes in the position of symmetry center or of the luminance threshold lead to slightly different result. The aspect of the final volume is also influenced by the method that uses it as input. Different methods will turn into different results.

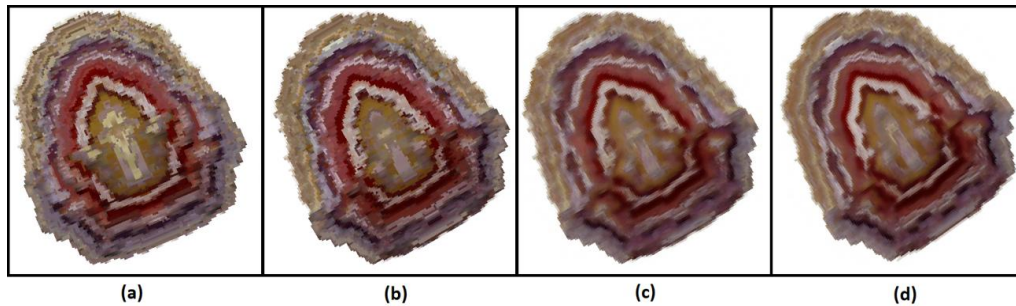


Figure 6.21: Differences in the volume resulting from external parameters.

Other limitations are related to the fact that the technique does not take into account the different structures inside the object. The only properties considered are the pixels' color and location. Thus, it is not possible to simulate, for example, agates which present some crystals in their interior, as shown in Figure 6.22. Furthermore, properties such translucence and other optical effects are not yet treated. Thus, in some cases, as for example in Figure 6.23, the *external surface* of the resulting volume may not look like a stone.



Figure 6.22: Agate with crystals in its interior (Source: <http://bibliotecaria-detodocomoenbotica.blogspot.com.br/2009/08/el-agata.html>. Access in June, 2012).

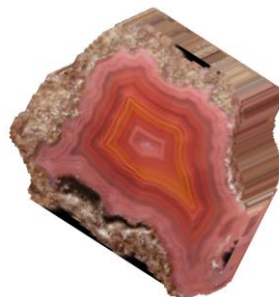


Figure 6.23: The external surface of the resulting volume generated with the proposed technique may not look like a stone.

7 RESULTS AND DISCUSSION

Our original goal was to simulate minerals in general. However, considering only the initial tests performed for determining the best methods to be used with pure minerals, with different impurities in different concentrations, and with structures containing different number of atoms (molecules and unit cells), we had to perform over 1,000 (one thousand) experiments. This huge number of experiments, and the time and computational resources needed to execute them forced us to restrict the scope of the work. Thus, we decided to focus on Silica, mainly because it could be used as a basis for working with the vast and interesting world of agates.

This chapter presents the results of our simulations with silica. We started working with a single SiO_2 molecule, then, we worked with the unit cell and, at last, with the unit cell expanded on Cartesian axes. We also present some results we obtained adding impurities to the unit cell.

7.1 Single Molecule

A silica unit cell is illustrated in Figure 7.1¹³. It consists of six silicon (Si) and six oxygen (O) atoms. Thus, we divided the unit cell into six different molecules and worked with them separately, as shown in Figure 7.2. Note that although atoms Si_1 - Si_5 , Si_2 - Si_4 and Si_3 - Si_6 are symmetrical to each other and, therefore, can be considered interchangeably, we decided to consider them separately to verify the consistency of the method.

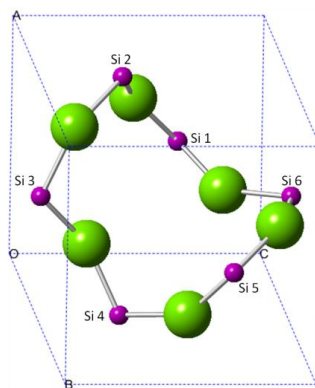


Figure 7.1: Silica unit cell. It is formed by six silicon (Si) and six oxygen (O) atoms.

¹³ This figure represents the same unit cell as the one presented in Figure 5.1(left), but, from a different point of view.

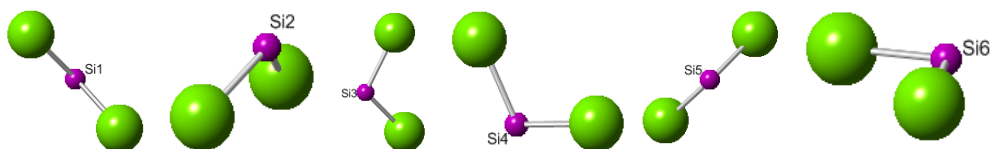
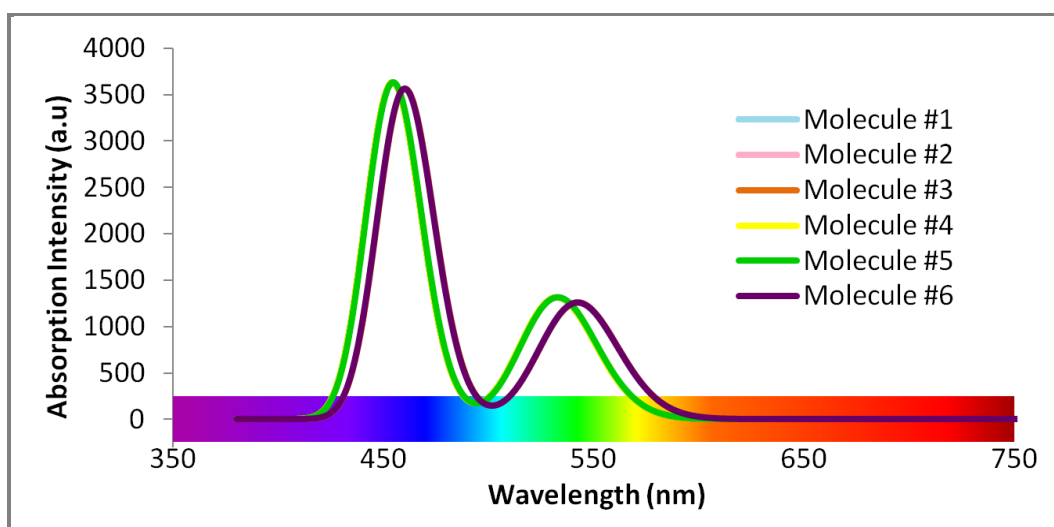


Figure 7.2: Molecules based on the unit cell, treated separately.

When plotting the absorption spectra resulted from the simulations of the six individual molecules shown in Figure 7.2, we obtained the chart and colors presented in Figure 7.3. In this chart, the molecules formed by Si atoms number 1, 2, 4 and 5 result in the same curve. This curve is slightly different from the one obtained by Si atoms number 3 and 6. This difference can be explained by the fact that these two set of molecules also present a small difference in their molecular angle. Therefore, their elements do not interact in the same way. As shown in Figure 7.4 (for only one of the symmetric atoms), molecules formed by atoms number 1, 2, 4 and 5 have a molecular angle of $110,43^\circ$, while molecules from atoms number 3 and 6 exhibit a molecular angle of $108,75^\circ$. Note that as the differences are small, the resulting colors are very similar.





Molecules 1, 2, 4 and 5	$RGB = \{250, 223, 165\}$	
Molecules 3 and 6	$RGB = \{247, 221, 169\}$	

Figure 7.3: Absorption spectra obtained from individual molecules (top) and the colors represented by the resulting curves (bottom). Molecules 1, 2, 4, and 5 have a molecular angle of $110,43^\circ$, while molecules 3 and 6 have a molecular angle of $108,75^\circ$. The small angular differences result in similar simulated colors.

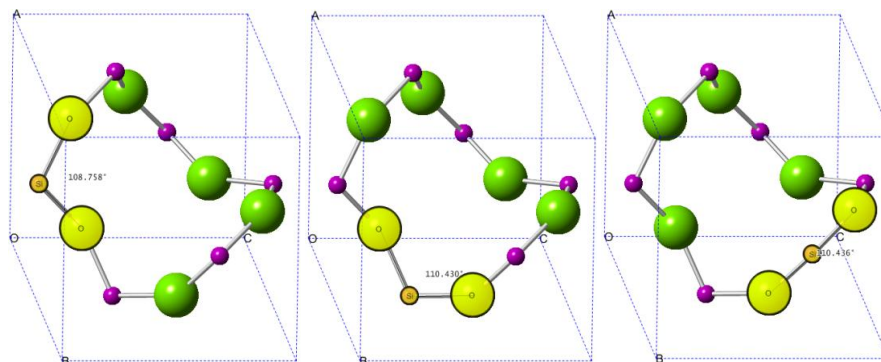


Figure 7.4: Molecular angles presented by the different molecules.

7.2 The Unit Cell

When more than one similar method for solving the same problem was available (*e.g.*, different methods for relativistic effects calculations) it was necessary to decide which method should be selected. The decision was made considering the method's accuracy and execution time. In general, the differences in accuracy for similar methods were not significant, resulting in the same curve. Thus, the selected method was the one with shortest execution time. The values considered for comparison were based on the results obtained executing them with the unit cell.

The most relevant result considering the differences between curves and execution time was obtained when we compared the methods B3LYP and RI-B2PLYP. As described in Section 5.3.2, B3LYP is more precise, but RI-B2PLYP is faster. We verified that for our sample the difference between the execution time was in the order of more than one day for the unit cell, which has a small number of atoms. When it comes to precision, we obtained the curves presented at Figure 7.5. At first glance, they look completely different. But, if we also plot the values outside the visible region of the spectrum (Figure 7.6), one notes some similarity. And, if one translates the RI-B2PLYP curve to the left until it meets the other curve (Figure 7.7), one notes that their absorption peaks are practically the same. Thus, we opted for the RI-B2PLYP method because it is faster, but the difference in precision should then be considered later, when extrapolating the results.

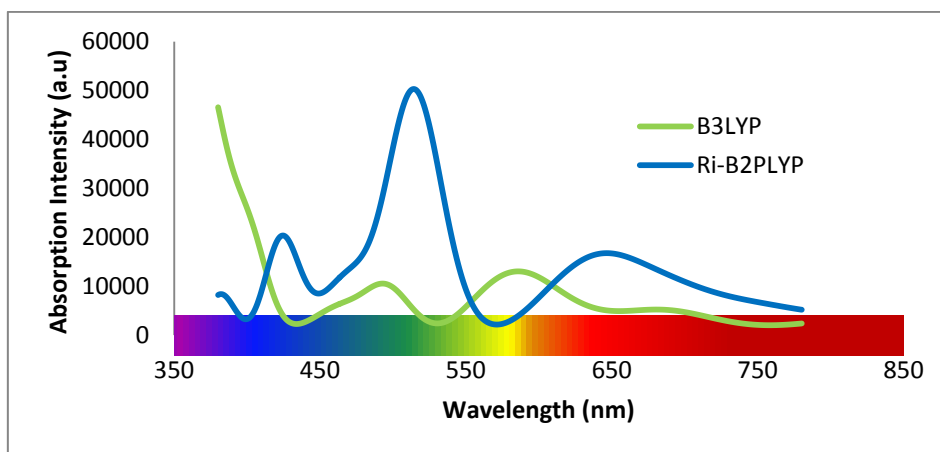


Figure 7.5 Absorption spectra for the silica unit cell inside the visible region of the spectrum, obtained using the methods B3LYP and RI-B2PLYP.

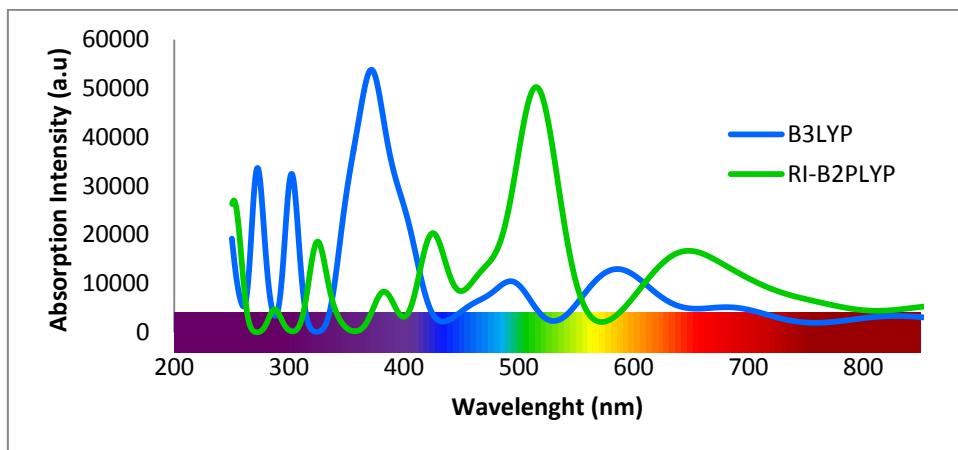


Figure 7.6: Absorption spectra for the silica unit cell for a larger portion of the electromagnetic spectrum obtained using the methods B3LYP and RI-B2PLYP.

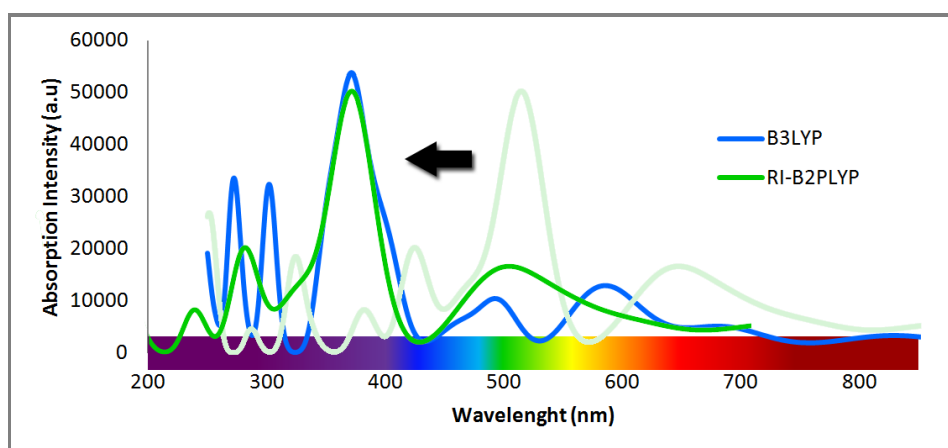


Figure 7.7: Absorption spectra for the silica unit cell for a larger portion of the electromagnetic spectrum obtained using the methods B3LYP and RI-B2PLYP, after the RI-B2PLYP curve has been translated to the left to better match the B3LYP curve.

7.3 Expansions

As stated before, our goal for this step was to increase the number of atoms in the simulation and then find a relationship between the number of atoms and the generated absorption curve. Thus, as the unit cell is the basic structure of a mineral, we incrementally expanded the unit cell along its Cartesian axes. These expansions were made using the CrystalMaker® software (CRYSTALMAKER SOFTWARE LTD, 2011).

We expanded the unit cell along the X, Y and Z axes, individually, and then combined them as XY, XZ, YZ and XYZ. However, due to technical problems that will be described in Section 7.5, we could only generate the absorption spectra of the expansions along the X, Y and Z directions. Figure 7.8 shows the unit cell expanded into X, Y and Z directions, respectively. Remember from Section 7.1 that there is a small difference between the angles presented by the molecules in the unit cell depending on their position. Thus, although the three resulting expansions look similar,

their bonding angles vary according to the original molecules that were replicated to originate each one of them.

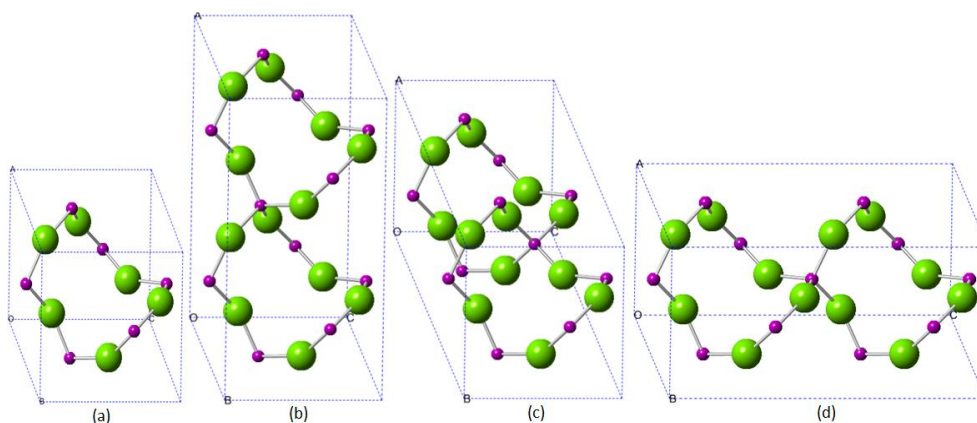


Figure 7.8: Unit cell (a) expanded along the X, Y and Z directions, (b), (c) and (d) respectively.

At first, except for a small overlap of expansions along the X and Y directions (Figure 7.8, (b) and (c)), the absorption spectra obtained seem different and unrelated, as seen in Figure 7.9.

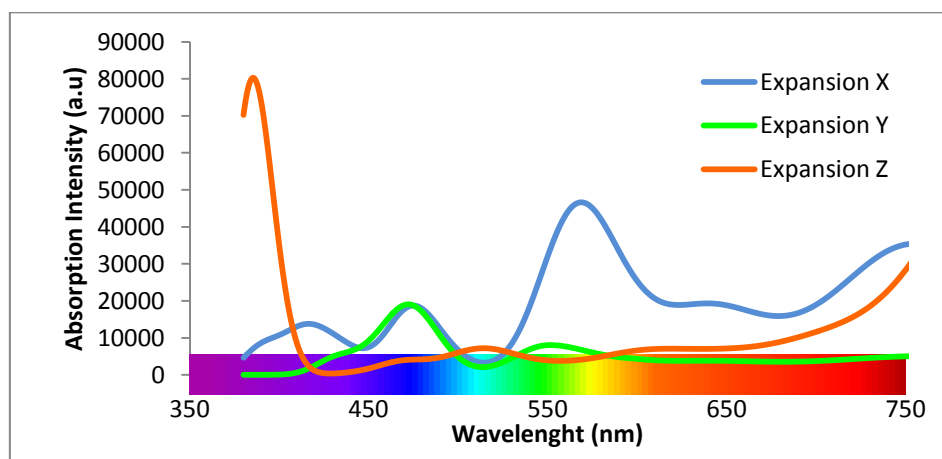


Figure 7.9: Absorption spectra of the unit cell expanded into X, Y and Z directions

However, scaling these curves to absorption intensity between 0 and 1 (Figure 7.10), one perceives that the peaks of the curves are similar, but translated. The same can be perceived even if we add the curves obtained by the molecular and unit cell simulation, Figure 7.11. This fact is interesting because it reinforces our hypothesis that it would be possible to extrapolate the results. Note that this translation in the curves represents absorption in different regions of the spectrum and, thus, that a different color is being re-emitted. So, to extrapolate the results, we would have to know how much to translate the curve and to each side. Unfortunately, with the results we have so far, it is not possible to establish such a relation, as the curves translate either to the left or to the

right. The combined expansions (along XY, XZ, YZ and XYZ axis) were necessary to determine, for example, the influence of the number of molecules and their positions to the resulting absorption spectrum.

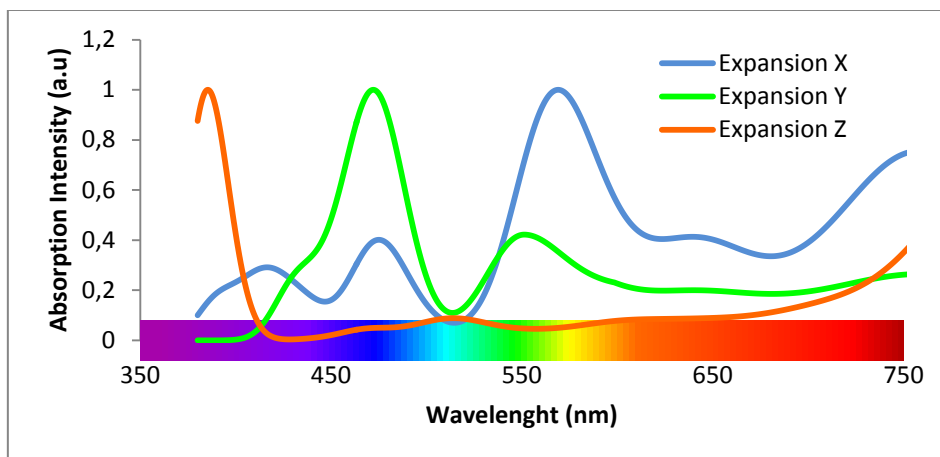


Figure 7.10: Scaled version of the absorption spectra of the expanded unit cell

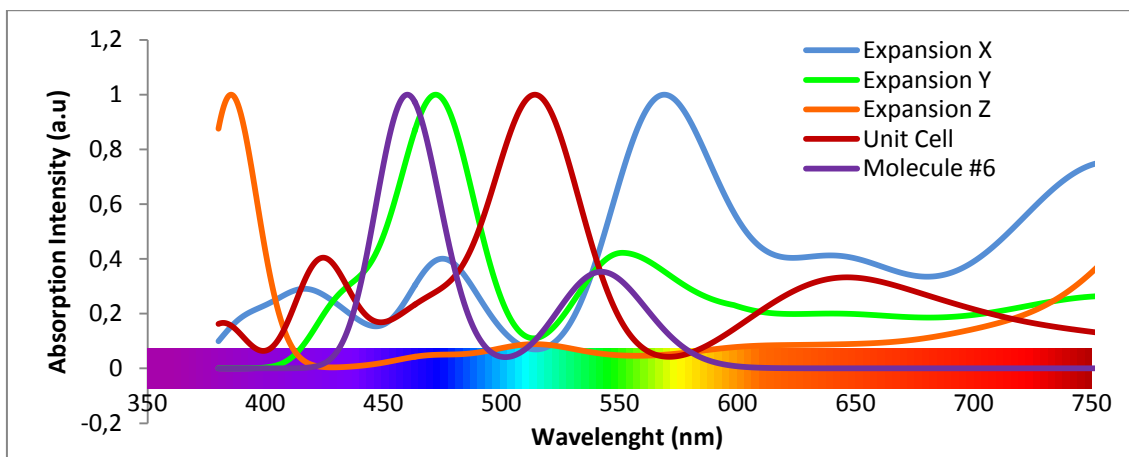


Figure 7.11: Absorption spectra of a molecule, the unit cell and its expanded versions

7.4 Unit Cell with Impurities

Besides the results presented so far, we also wanted to verify the influence of impurities to the absorption-spectrum curve. Thus, we replaced the *Si* atoms in the unit cell by titanium (*Ti*) and iron (*Fe*) atoms. Note that the samples we present here are not realistic, as in real life only traces or 1-2% of the atoms are replaced by impurities. Due to the small number of atoms used in our simulations, even if we replace only one of atom, the percentage of replacement tends to be big. We should note that we are not considering the changes in bonding angles due to the presence of other elements other than silica and oxygen.

Although not realistic when it comes to determination of color, these samples are very interesting for demonstrating the influence of concentration, type, and position of

an element to the final absorption spectrum. To verify the different possibilities, we defined a set of ten replacements as:

- One iron (*Fe*) atom in three different positions;
- Two *Fe* atoms simultaneously;
- One titanium (*Ti*) atom in three different positions;
- One *Ti* atom and one *Fe* atom with the *Fe* atom in two different positions;
- One *Ti* atom and one *Fe* atom with *Ti* atom in the position of the *Fe* atom and vice versa.

Figure 7.2 presents the unit cell after the impurities have been inserted: (a), (b) and (c) show iron atoms (in blue) inserted at positions #1, #2 and #3 respectively; (d) iron atoms inserted at positions #1 and #2 simultaneously; (e), (f) and (g) titanium atoms (shown in red) inserted at positions #1, #2 and #3 respectively; (h) and (i) titanium atoms inserted at position #3 and iron atoms inserted at positions #1 and #2 respectively; and (j) atoms of i) in inverted positions. Note that as the Si atoms in the original unit cell (shown in purple) present symmetry, if we replace one of them (e.g. atom #1) its symmetrical (atom #4) is also replaced. That is the reason for the apparent duplicate atoms.

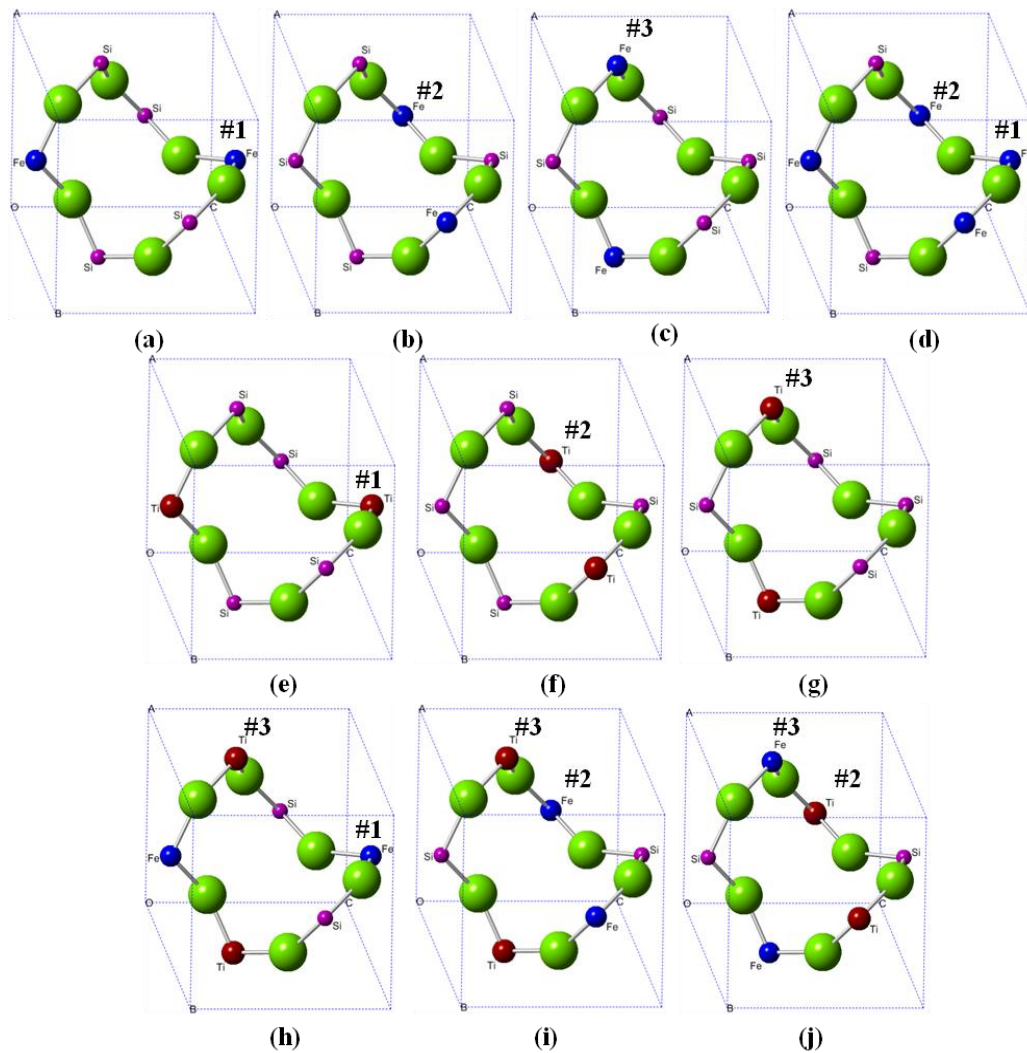


Figure 7.12: Unit cell after the insertion of impurities. The blue spheres represent iron (*Fe*) atoms, while the red spheres represent titanium (*Ti*) atoms.

The ten spectra obtained from these simulations plus the one from the pure unit cell can be seen in Figure 7.13. Due to the difficulty to understand and analyze such an intricate set of curves, we will analyze some combinations of them that can lead to interesting remarks. Note that the analyses within these samples are not limited to those presented here. Depending on what one wants to demonstrate, other combinations can be used. Also, if such curves are combined with results from bigger samples, even more interesting and accurate conclusions can be established.

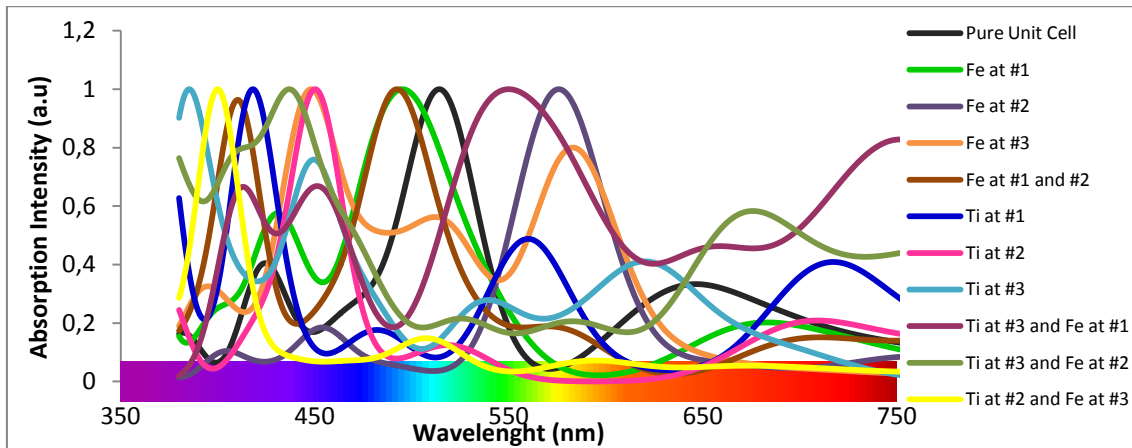


Figure 7.13: Set of obtained impure spectra from the configurations shown in Figure 7.12.

We start by presenting in Figure 7.14 the results of *Fe* (top) and *Ti* (bottom) atoms individually replaced. For such configurations, no obtained curve is equal to another. However, one perceives that both *Fe* and *Ti* present a similar behavior. At position #3, besides their main absorption peak, both have a peak which partially overlaps the one formed by the atom at position #2. Also, the peak of the curve corresponding to position #1 is situated between the other two.

This similarity demonstrates that the position of the impurity influences the final curve. By altering the position of the impurities, the variation in the obtained curves is not quantitatively equal for all elements. However, the way it influences the result is the same (*i.e.*, the final curve in a certain position will translate to left or right).

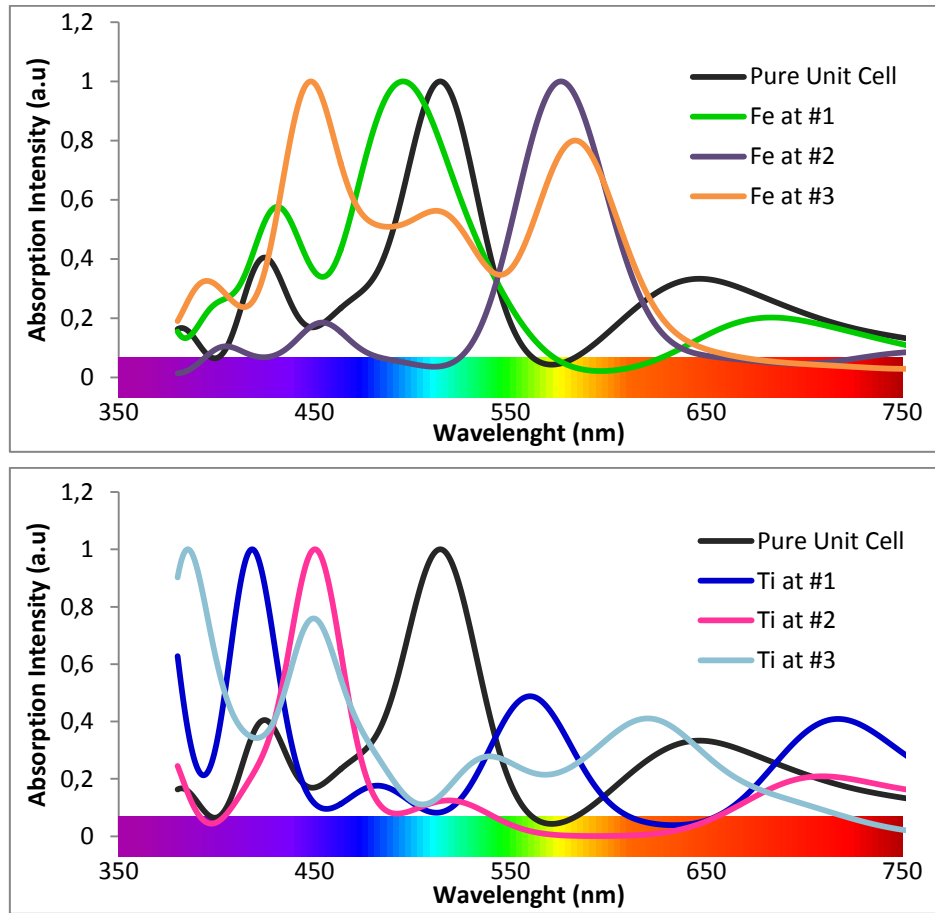


Figure 7.14: Spectra of *Fe* (top) and *Ti* (bottom) atoms individually replaced

Figure 7.15 presents a sample of the influence of concentration of an element. On top, we have the spectra formed by *Fe* atoms individually and simultaneously at positions #1 and #2. At the bottom, we have the same curves and also the simultaneous one translated to the right. We perceive that when two atoms are replaced, there is a formation of two peaks. In the first case (top), it partially overlaps the curve formed by the *Fe* atom at position #1. After translation (bottom), it practically overlaps both curves. This experiment suggests that each atom influences the final result of the combination.

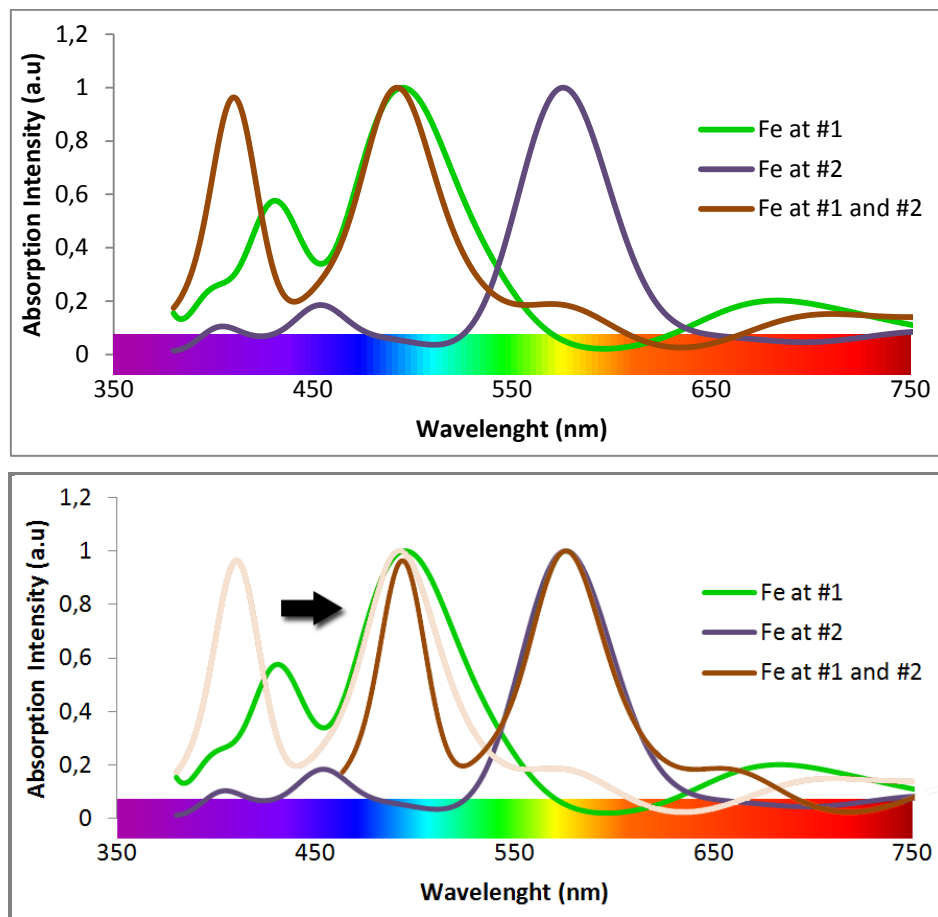


Figure 7.15: Influence of the concentration of an element.(top) The curve defined by Fe at #1 and #2 partially overlaps the curve formed by the Fe atom at position #1. After translation (bottom), it practically overlaps both curves.

Figure 7.16 presents the results of replacing a *Ti* atom at position #3 with a *Fe* atom at position #2 and the inverse situation. Remember from previous sections that the bonding angle at positions #2 and #3 is the same. Thus, if position and bonding angle were the only factors to influence the result, we would expect both curves to be the same. But, the different curves obtained allow us to verify that the element involved also influences as it considers the interactions with its surroundings (principle of MOT).

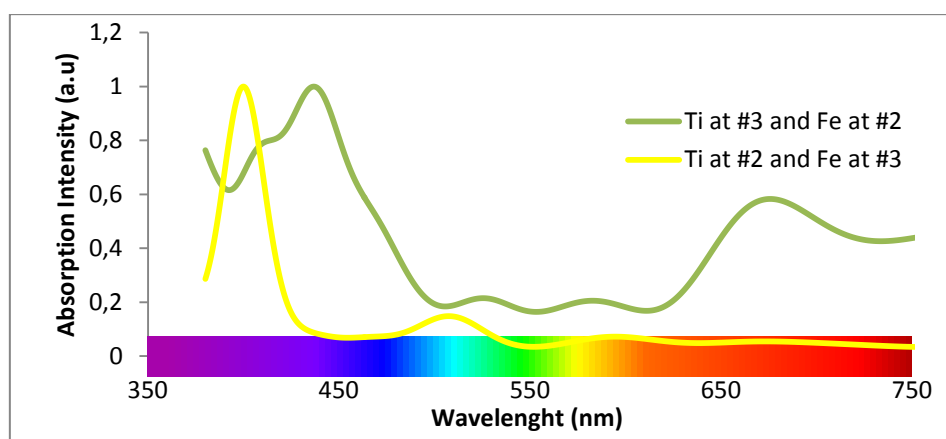


Figure 7.16: Ti atom at position #3 with Fe atom at #2 and the inverse situation

Our last analysis tries to verify the influence of the presence of certain elements to shape of the absorption-spectrum curve. Figure 7.17 presents the spectra obtained with atoms of *Ti* at position #3 and atoms of *Fe* at position #1 (top) and #2 (bottom), as well as their individual spectra. Keeping the *Ti* atom in a fixed position, we perceive that the resulting curve from the mixture of *Ti* and *Fe* translate in opposite direction to the one of the corresponding individual *Fe* atom. That is, if the spectrum of *Fe* #1 translates to the left of the pure unit cell, with the presence of the *Ti* atom, the curve translates to right. A similar opposite translation is observed in the spectrum of *Fe* #2. This behavior presented by the curves verifies once again the influence of the involved elements and of their positions.

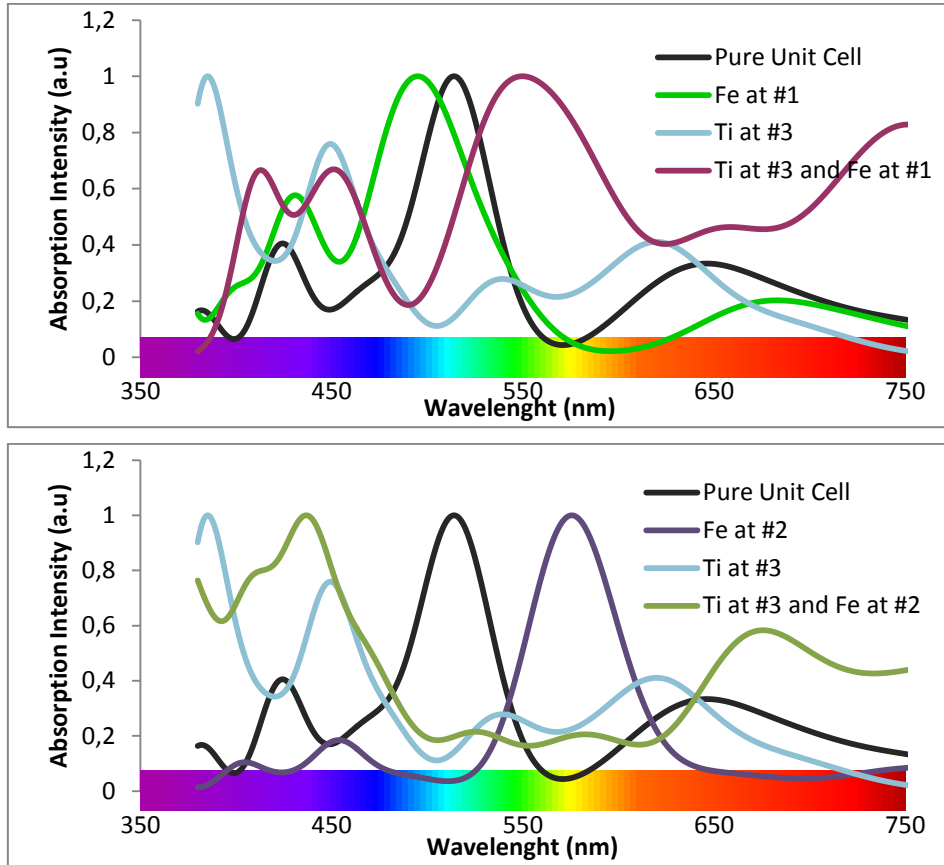


Figure 7.17: Spectra obtained from a mixture of *Ti* atoms at position #3 with *Fe* atoms at position #1 (top) and #2 (bottom)

7.5 Discussion

As we tried to increase the number of atoms in the simulation samples, we faced some difficulties due to the exponential increase in the computational cost. At first, we tried performing the simulations on fast PCs in our laboratory. However, it would take days to execute 1% of the simulation. Then, we started using the resources of the National Supercomputing Center (Centro Nacional de Supercomputação) (CESUP, 2012). Unfortunately, just after we started using these resources, their cluster began to present some refrigeration problems, resulting in abrupt stops of the executions, which forced us to restart the simulations, some of them days after being started. Despite the efforts of CESUP's staff, this and other problems persisted in the following months.

Every time we restart a process in Orca, it essentially recalculates everything. Also, it is important to note that sometimes the same sample needs to be executed more than once, until it converges, what demands additional time. For example, the impure unit cells presented in Section 7.1 required more than 10 executions each, for convergence.

Beside these problems, by just increasing the number of atoms in the sample, the program execution would be randomly interrupted due to different errors in different points of the process. The fact that these errors were not reproducible hindered the determination of their cause. Even working together for some weeks with people from the technical support of the cluster, it was not possible to determine what was happening. Sometimes, just by resubmitting the sample several times would end up resulting in an execution with no error at all. Such errors could occur due to various causes, including but not limited to: (i) errors in the program used to perform the quantum computation; (ii) non explicit divergences between the configuration of resources allocation in the cluster and in the program; (iii) differences between the configuration of the application programming interface (API) used by the cluster and by the program; and (iv) problems in the input files provided to the program.

Due to these setbacks and the limited time for the development of a Master thesis, it was not possible to perform all the required simulations to complete the work as originally intended. It would be necessary several months just to identify the causes of the errors: review all the configurations, try other clusters (if necessary), and perform tests with other simulation programs. We should say that, despite all the faced problems, the use of the cluster was crucial to the development of this work. Although we did not obtain all the desired results, without using it, we would probably have no results at all.

It is also important to note that the fundamental principle of the proposed simulation technique (*i.e.*, the use of the Molecular Orbital Theory, and Time-Dependent Density Functional Theory) would not be altered to complete all the originally-planned work. The theories we use have been suggested for obtaining absorption spectra (MENNUCCI, 2010). The steps described in the previous sections would also conceptually remain the same. They could, however, suffer some modifications in practical aspects, such as replacing Orca by another program.

This work was practically developed step by step in the same order as described in this chapter. Thus, it was very joyful and interesting to perceive that the obtained (although not all the desired) results behaved as predicted. These results reinforce our initial idea that, with a larger group of bigger samples, it would be possible to use a quantum physics approach for the determination of colors in minerals and maybe in other materials.

There are many things that could be considered as future work. Certainly, the first thing that must be done is to solve the problems mentioned in the previous paragraphs. It would allow us to work with bigger samples and thus be able to complete this work as we conceived it. The completeness would be accomplished by, for example, generating spectra for the expanded version of the silica unit cell, adding different impurities with various concentrations and building a framework with all the steps integrated. However, note that if we had been able to simulate samples with up to a few hundred atoms, we would have fulfilled the original plan; a new range of possibilities would emerge. It would be possible, for example, to work with other minerals or even other kinds of materials.

8 CONCLUSIONS AND FUTURE WORK

This thesis presented a general technique for simulating the colors of minerals based on a quantum approach. Starting from the unit cell that characterizes a mineral (*e.g.*, an agate), larger structures can be obtained by combining multiple such cells, with possible introduction of impurities. By applying the simulation to one such structure, we obtain its corresponding absorption spectrum, from which the resulting color can be obtained. The generality of the proposed solution makes it applicable to arbitrary materials. This should allow us to simulate the appearance not only of natural materials, but also of synthetic ones (even those that are not stable under natural conditions). Such a result should have a great impact in many fields, such as chemistry, engineering, mineralogy, and astrophysics, besides computer graphics. The considerable amount of computational power currently required for performing all necessary experiments and simulations makes this endeavor too big to be undertaken in the scope and time available for a single Master thesis. This work is, however, a first important step along this direction, providing supporting evidence about the correctness of the proposed strategy.

To the field of computer graphics, the main contribution of this thesis is the idea of using a quantum approach for image synthesis. It defines a whole new range of possibilities for mixing computational chemistry and computer graphics. For example, what if we could speed up the quantum calculations to the point of simulating the structure of a whole object (even a very small one) in all its complexity and richness of materials in real time? Or what if we could use molecular dynamics to simulate/develop new materials and see how they would look like, and analyze their properties, such as texture and shine. These are just some of the possibilities.

As future work, we would like to be able to perform all the experiments necessary to apply the proposed solution to arbitrary materials. This will, however, require faster and more reliable computer infrastructure than is currently available in most academic institutions worldwide. We would also like to develop a framework that could be used, for example, by agate producers and sellers. It would simulate not only cuts but also some different dyeing processes to which some agate are submitted in order to enhance their commercial value. This simulation would have to take into account the difference in porosities of agates layers. This is related to the organization of the microcrystalline structure, and interferes with the dyeing process, resulting in a non-uniform and sometimes messy colorization (DAKE, FLEENER and WILSON, 1938).

To obtain more realistic representations for agates, we would have to enhance the algorithm presented in Chapter 6 to treat cases where agates present some crystal formation in their structures. Also, by generating a mesh or other model that we might consider appropriate to work with our volume, we can treat the cases of translucence and other optical effects inside agates and objects sculptured from them.

9 REFERENCES

- ATKINS, P.; FRIEDMAN, R. **Molecular Quantum Mechanics**. 4th. ed. [S.l.]: Oxford Univ. Press, 2005.
- ATKINS, P.; PAULA, J. D. **Physical Chemistry**. 8th. ed. [S.l.]: Oxford University Press, 2006.
- BAIBICH, I. M. **Notas de Aula Química Inorgânica I**. UFRGS. [S.l.]. 2001.
- BARNARD, R.; URAL, S. **Rendering Translucency with Perlin Noise**. GRAPHITE '05. Dunedin, New Zealand: ACM. 2005. p. 131-134.
- BAUERNSCHMITT, R.; AHLRICHS, R. Stability Analysis for Solutions of the Closed Shell Kohn-Sham Equation. **Journal Of Chemical Physics**, v. 104, n. 22, p. 9047-9052, 1996.
- BECKWITH, J. A. **Gem Minerals of Idaho**. [S.l.]: Caxton Printers, 1972.
- BENVENUTTI, E. V. **Química Inorgânica - Átomos, Moléculas, Líquidos e Sólidos**. 3°. ed. [S.l.]: Editora da UFRGS, 2011. 219 p.
- BORN, M.; WOLF, E. **Principles of Optics: Electromagnetic Theory of Propagation, Interference and Diffraction of Light**. 7th. ed. [S.l.]: Cambridge University Press, 1999.
- BRITANNICA, I. E. **Rocks and Minerals**. [S.l.]: Encyclopaedia Britannica, 2008.
- BURKE, K.; WERSCHNIK, J.; GROSS, E. K. U. Time-Dependent Density Functional Theory: Past, Present, and Future. **The Journal of Chemical Physics**, v. 123, n. 6, p. 62206-9, 2005.
- BURKHARDT, C. E.; LEVENTHAL, J. J. **Foundations of Quantum Physics**. [S.l.]: Springer, 2008.
- BURNS, R. G. **Mineralogical Applications of Crystal Field Theory**. 2nd. ed. [S.l.]: Cambridge University Press, 1993.
- CARTER, J. **Lighting Marble**. Proceedings of the 45th Annual Southeast Regional Conference. Winston-Salem, North Carolina: ACM. 2007. p. 8-12.
- CESUP. Centro Nacional de Supercomputação, 2012. Available at: <www.cesup.ufrgs.br>. Access in: March 2012.
- CHVÁTAL, M.; LIMA, I. A. **Mineralogia para Principiantes: Cristalografia**. [S.l.]: Sociedade Brasileira de Geologia, 2007.
- CIBJO. **The Gemstone Book**. Italy: Confédération Internationale de la Bijouterie, Joaillerie, Orfèvrerie, des Diamants, Perles et Pierres, 2010.

CIE. Commission Internationale de L'Eclairage, 2012. Available at: <<http://www.cie.co.at/>>. Access in: January 2012.

CRAMER, C. J. **Essentials of Computational Chemistry: Theories and Models**. [S.l.]: John Wiley and Sons, 2004. 596 p.

CRYSTALMAKER SOFTWARE LTD. **CrystalMaker**, 2011. Available at: <www.crystallmaker.com>. Access in: December 2011.

CULL, S. **Rocks and Minerals**. [S.l.]: Facts on File, 2009.

DAKE, H. C.; FLEENER, F. L.; WILSON, B. H. **Quartz Family Minerals: A Handbook for the Mineral Collector**. [S.l.]: Whittlesey House, McGraw-Hill Book Company, inc., 1938.

DEER, W. A. et al. **Rock-Forming Minerals: Framework Silicates: Slica Minerals, Feldspathoids and the Zeolites**. [S.l.]: Geological Society, 2004.

DONG, Y. et al. **Lazy Solid Texture Synthesis**. Computer Graphics Forum (Proceedings of the Eurographics Symposium on Rendering). [S.l.]: [s.n.]. 2008.

DOUGLAS, B. E.; HO, S. M. **Structure and Chemistry of Crystalline Solids**. [S.l.]: Springer, 2006.

DYALL, K. G. **Introduction to Relativistic Quantum Chemistry**. [S.l.]. 1995.

DYAR, M.; GUNTER, M. E.; TASA, D. **Mineralogy And Optical Mineralogy**. [S.l.]: Mineralogical Society of America, 2007.

FLÖRKE, O. W. et al. Water in Microcrystalline Quartz of Volcanic Origin: Agates. **Contributions to Mineralogy and Petrology**, v. 80, p. 324-333, 1982.

FOX, M. A.; WHITESELL, J. K. **Organic Chemistry**. [S.l.]: Jones and Bartlett Publishers, 2004.

FRIEDMAN, H. **The Mineral and Gemstone Kingdom**, 2011. Available at: <<http://www.minerals.net/>>. Access in: December 2011.

GANCHEFF, J. S.; DENIS, P. A. Time-Dependent Density Functional Theory Investigation of the Electronic Spectra of Hexanuclear Chalcogenide Rhenium(III) Clusters. **The Journal of Physical Chemistry A**, v. 115, n. 2, p. 211-218, 2011.

GIL, V. M. S. **Orbitals in Chemistry: A Modern Guide for Students**. [S.l.]: Cambridge University Press, 2000.

GILLESPIE, R. J.; POPELIER, P. L. A. **Chemical Bonding and Molecular Geometry: From Lewis to Electron Densities**. [S.l.]: Oxford University Press, 2001.

GLICK, D. **Methods of Biochemical Analysis**. [S.l.]: John Wiley & Sons, 2009.

GÖETZE, J. et al. Defect Structure and Luminescence Behaviour of Agate; Results of Electron Paramagnetic Resonance (EPR) and Cathodoluminescence (CL) Studies. **Mineralogical Magazine**, v. 63, n. 2, p. 149-163, 1999.

GRANDE, L.; AUGUSTYN, A.; WEINSTEIN, J. **Gems and Gemstones: Timeless Natural Beauty of the Mineral World**. [S.l.]: University of Chicago Press, 2009.

GREINER, W. **Quantum Mechanics: An Introduction**. 4th. ed. [S.l.]: Springer, 2001.

GRIMME, S. Semiempirical Hybrid Density Functional with Perturbative Second-Order Correlation. **The Journal of Chemical Physics**, v. 124, n. 3, p. 034108, 2006.

GRIMME, S.; NEESE, F. Double-Hybrid Density Functional Theory for Excited Electronic States of Molecules. **The Journal of Chemical Physics**, v. 127, p. 154116, October 2007.

GUMEE, G. Agate Basics, 2011. Available at: <<http://www.agatelady.com/agate-basics.html>>. Access in: December 2011.

GUNTER, M. E. **Optical Mineralogy**. University of Idaho, Moscow. [S.l.]. 2008.

GUY, S.; SOLER, C. **Graphics Gems Revisited: Fast and Physically-Based Rendering of Gemstones**. [S.l.]: ACM. 2004. p. 231-238.

HALL, S. R.; ALLEN, F. H.; BROWN, I. D. The Crystallographic Information File (CIF): A New Standard Archive File for Crystallography. **Acta Crystallographica Section A**, v. 47, n. 6, p. 655-685, 1991.

HALLIDAY, D.; RESNICK, R.; WALKER, J. **Fundamentos de Física**. 6ed. ed. [S.l.]: LTC - Livros Técnicos e Científicos, v. 4, 2003.

HALLIDAY, D.; RESNICK, R.; WALKER, J. **Fundamentals Of Physics Extended**. 8th. ed. [S.l.]: Wiley India Pvt. Ltd., 2008.

HEANEY, P. J.; DAVIS, A. M. Observation and Origin of Self-Organized Textures in Agates. **Science**, v. 269, n. 5230, p. 1562-1565, 1995.

HERBERT, G. F. **Gemstones**. 13th. ed. [S.l.]: Pitman Pub. Corp., 1958.

HIRATA, F. **Molecular Theory of Solvation**. [S.l.]: Kluwer Academic Publishers, 2003.

HOLTEN, T.; JAMTVEIT, B.; MEAKIN, P. Self-Affine Fractal Geometry of Agate. **European Journal of Mineralogy**, v. 10, n. 1, p. 149-153, 1998.

HORNBACK, J. M. **Organic Chemistry**. [S.l.]: Thomson, 2005.

IBGM. **Manual Técnico de Gemas**. 3°. ed. Brasília: República Federativa do Brasil, Ministério de Minas e Energia, Secretaria de Minas e Metalurgia, Departamento Nacional de Produção Mineral, 2005.

IUPAC. **Compendium of Chemical Terminology (the "Gold Book")**. 2nd. ed. Oxford: Blackwell Scientific Publications, v. XML on-line corrected version: goldbook.iupac.org, 1997-2011.

JENSEN, F. **Introduction to Computational Chemistry**. [S.l.]: John Wiley & Sons, 2007.

KOHN, W.; SHAM, L. J. Self-Consistent Equations Including Exchange and Correlation Effects. **Physics Reviews**, v. 140, n. 4A, p. A1133--A1138, 1965.

KOPF, J. et al. **Solid Texture Synthesis from 2D Exemplars**. ACM Transactions on Graphics (TOG) - Proceedings of ACM SIGGRAPH 2007. New York: ACM. 2007.

LANDAU, L. D.; LIFSHITZ, E. M. **Quantum Mechanics: Non-Relativistic Theory**. 3rd. ed. [S.l.]: Butterworth-Heinemann, 1977.

LEE, H.-C. **Introduction to Color Imaging Science**. [S.l.]: Cambridge University Press, 2005.

- LEVIN, F. S. **An Introduction to Quantum Theory**. [S.l.]: [s.n.], 2002.
- LIPKOWITZ, K. B.; CUNDARI, T. R.; BOYD, D. B. (Eds.). **Reviews in Computational Chemistry**. [S.l.]: John Wiley and Sons, v. 26, 2008.
- LORENSEN, W. E.; CLINE, H. E. **Marching cubes**: A high resolution 3D surface construction algorithm. Proceedings of the 14th annual conference on Computer graphics and interactive techniques. [S.l.]: ACM. 1987. p. 7.
- LOWE, J. P.; PETERSON, K. A. **Quantum Chemistry**. 3rd. ed. New York: Academic Press, 2006. xvi, 599 p. : p.
- MACKENZIE, W. S.; GUILFORD, C. **Atlas of Rock-Forming Minerals in Thin Section**. [S.l.]: Longman Scientific & Technical, 1994.
- MCQUARRIE, D. A.; SIMON, J. D. **Physical Chemistry: A Molecular Approach**. [S.l.]: University Science Books, 1997.
- MENNUCCI, B. The Simulation of UV-Vis Spectroscopy with Computational Methods. In: GRUNENBERG, J. **Computational Spectroscopy: Methods, Experiments and Applications**. [S.l.]: John Wiley & Sons, 2010. Cap. 5.
- MESSLER, G. L. **Inorganic Chemistry**. [S.l.]: Prentice-Hall, Inc., 2003.
- MOSS, R. A.; PLATZ, M.; JONES, M. **Reactive Intermediate Chemistry**. [S.l.]: Wiley-Interscience, 2004.
- MOXON, T.; REED, S. J. B. Agate and Chalcedony from Igneous and Sedimentary Hosts Aged from 13 to 3480 Ma: A Cathodoluminescence Study. **Mineralogical Magazine**, v. 70, n. 5, p. 485-498, 2006.
- MUELLER, M. **Fundamentals of Quantum Chemistry: Molecular Spectroscopy and Modern Electronic Structure Computations**. [S.l.]: Springer, 2001.
- NARDY, A. J. R.; MACHADO, F. B. **Mineralogia Óptica**. Unesp. [S.l.]. 2002.
- NASSAU, K. The Origins of Color in Minerals. **American Mineralogist**, v. 63, n. 3-4, p. 219-229, 1978.
- NASSAU, K. **The Physics and Chemistry of Color: The Fifteen Causes of Color**. [S.l.]: Wiley, 2001.
- NEESE, F. ORCA – An Ab Initio, Density Functional and Semiempirical Program Package, Version 2.6. **University of Bonn**, 2008.
- NEESE, F. Some Thoughts on the Scope of Linear Scaling Self-Consistent Field Electronic Structures Methods. In: PAPADOPOULOS, M. G. **Linear-Scaling Techniques in Computational Chemistry and Physics: Methods and Applications**. [S.l.]: Springer, 2011. Cap. 11.
- NEESE, F.; WENNMÖHS, F. **Orca - An Ab Initio, DFT and Semiempirical SCF-MO Package**. [S.l.]. 2010.
- NICKEL, E. H. The Definition of a Mineral. **The Canadian Mineralogist**, v. 33, p. 689-690, 1995.
- O'DONOGHUE, M. **Gems: Their Sources, Descriptions and Identification**. [S.l.]: Butterworth-Heinemann, 2006.

OLMSTED, J.; WILLIAMS, G. M. **Chemistry, The Molecular Science**. [S.l.]: Mosby, 1996.

ORTOLEVA, P. J.; CHEN, Y.; CHEN., W. **Agates, Geodes, Concretions and Orbicules: Self-Organized Zoning and Morphology**. [S.l.]: Springer-Verlag. 1994. p. 283-305.

PACCHIONI, G. Theory of Metal Clusters on the MgO Surface: The Role of Point Defects. In: HEIZ, U.; LANDMAN, U. **Nanocatalysis**. [S.l.]: Springer, 2007. Cap. 2.

PAULING, L. **General chemistry**. 3rd. ed. [S.l.]: Dover Publications, 1988.

PERLIN, K. An Image Synthesizer. **SIGGRAPH '85**, v. 19, n. 3, p. 287-296, 1985.

PHARR, M.; HUMPHREYS, G. **Physically Based Rendering: From Theory to Implementation**. San Francisco, CA, USA: Morgan Kaufmann Publishers Inc., 2004b.

POLK, P. **Collecting Rocks, Gems and Minerals: Identification, Values, Lapidary Uses**. [S.l.]: Krause Publications, 2010.

PRICE, M.; WALSH, K. **Rocks and Minerals**. [S.l.]: Dorling Kindersley, 2005.

READ, P. G. **Gemmology**. 3rd. ed. [S.l.]: Butterworth-Heinemann, 2005.

REINHARDT, J. **Principles of Mineral Optics**. School of Geological Sciences, University of KwaZulu-Natal. [S.l.]. 2008.

SCHÄFER, A.; HORN, H.; AHLRICHS, R. Fully Optimized Contracted Gaussian Basis Sets for Atoms Li to Kr. **The Journal of Chemical Physics**, v. 97, n. 4, p. 2571-2577, 1992.

SCHUMANN, W. **Gemstones of the World**. 4th. ed. [S.l.]: Sterling, 2009.

SHARMA, S. K. **Atomic and Nuclear Physics**. [S.l.]: Pearson Education, 2008. 620 p.

SHEVELL, S. K. (Ed.). **The Science of Color**. 2nd. ed. [S.l.]: Optical Society of America, 2003.

SHOLL, D.; STECKEL, J. A. **Density Functional Theory: A Practical Introduction**. [S.l.]: John Wiley & Sons, 2011.

SMART, L. E.; MOORE, E. A. **Solid State Chemistry: An Introduction**. 3rd. ed. [S.l.]: CRC Press, 2005.

SMOOT, R. C.; PRICE, J.; SMITH, R. G. **Chemistry: a modern course**. [S.l.]: Charles E. Merrill, 1983. Available at: <<http://boomeria.org/chemlectures/crystals/basic.jpg>>. Access in: December 2011.

SOLÉ, J. G.; BAUSÁ, L. E.; JAQUE, D. **An Introduction to the Optical Spectroscopy of Inorganic Solids**. [S.l.]: Wiley, 2005.

SUN, Y.; FRACCHIA, F. D.; DREW, M. S. **Rendering the Phenomena of Volume Absorption in Homogeneous Transparent Materials**. The 2nd Annual IASTED International Conference on Computer Graphics and Imaging (CGIM'99). [S.l.]: [s.n.]. 1999. p. 283-288.

SUN, Y.; FRACCHIA, F. D.; DREW, M. S. **Rendering Diamonds**. Western Computer Graphics Symposium 2000. [S.l.]: [s.n.]. 2000a.

SUN, Y.; FRACCHIA, F. D.; DREW, M. S. **Rendering Light Dispersion With a Composite Spectral Model**. International Conference on Color Graphics and Image Processing - CGIP '2000. [S.l.]: [s.n.]. 2000b.

SYMES, R. F.; HARDING, R. R. **Eyewitness Guides: Crystal & Gem**. 3rd. ed. New York: Dorling Kindersley Limited, 2007.

SZABÓ, A.; OSTLUND, N. S. **Modern Quantum Chemistry: Introduction to Advanced Electronic Structure Theory**. Mineola, New York: Courier Dover Publications, 1996.

TAKAYAMA, K. et al. Lapped Solid Textures: Filling a Model with Anisotropic Textures. **ACM Transactions on Graphics (TOG) - Proceedings of ACM SIGGRAPH 2008**, v. 27, n. 3, p. 1-9, 2008.

TAKAYAMA, K. et al. Volumetric Modeling with Diffusion Surfaces. **ACM Transactions on Graphics (TOG) - Proceedings of ACM SIGGRAPH Asia 2010**, v. 29, n. 6, p. 180:1--180:8, 2010.

TAKAYAMA, K.; IGARASHI, T. **Layered Solid Texture Synthesis from a Single 2d Exemplar**. Proceeding SIGGRAPH '09: Posters. New York: ACM. 2009. p. 86:1--86:1.

TANNENBAUM, D. C.; TANNENBAUM, P.; WOZNY, M. J. **Polarization and Birefringency Considerations in Rendering**. Proceeding SIGGRAPH '94. New York: ACM. 1994. p. 221-222.

THOMAS, A. **Gemstones: Properties, Identification and Use**. [S.l.]: New Holland, 2008.

VAN LENTHE, E.; BAERENDS, E. J.; SNIJDERS, J. G. Relativistic Regular Two-Component Hamiltonians. **The Journal of Chemical Physics**, v. 99, n. 6, p. 4597-4610, 1993.

VAN VLECK, J. H. Quantum Mechanics - The Key to Understanding Magnetism. **Reviews of Modern Physics**, v. 50, n. 2, p. 181-189, 1978.

VANDEVENNE, L. Texture Generation using Random Noise, 2004. Available at: <<http://lodev.org/cgtutor/randomnoise.html#Turbulence>>. Access in: December 2011.

VASILIEV, I.; ÖGÜT, S.; CHELIKOWSKY, J. R. First-Principles Density-Functional Calculations for Optical Spectra of Clusters and Nanocrystals. **Physical Review B**, v. 65, n. 11, p. 115416, March 2002.

WANG, L. et al. Vector Solid Textures. **ACM Transactions on Graphics - Proceedings of ACM SIGGRAPH 2010**, New York, v. 29, n. 4, p. 86:1--86:8, 2010.

WANG, L. et al. Multiscale Vector Volumes. **ACM Transactions on Graphics (TOG) - Proceedings of ACM SIGGRAPH Asia 2011**, New York, v. 30, n. 6, p. 167:1--167:8, 2011.

WANG, Y.; MERINO, E. Self-Organizational Origin of Agates: Banding, Fiber Twisting, Composition, and Dynamic Crystallization Model. **Geochimica et Cosmochimica Acta**, v. 54, n. 6, p. 1627-1638, 1990.

WEIDLICH, A.; WILKIE, A. **Modeling Aventurescent Gems with Procedural Textures**. Proceedings of the 24th Spring Conference on Computer Graphics. New York: ACM. 2008a. p. 51--58.

WEIDLICH, A.; WILKIE, A. Realistic Rendering of Birefringency in Uniaxial Crystals. **ACM Transactions on Graphics**, New York, v. 27, n. 1, p. 6:1--6:12, 2008b.

WEIDLICH, A.; WILKIE, A. **Rendering the Effect of Labradoescence**. [S.l.]: Canadian Information Processing Society. 2009. p. 79-85.

WEIGEND, F.; AHLRICHS, R. Balanced Basis Sets of Split Valence, Triple Zeta Valence and Quadruple Zeta Valence Quality for H to Rn: Design and Assessment of Accuracy. **Physical Chemistry Chemical Physics**, v. 7, n. 18, p. 3297-3305, August 2005.

WHITTED, T. **An improved illumination model for shaded display**. SIGGRAPH '79: Proceedings of the 6th annual conference on Computer graphics and interactive techniques. New York: ACM. June 1979. p. 7.

WILKIE, A.; TOBLER, R. F.; PURGATHOFER, W. **Raytracing of Dispersion Effects in Transparent Materials**. In WSCG 2000 Conference Proceedings. [S.l.]: [s.n.]. 2000.

WOLFRAM. Mathematica, 2010a. Available at: <<http://www.wolfram.com/mathematica/>>. Access in: 2010.

WOLFRAM. MathLink API, 2010b. Available at: <<http://reference.wolfram.com/mathematica/guide/MathLinkAPI.html>>. Access in: 2010.

WOLTER, S. F. **Lake Superior Agate**. [S.l.]: Burgess Pub., 1996.

WOON, D. E.; DUNNING, T. H. Gaussian Basis Sets for Use in Correlated Molecular Calculations. III. The Atoms Aluminum Through Argon. **The Journal of Chemical Physics**, v. 98, n. 2, p. 1358-1371, 1993.

WULFSBERG, G. **Inorganic Chemistry**. [S.l.]: University Science Books, 2000.

ZHANG, W.-Q. General Ray-Tracing Formulas for Crystal. **Applied Optics**, v. 31, n. 34, p. 7328-7331, 1992.

ZIM, H. S.; SHAFFER, P. R.; PERLMAN, R. **Rocks and Minerals**. [S.l.]: Turtleback Books, 1989.

ZUMDAHL, S. S.; ZUMDAHL, S. A. **Chemistry**. 8th. ed. [S.l.]: Brooks/Cole, Cengage Learning, 2010.

APPENDIX A: PHYSICAL AND CHEMICAL BACKGROUND

This appendix presents a brief overview of some physical and chemical background related to the subjects covered by this thesis. It is not intended to replace the reading of a good chemistry book, such as (BENVENUTTI, 2011), (ATKINS and FRIEDMAN, 2005), (WULFSBERG, 2000), or (PAULING, 1988), or cover the state of art definitions in chemistry and physics about the mentioned subjects. Its goal is to give a general introduction and understanding of the principles that guide the proposed technique.

A.1 Orbitals

The Heisenberg **Uncertainty Principle** states that is not possible to determine the position and momentum (*i.e.*, speed and direction) of a small particle, such as an electron, at the same time. This implies that we cannot describe precisely the electrons motion. Thus, we can only define the region in the space where there is the highest probability of finding a specific electron (ATKINS and FRIEDMAN, 2005). This region is called **orbital**. The equation that defines this probability is the Schrödinger wave equation, which treats the electron as a wave function and is given by (NASSAU, 2001):

$$\int \psi^2 dv,$$

where ψ is the wave function which describes the electron as a wave; dv is the volume element given by $dv = dx \cdot dy \cdot dz$, and $\psi^2 dv$ is the orbital.

A solution of the Schrödinger wave equation describes the position and energy of an electron in an atom, *i.e.*, describes an atomic orbital. These atomic orbitals can be expressed in terms of four quantum numbers, which are going to be described next.

A.1.1 Quantum Numbers

When a system is described in terms of quantum mechanics, the result of the Schrödinger wave equation does not present a single solution, but rather a set of solutions. Each individual solution is a wave function ψ containing a variable number of parameters: the *quantum numbers* (NASSAU, 2001). Appropriate solutions for ψ are only obtained if the quantum numbers have specific values. For each set of values, the energy of the system can be calculated. Thus, the quantum numbers are a set of four values used as parameters of the Schrödinger wave equation and, therefore, describe the highly-probable location of an electron in an atom (SHARMA, 2008), (ATKINS and PAULA, 2006). The following sections present these numbers. Their contents were based on (BURKHARDT and LEVENTHAL, 2008) and (ATKINS and PAULA, 2006).

A.1.1.1 Principal Quantum Number: n

It accepts any integer number bigger than zero ($n = 1, 2, 3 \dots$). It is limited to the number of shells presented in the atom. It is the indicator of the number of the shell in which the electron is. Thus, it is related to the electron's distance to the nucleus. This value is used to determine the amount of energy of an atom.

A.1.1.2 Azimuthal Quantum Number (Angular Momentum): l

It accepts any integer value smaller than n and specifies a sub-level in an orbital. It is related to the orbital angular momentum of a particle in uniform circular motion. It is also related to the shape of the orbital. Although the values of l admit integer numbers, they are best known by their historical names “s”, “p”, “d” and “f”. Where, s is 0, p is 1, d is 2 and f is 3. These names are due to the fact that the quantum numbers have been discovered from the study of light. The lines of the electromagnetic spectrum were classified according to their quality: *sharp*, *principal*, *diffuse*, and *fundamental*. A transition element is one for which the shells d or f are not completely filled. If an ion is isolated, the probability of an electron be in any of the d orbitals is the same. But in a crystal structure, the electrostatic field splits the d orbitals into different energy levels. The way the orbital is split depends on the type, positions, and symmetry of the ligands around the ion (BURNS, 1993).

A.1.1.3 Magnetic Quantum Number: m_l

It accepts any positive or negative integer value ranging from $-l$ to $+l$.

Each sublevel is composed of one or more orbitals. When $l = 1$, for example, m accepts three values: - 1, 0 and +1. As we have seen in previous section, the sublevel for $l = 1$ is p . And, in conjunction with analyzing the value of m , it is concluded that the p orbital has three components which are usually called p_x , p_y and p_z . These names are related to the x, y and z axes of a 3D coordinate system and, as will be discussed in Section A.1.3, are directly related to the orbital position relative to these axes in space. According to the shape of the orbital, it can have a different direction when in presence of a magnetic field. The s orbital can have one direction, p can have three (three fold degeneracy: p_x , p_y , p_z), d five (five fold degeneracy: d_{xy} , d_{yz} , d_{xz} , $d_{x^2-y^2}$, d_{z^2}) and so on. Table A.1 presents the possible values for n , l and m . In this table only the values of n ranging from one to three are represent. For values of n greater than three, the logic for setting up the table would be similar.

Table A.1: Possible values for n , l and m .

n	l	m	DENOMINATION
1		0	1s
2	0	0	2s
	1	-1	2p _x
		0	2p _y
		+1	2p _z
3	0	0	3s
	1	-1	3p _x
		0	3p _y
		+1	3p _z
	2	-2	3d _{xy}
		-1	3d _{xz}
		0	3d _{yz}
		+1	3d _{x²-y²}
		+2	3d _{z²}

A.1.1.4 Spin: s

It accepts the values $+1/2$ and $-1/2$.

The electron is a wave, but it is also a particle, therefore, it has rotational motion. This rotation causes it to create electromagnetic energy. Spin are moves for or against the magnetic field where the electron was placed. They indicate the orientations of the electron (clockwise or anticlockwise).

A.1.2 Electron configuration

Knowing the electron configuration of an atom is important because it determines the shape of the orbitals. Each orbital corresponds to an energetic level. For an electron to go from one level to another they need to emit/absorb energy. The Pauli Exclusion Principle states that two electrons in an atom cannot have the same set of quantum numbers. If they were equal, it would be like if two bodies were occupying the same place in space. An orbital can have two electrons as long as they are spinning in opposite directions. The filling sequence of layers is always performed through the addition of electrons one by one in the available level which has the least energy.

When the levels s and p for any value of n are complete, this represents a steady state of noble-gas configuration. It takes a lot of energy to interact with these internal arrangements. Thus, the electrons that have acquired a noble-gas configuration will no longer combine with electrons from other atoms. This is the reason why when an atom combines with another and gains or losses electrons, forming ions, this exchange occurs only in the valence shell (outermost layer) (NASSAU, 2001). Below, we have the electron configuration Beryllium (element Be of the Periodic Table):



Where $[\text{He}]$ represents the electron configuration of the noble-gas immediately before the element Be in the table. In other words, they are the electrons that are not going to react anymore. Only the two electrons of the $2s$ layer are going to interact with electrons from other atoms. Figure A.1 presents a simplified representation of the Periodic Table. The values above the columns directly indicate the electron configuration of the corresponding element and n is the Principal quantum number.

ns												np					
1	2											1	2	3	4	5	6
		(n-1)d															
		1	2	3	4	5	6	7	8	9	10						
		LA															
		AC															

(n-2)f														
	1	2	3	4	5	6	7	8	9	10	11	12	13	14
LA														
AC														

Figure A.1: Simplified representation of the Periodic Table.

Hence, based on Figure A.1, it is possible to directly obtain the electron configuration of the elements. Some examples are given below:

$\text{Na} = [\text{Ne}] 3s^1$	(Sodium)
$\text{Pb} = [\text{Xe}] 6s^2 5d^{10} 6p^2$	(Lead)
$\text{Fe} = [\text{Ar}] 4s^2 3d^6$	(Iron)
$\text{Fe}^{+2} = [\text{Ar}] 3d^6$	(Iron ion)
$\text{Fe}^{+3} = [\text{Ar}] 3d^5$	(Iron ion)

In these examples it is clear that the electrons from the element Fe that are being lost are always being removed from the outer level. However, observe that to fill the layers, you must first fill out all possible orbitals. For, to enter the same orbital, the electron spin would have to change, what would require the electron to spend a lot of energy. It is the Principle of Maximum Multiplicity of Hund.

For example, the configuration of two electrons in a p orbital is: $\boxed{\uparrow}\boxed{\uparrow}\boxed{}$

And not as it would be initially expected: $\boxed{\uparrow\downarrow}\boxed{}\boxed{}$

Due to this principle there are some exceptions in the electron configuration of certain elements, which try to be more stable. Table A.2 presents these exceptions and their expected and real settings (BAIBICH, 2001).

Table A.2: Exceptions of the electron configuration.

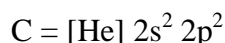
Element	Expected	Obtained	Element	Expected	Obtained
Cr	$[\text{Ar}] 4s^2 3d^4$	$ns^1(n-1)d^5$	Cu	$[\text{Ar}] 4s^2 3d^9$	$ns^1(n-1)d^{10}$
Mo	$[\text{Kr}] 5s^2 4d^4$		Ag	$[\text{Kr}] 5s^2 4d^9$	
W	$[\text{Xe}] 6s^2 5d^4$		Au	$[\text{Xe}] 6s^2 5d^9$	

It is noteworthy that these configurations are from the ground state of the atom, its most stable state.

A.1.2.1 Hybridization

The reorganization of the electrons in orbitals does not occur only in individual orbitals as seen in the previous session. It can also occur between orbitals, resulting into hybrid orbitals. This process is called hybridization.

As an example, we can examine the electron configuration of the Carbon:



If we use arrows to represent its orbitals we obtain:

$\uparrow\downarrow$	\uparrow	\uparrow	
2s	2p _x	2p _y	2p _z

However, to achieve a more stable state, there is a promotion of one electron from the s orbital to the p orbital:

\uparrow	\uparrow	\uparrow	\uparrow
2s	2p _x	2p _y	2p _z


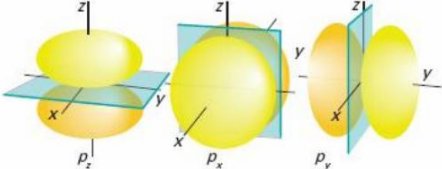
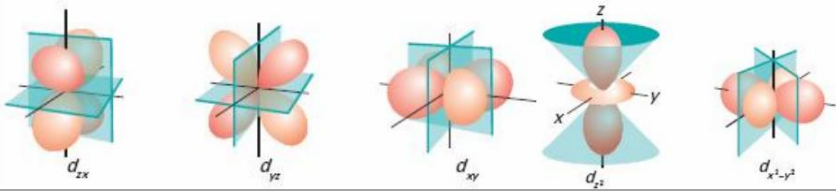
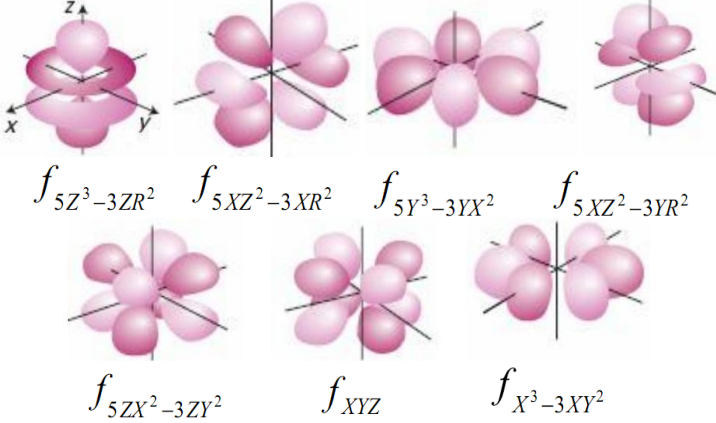
This is just a brief introduction to the process of hybridization. More information can be found at (FOX and WHITESELL, 2004) and (HORNBACK, 2005).

A.1.3 The Shape of Orbitals

The wave functions resulting from Schrödinger's equation may have positive or negative sign. If squared and normalized, the result will always be positive and represents the density of the electron cloud. However, the signal is important because it is responsible for controlling the interaction between electrons (ZUMDAHL and ZUMDAHL, 2010), (WULFSBERG, 2000).

All s orbitals have a spherical symmetric distribution of the electrons. The nucleus is located in the center and the size of the orbital depends on the value of n. A larger n results in a bigger electron cloud. It is important to note that the figures usually used to represent the orbitals are only schematic, since they do not have fixed borders. The three p orbitals are no longer spherically symmetric, but are made up of two lobes, one derived from a positive value of the equation and the other from a negative (NASSAU, 2001). The shape of the orbitals d and f is also no longer spherical. Table A.3 presents a graphical representation of the possible individual orbitals. Electrons which participate in processes of hybridization have an orbital which is a hybrid of the individual orbitals involved (MCQUARRIE and SIMON, 1997).

Table A.3: Graphical representation of the orbitals.

Orbital	Possible Shapes
s	
p	
d	
f	

(Source: <http://pt.scribd.com/doc/14420276/Quimica-Inorganica-I>. Access in June, 2012).

A.2 Definition of Mass and Matter

The mass in the universe presents itself in two basic forms: as radiation (photons) and as matter. Under normal conditions of the human beings' environment, the matter comes basically in three physical states: gas, liquid and solid. The physical state of matter varies according to the environment where it is located, specially, with temperature and pressure. Theoretically, therefore, regardless of their chemical composition, each matter may occur in each of these three physical states (CHVÁTAL and LIMA, 2007). Figure A.2 presents a phase diagram. Consisting of a graph representing the state in which a compound is according to a certain temperature and pressure.

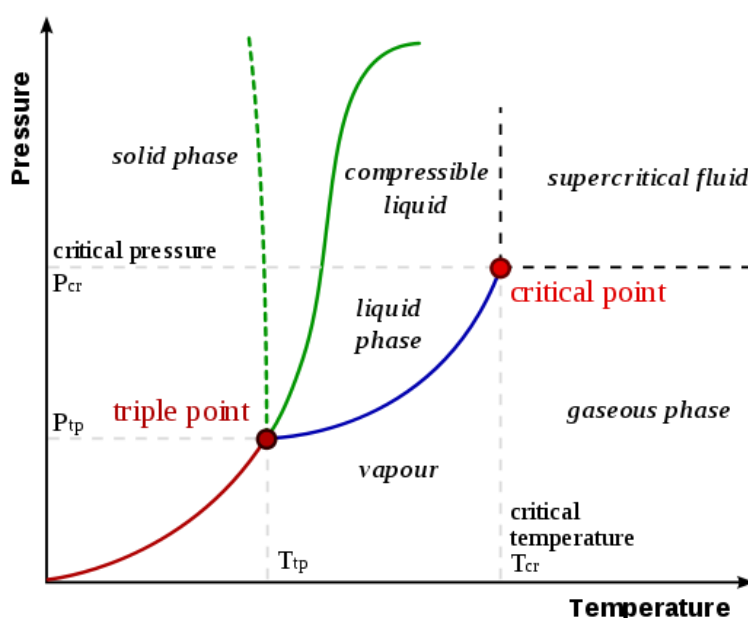


Figure A.2: Phase Diagram(Source: http://en.wikipedia.org/wiki/Phase_diagram. Access in June, 2012.).

The gaseous state is characterized by a relatively small number of identities (atoms, ions, molecules) per unit of volume and a small number of collisions between them. For liquids, it is typical a greater number of identities per unit of volume, as well as a larger number of collisions between them. The solids are characterized by greater proximity between their constituents. The movement of these identities is limited to a relatively small space in the vicinity of certain points (the equilibrium position), given that the binding energy between the atoms (ions, molecules) that requires the energy of their thermal motion (CHVÁTAL and LIMA, 2007).

The solid matter is the focus of this work; it can be classified into two groups: (i) crystalline material and (ii) amorphous materials. Crystal is a body with regular and periodic three-dimensional arrangement. This type of arrangement is called the crystal structure. On the other hand, in amorphous materials, the distribution is irregular. From this point of view, amorphous materials are similar to liquids and, indeed, may be taken by very slow fluid flow; glass, for example, stands out among the amorphous material

(CHVÁTAL and LIMA, 2007). Figure A.3 shows the structure of a crystalline material (left) and amorphous (right).

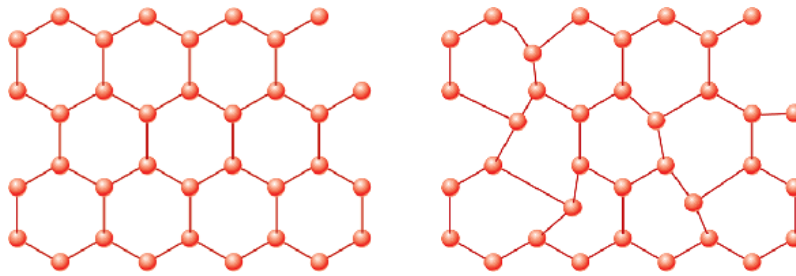


Figure A.3: Structure of a crystalline (left) and an amorphous material (right) (CHVÁTAL and LIMA, 2007).

It is important to note that a crystal is defined by its internal three-dimensional periodic structure, and not based on its outer edge. That is, the crystals are not only those perfect bodies, bound by their smooth faces, displayed in museums, but also the slivers of varying size, the nuggets, the grains irregularly limited, etc. The flat crystal faces are developed only in crystals that are not prevented from growth by the environment in which they are, so that the external format of a crystal is not a mere reflection of its structure. On the other hand, the polishing of an amorphous material (glass, for example) into a perfect crystalline shape does not result in a perfect crystal, because it does not fulfill the condition of having three-dimensional periodic internal structure (CHVÁTAL and LIMA, 2007). In Figure A.4 only items (a), (b) and (c) are crystals. Item (d) shows only regular external structure.

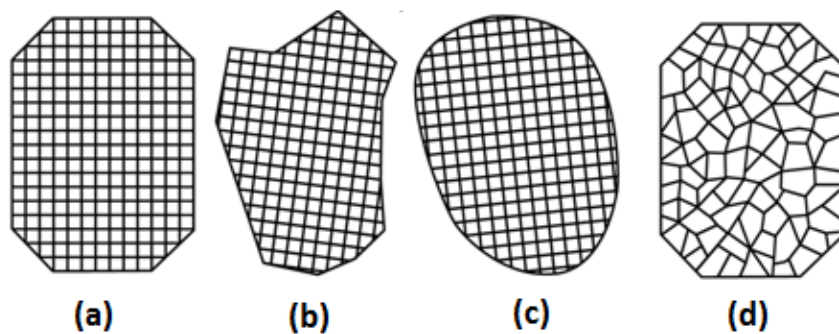


Figure A.4: Only items (a), (b) and (c) are crystals (CHVÁTAL and LIMA, 2007).

A.3 Light

In this section we will present theories on light. There are innumerable books about physics and optics which cover this subject in a very detailed and advanced form. Therefore, we are going to briefly mention the basic concepts of some aspects related to this subject such as: definition of light, refractive and reflective indices, interaction of light with matter, etc.

A.3.1 Definition of Light

James Maxwell showed that a light ray is a progressive wave of electric and magnetic fields, that is, an electromagnetic wave. As can be seen in Figure A.5, we know a broad spectrum of electromagnetic waves. The visible region of the spectrum is the one we are most interested in. The wavelengths' intervals corresponding to the different colors of the spectrum are not well defined. So the colors changes from one to the other gradually. The sensitivity limits of the human eye are approximately 430 and 690nm and may be higher if the radiation is intense enough (HALLIDAY, RESNICK and WALKER, 2003).

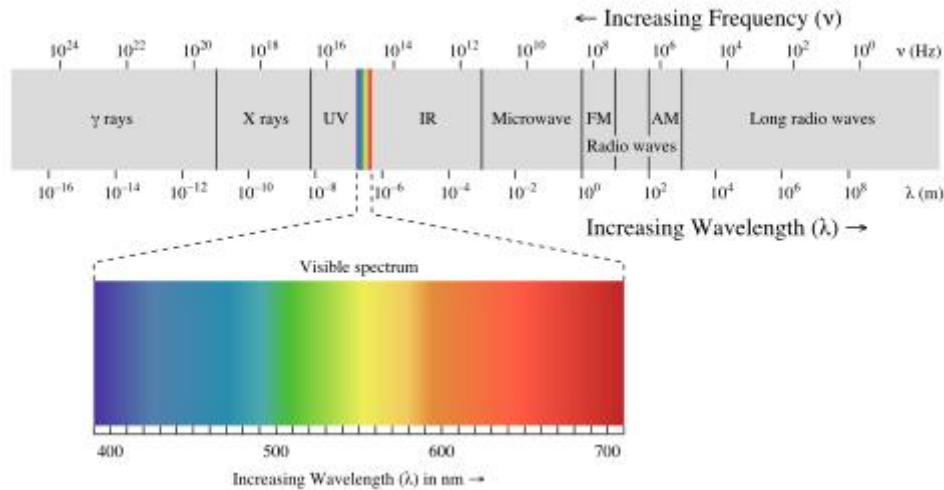


Figure A.5: Electromagnetic spectra (HALLIDAY, RESNICK and WALKER, 2008).

An electromagnetic wave is a transverse wave. That is, the electric and magnetic fields are perpendicular to the direction of wave propagation. These fields are also perpendicular to each other. Figure A.6 shows a wave propagating in the direction c and their respective electric and magnetic fields (HALLIDAY, RESNICK and WALKER, 2003).

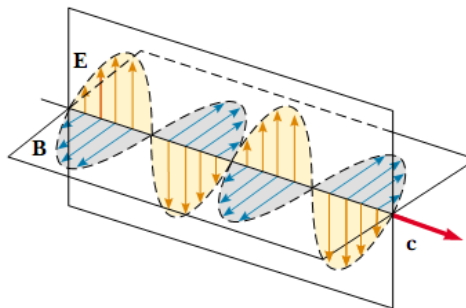


Figure A.6: Wave propagation in the c direction and its electric and magnetic fields (HALLIDAY, RESNICK and WALKER, 2008).

Electromagnetic waves do not require a medium to propagate.

If at the human retina arrive simultaneously waves with wavelengths from 3900 to 7700 Å, the brain interprets this radiation as white light. In other words, white light is the "mixture" of all the colors of the visible light spectrum.

The frequency of light is given by:

$$f = \frac{v}{\lambda}$$

where v is the speed of light in the medium and λ is the wavelength.

This frequency is fixed for a given light source and remains constant even if the light passes through different media (REINHARDT, 2008).

The following is a series of concepts and definitions adapted from (NARDY and MACHADO, 2002).

Wavelength (λ): It is the distance between two consecutive and identical positions (or in phase) in the direction of the propagation of a wave. The wavelength in the case of visible light, is given in Angstroms, \AA , where $1\text{\AA} = 1 \times 10^{-7} \text{ mm} = 1 \times 10^{-1} \text{ m}\mu$. Figure A.7 shows the distance of a wavelength λ , with amplitude A .

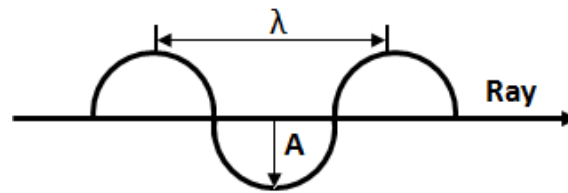


Figure A.7: Distance of a wavelength λ , with amplitude A .

Period (T): It is the time spent to complete an oscillation, that is, the time needed to travel to a distance equal to one wavelength (λ). The period is expressed in seconds.

Frequency (N): The number of oscillations completed in a certain unit of time. The frequency is expressed in cycles per second or Hz. Note that the period is the inverse of frequency, that is:

$$N = \frac{1}{T}$$

Speed of light (c): The speed of light in vacuum is the same for all colors and it is equal to: $c = 299.776(\pm 4) \text{ Km/s}$. The relationship between these quantities is:

$$N = \frac{c}{\lambda}$$

It should also be considered that the frequency of the oscillations does not change when the waves pass through different media. When a ray of light undergoes refraction there might be changes in speed and/or in its wavelength, but never in its frequency.

Monochromatic light: This is light composed of a single wavelength or several which vary in a fairly narrow range, i.e.: The Sodium vapor lamp with λ ranging between 5890 and 5896 \AA .

Polychromatic light: It is the light composed of a wide range of wavelengths, i.e.: Sunlight, household light bulb, etc. The petrographic microscope uses a polychromatic light source, obtained through a tungsten filament lamp (similar to a household light bulb), yellowish, to which is added a blue filter to make it white. The use of polychromatic light in the microscope is desirable because it promotes the phenomenon of dispersion of the refractive indices in minerals. The monochromatic light in turn, is used only in precision optical measurements, as in refractometers (equipment that measures the refractive index of minerals and liquids).

Ray: It is the direction of propagation of light from the point of origin to any other point. In homogeneous media, the rays are straight.

Beam: It's a set of light rays that start from the same source.

A.3.2 Photons

A quantized magnitude is the one that has only integer multiples of an elemental amount. Quantum is the elemental amount of this quantized magnitude. Einstein proposed that electromagnetic radiation is quantized. Photon is as it is called the elemental amount of light (HALLIDAY, RESNICK and WALKER, 2003).

The energy of a photon (light quantum) of frequency f is given by:

$$E = hf,$$

where h is Planck's constant. The energy of a single photon (hf) is the lowest energy that a light wave of frequency f can have.

When light interacts with an object, it is absorbed or emitted by the atoms that constitute this object. When the absorption of a photon occurs, the atom acquires the energy contained in this photon which is thus annihilated. When the emission of a photon occurs, it means that the atom is releasing energy as light, it is the creation of a photon. Not necessarily the same amount of absorbed photons will be emitted and vice versa (HALLIDAY, RESNICK and WALKER, 2003).

A.3.3 Wave-Particle Duality

The light can be seen as both a wave and a particle depending on the physical process that is being studied. The colors of the visible light are defined in terms of wavelength. The perception of color by an individual is related to the sensitivity of your eyes. The theory of light as wave describes the light as a longitudinal wave whose direction of propagation and energy transfer are perpendicular. The theory of light as a particle describes the light as composed of photons of different energies and with these energies related to the wavelength in the electromagnetic theory (GUNTER, 2008).

A.3.4 Polarized Light

Light behaves like an electromagnetic wave. This wave propagates according to a transverse undulatory motion in which the direction of vibration is perpendicular to the direction of propagation. In natural light, or non-polarized, the electric field changes randomly with time, but remains perpendicular to the direction of propagation of the ray. Figure A.8 presents an example of non-polarized light, where the arrows represent the different directions taken by the electric field. The polarized light, in turn, has an electric field that oscillates in only one direction, as shown in Figure A.9.

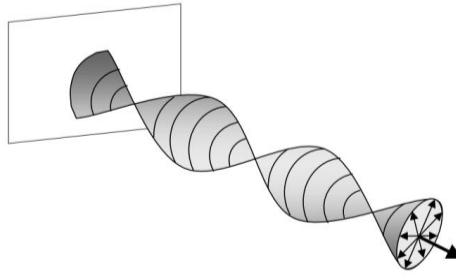


Figure A.8: Non polarized light (GUNTER, 2008).

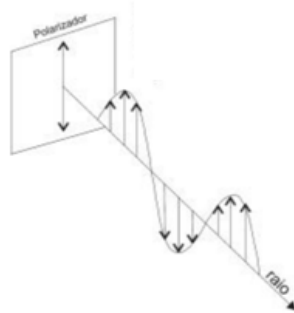


Figure A.9: Polarized light(NARDY and MACHADO, 2002).

A.3.5 Refraction and Reflection

Geometrical optics is the study of the properties of light waves which is based on the assumption that light travels in a straight line. And thus, it is possible to determine the behavior that a ray of light will have when reaching a surface.

Figure A.10 shows an example of the propagation of a light wave, where a beam of light falls on a flat surface. Some of the light is reflected, i.e., it is re-emitted by the surface. Part penetrates, forming a beam that propagates down the surface. If it is a transparent material, the light that penetrated will be refracted. Refraction is the passage of light through a surface that separates two different media. The light beams in Figure A.10 represent the incident ray, the reflected, the refracted and the angles associated. The orientation of these rays is measured relative to the surface normal. The plane containing the normal and the incident ray is the plane of incidence (HALLIDAY, RESNICK and WALKER, 2003).

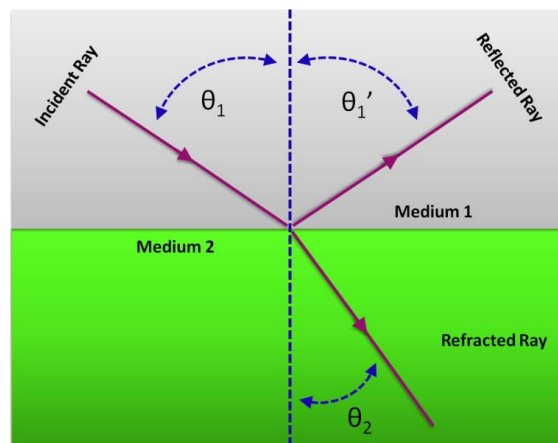


Figure A.10: Propagation of a light wave.

The law of reflection says that the reflected ray is in the plane of incidence and has a reflection angle equal to the incidence angle which, following the denomination of Figure A.10, is $\theta'_1 = \theta_1$.

As for the refraction, its behavior depends on the medium where the light is propagating. The Refractive Index (η) exists to consider this aspect. It is a dimensionless constant that represents the change in the speed of light as it passes from one medium to another and can be defined as:

$$\eta = \frac{v_v}{v_m}$$

where η is the refraction index; v_v is the speed of light in vacuum and v_m is the speed of light for an specific wavelength in a certain medium.

The quantum theory of light is used to explain the changes in refractive index. When photons penetrate into a material they are decelerated by the interaction with electrons and, the greater the deceleration, the higher refractive index. Likewise, increasing the electron density increases the value of the index. This value is also related to the bonds of the atom. In general, ionic compounds have lower values than covalent. In covalent bonds there are more electrons being shared, thus, there are more electrons distributed through the structure and interacting with the incident photons (GUNTER, 2008).

Geometrically, the light passes through a crystal with the incident and transmitted rays following Snell's law:

$$n_i \sin(\theta_i) = n_t \sin(\theta_t)$$

where n_i is the index of refraction of the incident medium; n_t is the index of refraction of the transmission medium; θ_i is the incident angle and θ_t is the transmission or refraction angle. Many concepts of physical optics and ray tracing algorithms are based on this formula. It is obeyed by all isotropic materials.

The refractive index of a material is dependent on the wavelength of incident light. That is, a light beam formed by rays of different wavelengths, will have different angles of refraction for each ray. Resulting in a scattering of rays called chromatic dispersion (HALLIDAY, RESNICK and WALKER, 2003). The rainbow is an example of dispersion. White light is composed of different wavelengths and each has a different refractive index, which causes the different colors of the rainbow. Figure A.11 presents the propagation of a beam of white light through a glass prism of triangular cross section. It can be seen that dispersion occurs when light enters the glass and intensification when the light leaves the glass.

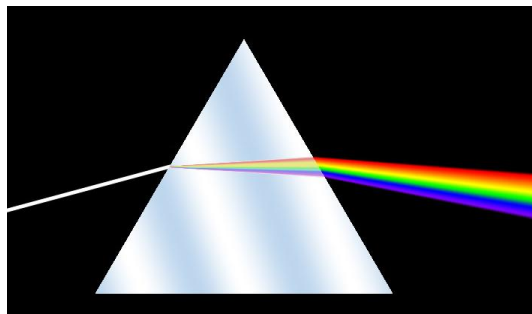


Figure A.11: Propagation of a white light beam through a prism(Source: http://en.wikipedia.org/wiki/File:Dispersion_prism.jpg. Access in June, 2012).

APPENDIX B: THE CAUSES OF COLOR

Nassau (NASSAU, 2001) makes a detailed analysis of the physical and chemical principles that cause color. Altogether, the author points to 15 causes of colors for the existing materials:

- 1) Incandescence
- 2) Gas excitation
- 3) Vibrations and rotations
- 4) Presence of transition metal in the original compound
- 5) Presence of transition metal as an impurity
- 6) Molecular orbitals
- 7) Charge transfer
- 8) Band theory for metals
- 9) Band theory for semiconductors
- 10) Impurities in semiconductors
- 11) Color centers
- 12) Dispersion
- 13) Scattering
- 14) Interference without diffraction
- 15) Diffraction

This work does not intend to replicate the information contained in (NASSAU, 2001) and (SHEVELL, 2003). Thus, in the following sections only a summary of each cause will be provided, so that the reader can get an overview of them. What can be concluded is that, in essence, all these mechanisms of color production are based on the interaction of incident light rays with the electrons and chemical bonds that form the material.

B.1 Incandescence

When one heats any object, its color changes as the temperature increases. The increase in temperature is derived from the increase in vibrational energy of this object. Atoms and molecules then emit some of this energy as photons, i.e., they emit light. The hotter the object, the greater the energy of vibration of its atoms, and therefore, the greater the frequency of the emitted light. Thus, with the increase in temperature, the color sequence black, red, orange, white and bluish white is formed. Figure B.1 shows the spectrum of colors and three ways of expressing it: (i) frequency (vibrations per second), (ii) wavelength, and (iii) energy. Figure B.2 shows a piece of hot iron where it is possible to observe part of the sequence of colors.

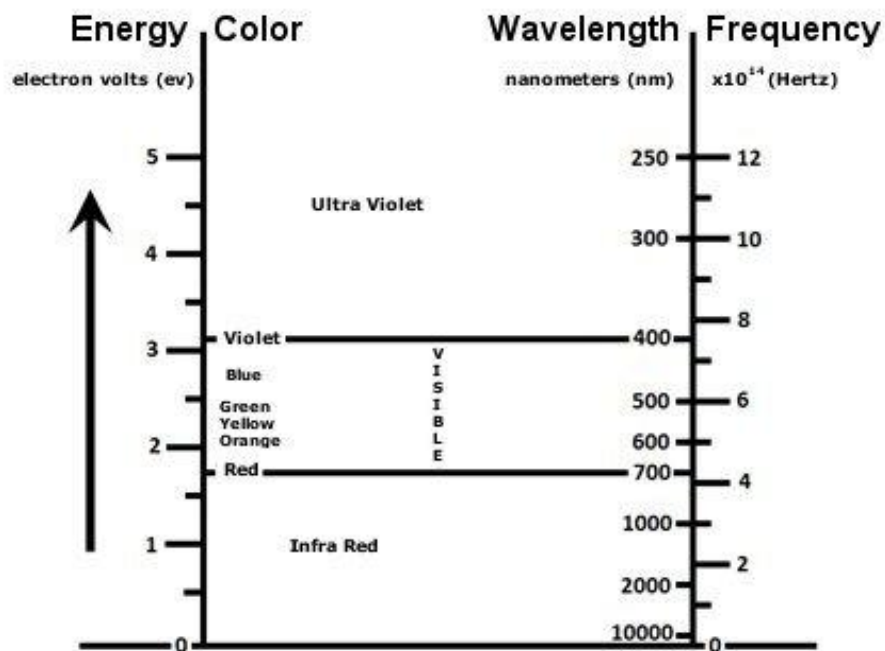


Figure B.1: Spectrum of colors (NASSAU, 2001).



Figure B.2: Piece of hot iron(Source: <http://s3.amazonaws.com>. Access in March, 2009).

B.2 Gas Excitation

Unlike incandescent light that may be emitted by any hot object, in the excitement of gases it is a specific chemical element that emits light. An atom in a gaseous or vapor state may have its electrons excited to higher energy levels. The light is then emitted when part of this energy is released as photons. The electron configuration of the atom will determine the energy levels that can be achieved and the possible transitions between energy levels. And so, determine the wavelength of the emitted photons.

There are various ways of exciting a gas, for example, using an electric current, as in the neon tubes, and in the sodium and mercury lamps. Figure B.3 presents the light emitted by a sodium lamp.

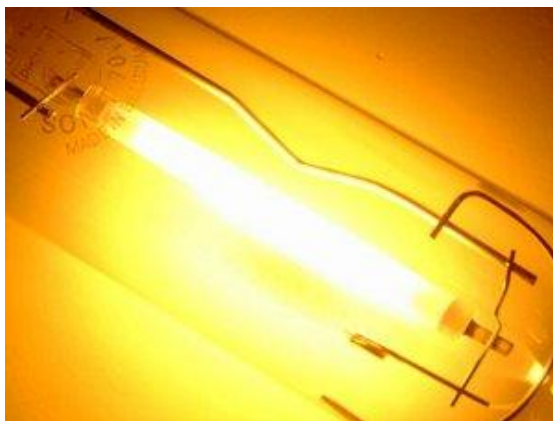


Figure B.3: Light emitted by a sodium lamp(Source: http://www.lightsoftherockies.net/-Green_Lighting.html. Access in June, 2012).

B.3 Vibrations and Rotations

Consider, for example, a molecule of iodine (I_2) in the gaseous state. We can represent it as two sphere connected by a spring representing the chemical bond. If the system is disturbed, it will vibrate. Figure B.4 presents the possible directions of vibration for the molecules of iodine (left), and water (right).

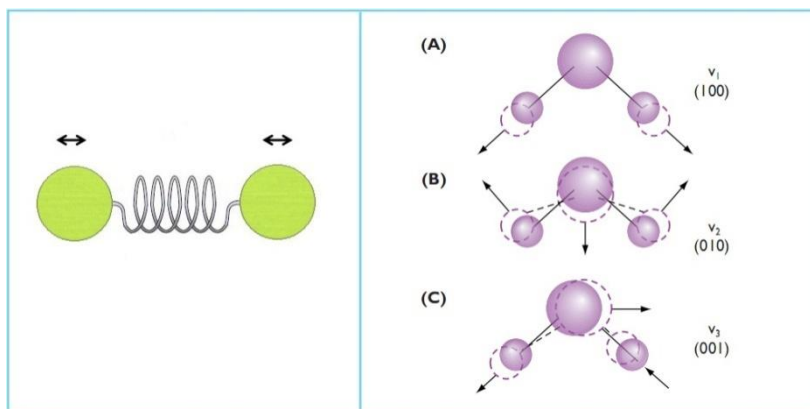


Figure B.4: Directions of vibration for molecules of iodine (left), and water (right) (SHEVELL, 2003).

The frequency of vibration of all the molecules is so low that the energy involved is too small to directly interact with visible light. Consequently, the absorptions due only to vibrations are restricted to the infrared. As the systems involved are very small (we are dealing at atomic level) and contains low energy, only a few vibrational energies are possible.

The vibrational energy levels are much closer than the electronics. Thus, each electronic level has a series of vibrational levels called v_1, v_2, v_3, \dots for the ground state; $v_1', v_2', v_3' \dots$ for the first excited state and so on. There are cases, such as the color of ice and water, in which only the vibrations are responsible for their coloration. But besides the vibrational energy levels, there are still the rotational energy levels, resulting from the rotation of molecules. Figure B.5 presents the possibilities of rotation

of a diatomic molecule, which, together with the vibration, determines the color of the compound.

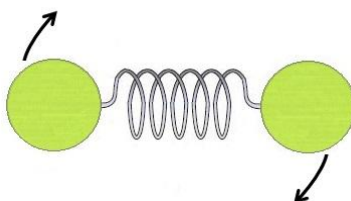


Figure B.5: Possibilities of rotation for a diatomic molecule.

That is, vibrations and rotations provide different levels of energy for each electronic level what modifies the absorption and emission spectrum. This is what happens, for example, with iodine. Figure B.6 presents iodine in solid state (left) and vaporized (right). Note that in the image of solid iodine it is possible to see a light purple color over the black solid, indicating the onset of vaporization.

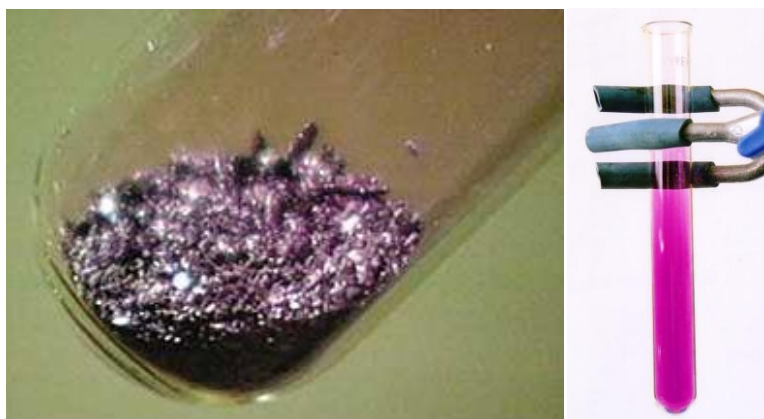


Figure B.6: Iodine in solid state (left), and vaporized (right)(Source: <https://www.chem.wisc.edu/deptfiles/genchem/lab/ptl/Elements/i/I.html>. Access in June, 2012)

B.4 Presence of transition metal in the original compound or as an impurity

The presence of transition metals either in the original compound or as in the form of impurities is the best known cause of color. It is responsible for the color of many minerals and gems. The energy required to excite an electron that is paired is very high. Thus, the absorption of visible light occurs in inorganic compounds containing metallic ions with unpaired electrons in the d or f orbitals

Consider a crystal of aluminum oxide (Al_2O_3), which, as seen in Figure B.7 consists of an aluminum atom surrounded by six atoms of oxygen in the form of a slightly distorted octahedron. Since all electrons are paired, this results in a colorless crystal.

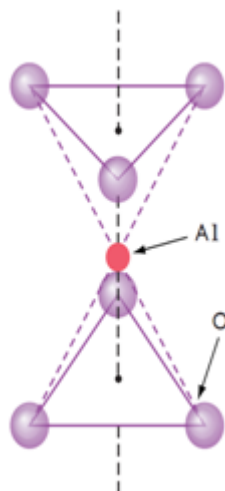


Figure B.7: Aluminum atom surrounded by six atoms of oxygen (SHEVELL, 2003).

If we exchange 1% of the Al^{+3} ions by Cr^{+3} ions, which has unpaired electrons in the orbital 3d, the mineral will acquire a beautiful red color, and it will be called ruby. With emerald also occurs the substitution of the aluminum ions by chromium ions. However, the mineral that will lead to the emerald before replacement (i.e., the mineral without impurities) is beryllium ($\text{Be}_3\text{Al}_2\text{Si}_6\text{O}_{18}$). Thus, despite the fact that the substitution that occurs is the same, the green color of emerald is due to the presence of beryllium and silicates in its composition. Figure B.8 presents from left to right, the crystals of aluminum oxide, ruby, and emerald.



Figure B.8: From left to right, the crystals of aluminum oxide, ruby and emerald (Source: <http://www.chm.davidson.edu/vce/coordchem/cft.html>. Access in June, 2012) (Source: <http://en.wikipedia.org/wiki/Ruby>. Access in June, 2012) (Source: <http://en.wikipedia.org/wiki/Emerald>. Access in June, 2012).

The Alexandrite mineral has an interesting effect. Consisting of beryllium aluminate containing a little bit of chromium, it has an intermediate behavior between ruby and emerald. As can be seen in Figure B.9, when illuminated by daylight or by a fluorescent light, it has a blue-green color. And, under the light of an incandescent lamp, one

perceives a deep red color. This rare effect (called Alexandrite Effect) can be observed in other gemstones and it is not related to pleochroism¹⁴.



Figure B.9: Alexandrite effect(Source: <http://www.geocities.jp/senribb/jewels/gem1st.html>. Access in June, 2012).

B.5 Molecular Orbitals

The Molecular Orbital Theory (MOT) is used to explain the color in organic compounds. This category includes all types of dyes and pigments. As these compounds are beyond the scope of this work, they will not be addressed and an overview of MOT was given in Section 5.2.1.

B.6 Charge transfer

As can be seen in Figure B.10 (left), a crystal of aluminum oxide is colorless. When iron impurities are present, it acquires a pale yellow color (Figure B.10 center). If besides iron titanium is also present, the result is the intense blue of the Blue Sapphire (Figure B.10 right). The mechanism responsible for this is charge transfer. That is, due to the energy produced by the absorption of a photon, an electron from an ion of a transition metal passes to another transition metal, resulting in a temporary change in the valence states of both ions.

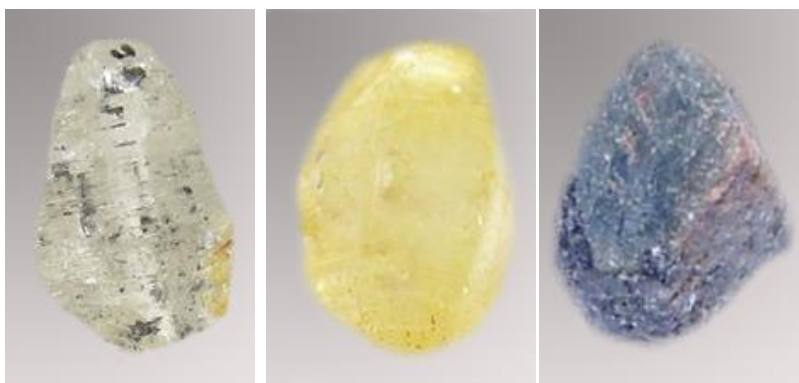


Figure B.10: A crystal of aluminum oxide (left). Iron impurities result in a pale yellow color (center). Iron plus titanium impurities result in the blue (right) (Source: <http://en.wikipedia.org/wiki/Corundum>. Access in June, 2012).

¹⁴ See Section 2.1.6.2 for definition

Consider two slightly distorted octahedral adjacent aluminum sites occupied by Fe^{+2} and Ti^{+4} , as shown in Figure B.11. The transfer of an electron from iron to titanium results in the variation of the valence of both ions:

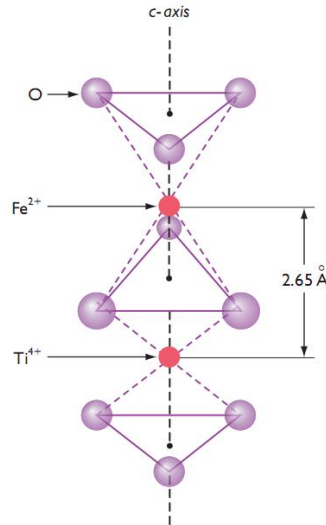
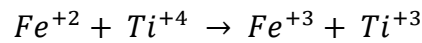


Figure B.11: Slightly distorted octahedral aluminum sites occupied by Fe^{+2} and Ti^{+4} (SHEVELL, 2003).

This process requires absorbing energy corresponding to the yellow color in the spectrum, thus, it results in the emission of the complementary color, blue. This exchange can occur both with ions of different elements, as well as with ions of the same elements, as it occurs with Fe^{+2} and Fe^{+3} in magnetite.

B.7 Band theory

Consider two hydrogen atoms that connect to form a bond. Two atomic orbitals interact and form two molecular orbitals. If now we have four atoms, we expect that four molecular orbitals are going to be formed. Extrapolating this approach to a piece of metal containing 10^{23} atoms interacting per cubic centimeter, we expect 10^{23} of these orbitals, forming something as an "energy band", as can be seen in Figure B.12.

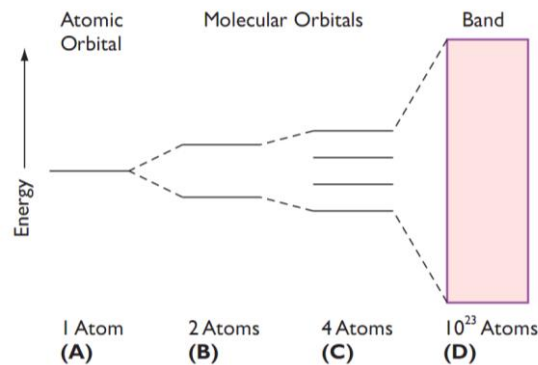


Figure B.12: Energy band (SHEVELL, 2003).

The band theory is used to explain the properties of metals and their alloys. The format of the band depends on the atomic orbitals involved, on the number of atoms present, on the geometry and the space between the atoms. The total number of electrons involved is the sum of all valence electrons of all atoms present.

The ability to hold electrons varies with different energies through the band. The highest energy level filled is called the *Fermi surface*. In a metal, the bonding electrons no longer belong to individual atoms, but to the piece of metal as a whole. They are "delocalized".

When light falls on a metal, electrons below the Fermi surface can be excited to higher levels of energy in the empty part of the band. The light is so intensely absorbed that it cannot penetrate far into the metal. As the metal is a conductor of electricity, the light absorbed will induce an electrical current in the metal surface. The electromagnetic theory shows that these currents immediately emit light back out of the metal, resulting in large reflection of a polished metal surface. Figure B.13 shows a silver ore, where this property can be perceived.



Figure B.13: Silver ore (Source: <http://en.wikipedia.org/wiki/Ore>. Access in June, 2012).

In some materials, such as insulators and semiconductors, there is a gap in the band, affecting the color. This gap is the difference between the energy of the valence band¹⁵ and the conduction band¹⁶. Thus, the color of pure material varies with the size of the gap as a larger gap means that a larger amount of energy is required to excite an electron from the valence band to the conduction band. Therefore, for example, if the required energy is superior to those corresponding to the visible spectrum, the material will be colorless.

If a substance forms an impurity level in the band gap, then the light can be absorbed (or emitted) by a semiconductor with energy smaller than the gap. This principle is responsible, for example, for yellow diamonds. This results from the presence of some nitrogen atoms in the carbon structure. The variation in the size of the gap is demonstrated by the mixture of the yellow crystals of cadmium sulfide (CdS) and the black ones of cadmium selenide (CdSe). These compounds have the same structure and form a continuous series whose sequence of colors is represented in Figure B.14.

¹⁵ Valence band is the band where the electrons are bound to one atom.

¹⁶ Conduction band is the band where the electrons can move freely through the material



Figure B.14: Color sequence of a continuous series formed by crystals of CdS and CdSe (SHEVELL, 2003).

B.8 Color centers

Color centers involve the displacement of an electron through radiation or other techniques with the formation of a hole. For example, in Figure B.15, atom A is irradiated and its electron is displaced, forming a hole center. This displaced electron is trapped in atom B and forms an electronic center. The hole center in atom A and/or the electronic center in atom B may become the center of color that absorbs light.

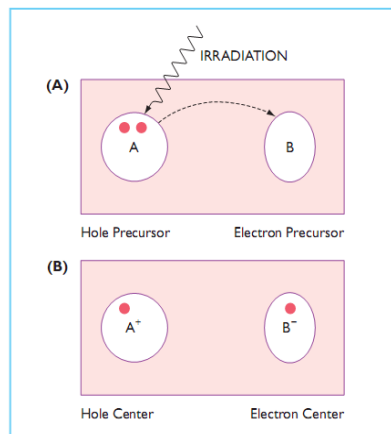


Figure B.15: Example of the formation of color centers(SHEVELL, 2003).

Color centers may or may not be stable. The non-stable ones can be undone by the presence of light or by heating. The stable ones can only be undone by heating. Some have the opposite behavior and form in the dark. Color centers are responsible, for example, for the different colors of topaz, seen in Figure B.16.



Figure B.16: Different colors of topaz (Source: <http://en.wikipedia.org/wiki/Topaz>. Access in June, 2012.).

B.9 Dispersion

Dispersion involves the reduction of the refractive index with the increasing of the wavelength. Anomalous dispersion occurs in regions where there is absorption of incident light. The color is generated by the dispersion in prisms and lenses, faces of gems, water drops, ice crystals, and the atmosphere. An example of dispersion is the sparkles presented by a diamond cut such as shown in Figure B.17.



Figure B.17: Sparkles in a diamond (Source: <http://www.whiteflash.com/about-diamonds/diamond-education/diamond-light-return---is-maximization-really-the-answer-1158.htm>. Access in June, 2012.).

B.10 Scattering

When the air is apparently clean, it is difficult to witness the scattering effect. However, if there is dust in the air, we can see, for example, the sun's rays coming through the window. And, most atmospheric phenomena such as the blue sky and the red sunset (represented in Figure B.18), is due to different types of scattering.



Figure B.18: Red sunset (Source: <http://www.123rf.com>. Access in June, 2012).

Lord Rayleigh was the first to understand that even the purest substances, including gases, have fluctuations in their refractive indices and can spread the light. He demonstrated that the intensity of scattered light I_s is related to the incident light I_0 by the inverse of the fourth power of the wavelength:

$$\frac{I_s}{I_0} = \text{const } \lambda^{-4}$$

The Rayleigh scattering produces blue colors when the scattering centers are larger than the wavelength of light, resulting, for example, in the blue of the sky, in the red sunset and in the green and purple colors of some animals. And when they are larger than the wavelength, it usually results in white, but it can also result in the phenomenon of blue moon.

B.11 Interference and Diffraction

Two light beams of the same wavelength can interfere with each other constructively or destructively, as shown in Figure B.19.

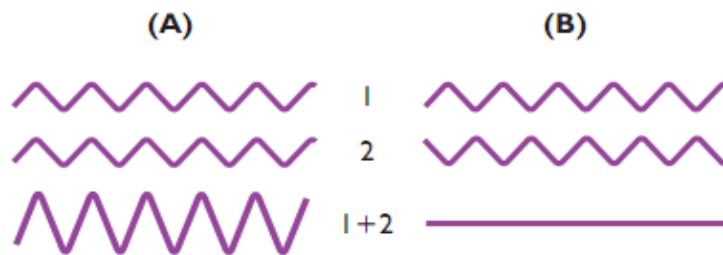


Figure B.19: Constructive (left) and destructive (right) interference (SHEVELL, 2003).

If two monochromatic beams are focused onto a thin surface the result is black and white fringes. If the beam is of white light, it produces the range of Newton's colors. These colors can be observed, for example, on the surface of soap bubbles, as in Figure B.20.



Figure B.20: Bubble soap (Source: <http://www.123rf.com>. Access in June, 2012).

Diffraction describes the propagation of light at the edges of an object. As two diffracted light beams from opposite sides of a small particle can cause interference, diffraction always involves interference. Thus, it results in colored fringes around and within the shadow of the object. When there are many small particles as in the case of clouds and fog, it produces effects such as the corona shown in Figure B.21 (left), or the iridescent clouds (right), and many others.



Figure B.21: Corona (left) and iridescent clouds (right) (Source: <http://astrobob.areavoices.com/2008/09/13/through-fog-into-another-dimension>. Access in June, 2012) (Source: <http://www.flickr.com/photos/pixieledpictures/2570791174>. Access in June, 2012).

ANNEX A

```
#-----
##Date: 2010-01-30 13:59:17 +0000 (Sat, 30 Jan 2010) $
##Revision: 966 $
##URL: svn://cod.ibt.lt/cod/cif/5/5000035.cif $
#-----
#
# This file is available in the Crystallography Open Database (COD),
# http://www.crystallography.net/
#
# All data on this site have been placed in the public domain by the
# contributors.
#
data_5000035
 _chemical_name_systematic      'Silicon oxide'
 _chemical_name_mineral         'Quartz'
 _chemical_formula_structural   'Si O2'
 _chemical_formula_sum          'O2 Si'
 _publ_section_title
;
Crystal structures of quartz and magnesium germanate by profile
analysis of synchrotron-radiation high-resolution powder data.
;
loop_
 _publ_author_name
   'Will, G'
   'Bellotto, M'
   'Parrish, W'
   'Hart, M'
 _journal_name_full             'Journal of Applied Crystallography'
 _journal_volume                21
 _journal_year                  1988
 _journal_page_first            182
 _journal_page_last             191
 _cell_length_a                 4.91239(4)
 _cell_length_b                 4.91239(4)
 _cell_length_c                 5.40385(7)
 _cell_angle_alpha              90
 _cell_angle_beta               90
 _cell_angle_gamma              120
 _cell_volume                   112.9
 _cell_formula_units_Z          3
 _symmetry_space_group_name_H-M 'P 32 2 1'
 _symmetry_Int_Tables_number    154
 _symmetry_cell_setting         trigonal
loop_
 _symmetry_equiv_pos_as_xyz
   'x,y,z'
   '-y,x-y,2/3+z'
   'y-x,-x,1/3+z'
   'y,x,-z'
   'x-y,-y,1/3-z'
   '-x,y-x,2/3-z'
loop_
 _atom_type_symbol
 _atom_type_oxidation_number
Si4+  4.000
O2-   -2.000
loop_
 _atom_site_label
 _atom_site_type_symbol
 _atom_site_symmetry_multiplicity
 _atom_site_Wyckoff_symbol
 _atom_site_fract_x
 _atom_site_fract_y
 _atom_site_fract_z
 _atom_site_occupancy
 _atom_site_attached_hydrogens
 _atom_site_calc_flag
Si1  Si4+  3 a 0.4701(4) 0. 0.6667 1. 0 d
O1   O2-   6 c 0.4139(7) 0.2674(7) 0.7856(6) 1. 0 d
_refine_ls_R_factor_all          0.022
_cod_database_code 5000035
```

Figure AnnexA.1: Example of a silica CIF file.

ANNEX B

Table Annex B.1: CIE 1931 standard colorimetric observer(CIE, 2012).

λ , nm	$\bar{x}(\lambda)$	$\bar{y}(\lambda)$	$\bar{z}(\lambda)$	λ , nm	$\bar{x}(\lambda)$	$\bar{y}(\lambda)$	$\bar{z}(\lambda)$
380	0,001368	0,000039	0,006450	585	0,978600	0,816300	0,001400
385	0,002236	0,000064	0,010550	590	1,026300	0,757000	0,001100
390	0,004243	0,000120	0,020050	595	1,056700	0,694900	0,001000
395	0,007650	0,000217	0,036210	600	1,062200	0,631000	0,000800
400	0,014310	0,000396	0,067850	605	1,045600	0,566800	0,000600
405	0,023190	0,000640	0,110200	610	1,002600	0,503000	0,000340
410	0,043510	0,001210	0,207400	615	0,938400	0,441200	0,000240
415	0,077630	0,002180	0,371300	620	0,854450	0,381000	0,000190
420	0,134380	0,004000	0,645600	625	0,751400	0,321000	0,000100
425	0,214770	0,007300	1,039050	630	0,642400	0,265000	0,000050
430	0,283900	0,011600	1,385600	635	0,541900	0,217000	0,000030
435	0,328500	0,016840	1,622960	640	0,447900	0,175000	0,000020
440	0,348280	0,023000	1,747060	645	0,360800	0,138200	0,000010
445	0,348060	0,029800	1,782600	650	0,283500	0,107000	0,000000
450	0,336200	0,038000	1,772110	655	0,218700	0,081600	0,000000
455	0,318700	0,048000	1,744100	660	0,164900	0,061000	0,000000
460	0,290800	0,060000	1,669200	665	0,121200	0,044580	0,000000
465	0,251100	0,073900	1,528100	670	0,087400	0,032000	0,000000
470	0,195360	0,090980	1,287640	675	0,063600	0,023200	0,000000
475	0,142100	0,112600	1,041900	680	0,046770	0,017000	0,000000
480	0,095640	0,139020	0,812950	685	0,032900	0,011920	0,000000
485	0,057950	0,169300	0,616200	690	0,022700	0,008210	0,000000
490	0,032010	0,208020	0,465180	695	0,015840	0,005723	0,000000
495	0,014700	0,258600	0,353300	700	0,011359	0,004102	0,000000
500	0,004900	0,323000	0,272000	705	0,008111	0,002929	0,000000
505	0,002400	0,407300	0,212300	710	0,005790	0,002091	0,000000
510	0,009300	0,503000	0,158200	715	0,004109	0,001484	0,000000
515	0,029100	0,608200	0,111700	720	0,002899	0,001047	0,000000
520	0,063270	0,710000	0,078250	725	0,002049	0,000740	0,000000
525	0,109600	0,793200	0,057250	730	0,001440	0,000520	0,000000
530	0,165500	0,862000	0,042160	735	0,001000	0,000361	0,000000
535	0,225750	0,914850	0,029840	740	0,000690	0,000249	0,000000
540	0,290400	0,954000	0,020300	745	0,000476	0,000172	0,000000
545	0,359700	0,980300	0,013400	750	0,000332	0,000120	0,000000
550	0,433450	0,994950	0,008750	755	0,000235	0,000085	0,000000
555	0,512050	1,000000	0,005750	760	0,000166	0,000060	0,000000
560	0,594500	0,995000	0,003900	765	0,000117	0,000042	0,000000
565	0,678400	0,978600	0,002750	770	0,000083	0,000030	0,000000
570	0,762100	0,952000	0,002100	775	0,000059	0,000021	0,000000
575	0,842500	0,915400	0,001800	780	0,000042	0,000015	0,000000
580	0,916300	0,870000	0,001650				

Table Annex B.2: CIE Standard Illuminant D65(CIE, 2012).

λ , nm	D65	λ , nm	D65
380	49,975500	585	92,236800
385	52,311800	590	88,685600
390	54,648200	595	89,345900
395	68,701500	600	90,006200
400	82,754900	605	89,802600
405	87,120400	610	89,599100
410	91,486000	615	88,648900
415	92,458900	620	87,698700
420	93,431800	625	85,493600
425	90,057000	630	83,288600
430	86,682300	635	83,493900
435	95,773600	640	83,699200
440	104,865000	645	81,863000
445	110,936000	650	80,026800
450	117,008000	655	80,120700
455	117,410000	660	80,214600
460	117,812000	665	81,246200
465	116,336000	670	82,277800
470	114,861000	675	80,281000
475	115,392000	680	78,284200
480	115,923000	685	74,002700
485	112,367000	690	69,721300
490	108,811000	695	70,665200
495	109,082000	700	71,609100
500	109,354000	705	72,979000
505	108,578000	710	74,349000
510	107,802000	715	67,976500
515	106,296000	720	61,604000
520	104,790000	725	65,744800
525	106,239000	730	69,885600
530	107,689000	735	72,486300
535	106,047000	740	75,087000
540	104,405000	745	69,339800
545	104,225000	750	63,592700
550	104,046000	755	55,005400
555	102,023000	760	46,418200
560	100,000000	765	56,611800
565	98,167100	770	66,805400
570	96,334200	775	65,094100
575	96,061100	780	63,382800
580	95,788000		